Dissolution of biogenic silica:
Roles of pH, salinity, pressure, electrical charging and reverse weathering

Socratis Loucaides

GEOLOGICA ULTRAIECTINA

Mededelingen van de
Faculteit Geowetenschappen
departement Aardwetenschappen
Universiteit Utrecht

No. 302

Members of the dissertation committee:

Joan D. Willey
University of North Carolina
Wilmington, USA

David J. DeMaster
North Carolina State University
USA

Patricia M. Dove
Virginia Polytechnic Institute and State University
USA

Daniel Conley
Lund University
Sweden

Jack Middelburg
Utrecht University/Netherlands Institute of Ecology
The Netherlands

ISBN/EAN 978-90-5744-164-6

Graphic design: GeoMedia [7430], Faculty of Geosciences, Utrecht University

Dissolution of biogenic silica: Roles of pH, salinity, pressure, electrical charging and reverse weathering

Oplossen van biogeen silica:
De rol van pH, saliniteit, druk, electrische lading en omgekeerde verwering

(met een samenvatting in het Nederlands)

Διαλυτότητα βιογενούς χαλαζία:
Επίδραση του pH, της αλατότητας, της πίεσης, του δυναμικού φορτίου και της ανάδρομης διάβρωσης

(με περίληψη στα Ελληνικά)

PROEFSCHRIFT

ter verkrijging van de graad van doctor aan de Universiteit Utrecht
op gezag van de rector magnificus, prof. dr. J.C. Stoof,
ingevolge het besluit van het college voor promoties
in het openbaar te verdedigen
op dinsdag 17 maart 2009 des middags te 12.45 uur

door

Socratis Loucaides
geboren op 22 maart 1977 te Limassol, Cyprus

Promotor:
Prof. dr. P. Van Cappellen
Department of Earth Science-Geochemistry
Faculty of Geoscience, Utrecht University

Co-promotor:
Dr. T. Behrends
Department of Earth Science-Geochemistry
Faculty of Geoscience, Utrecht University

"An unexamined life is not worth living"

Socrates (469-399 BC)

For my son, Dylan

Contents

CHAPTER 1

General introduction

1.1 The biogeochemical cycle of Si

Silicon is the second most abundant element in the Earth's crust, after oxygen, comprising about 26% of the crust by weight. Weathering of silicate rocks releases dissolved silica (dSi, mostly as silicic acid, H_4SiO_4) which is an essential nutrient for aquatic and terrestrial plants. Framework silicate minerals are ordered solids containing strong siloxane bonds (>Si-O-Si<), therefore, on biological time scales their dissolution is relatively slow (Lucas and Dolan, 1939; Mackenzie and Garrels, 1965).

On land, higher plants take up dSi, which they deposit in their tissues as phytoliths, a form of biogenic silica ($bSiO_2$) (Alexandre et al., 1997). On a dry weight basis, $bSiO_2$ can make up to 10% of plant biomass (Epstein, 1999). The accumulation of silica in plants is thought to play an important role in their health and resistance to biological, chemical, and physical stress (Datnoff et al., 2001; Epstein, 1999). Aquatic organisms including diatoms, radiolarian, chrysophytes, silicoflagellates, and sponges take up dSi to build their silica skeletons, which provide structural integrity, ballast, and protection from predators (Conley and Kilham, 1989; Hamm et al., 2003; Pondaven et al., 2007).

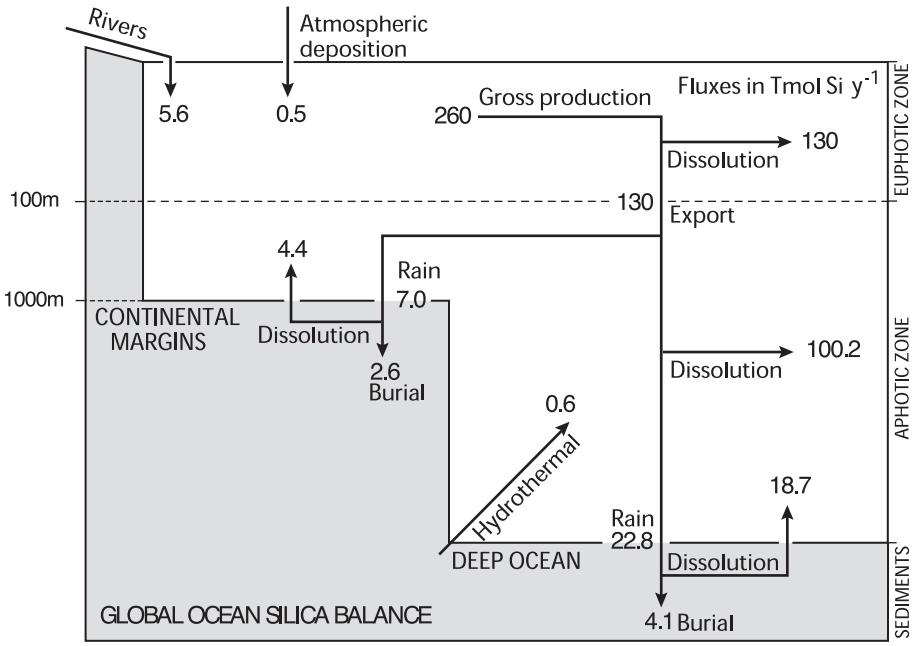

Figure 1.1 The oceanic Si budget by Sarmiento and Gruber (2006), calculated based primarily on the work of Trequer et al. (1995), Nelson et al. (1995) and DeMaster (2002).

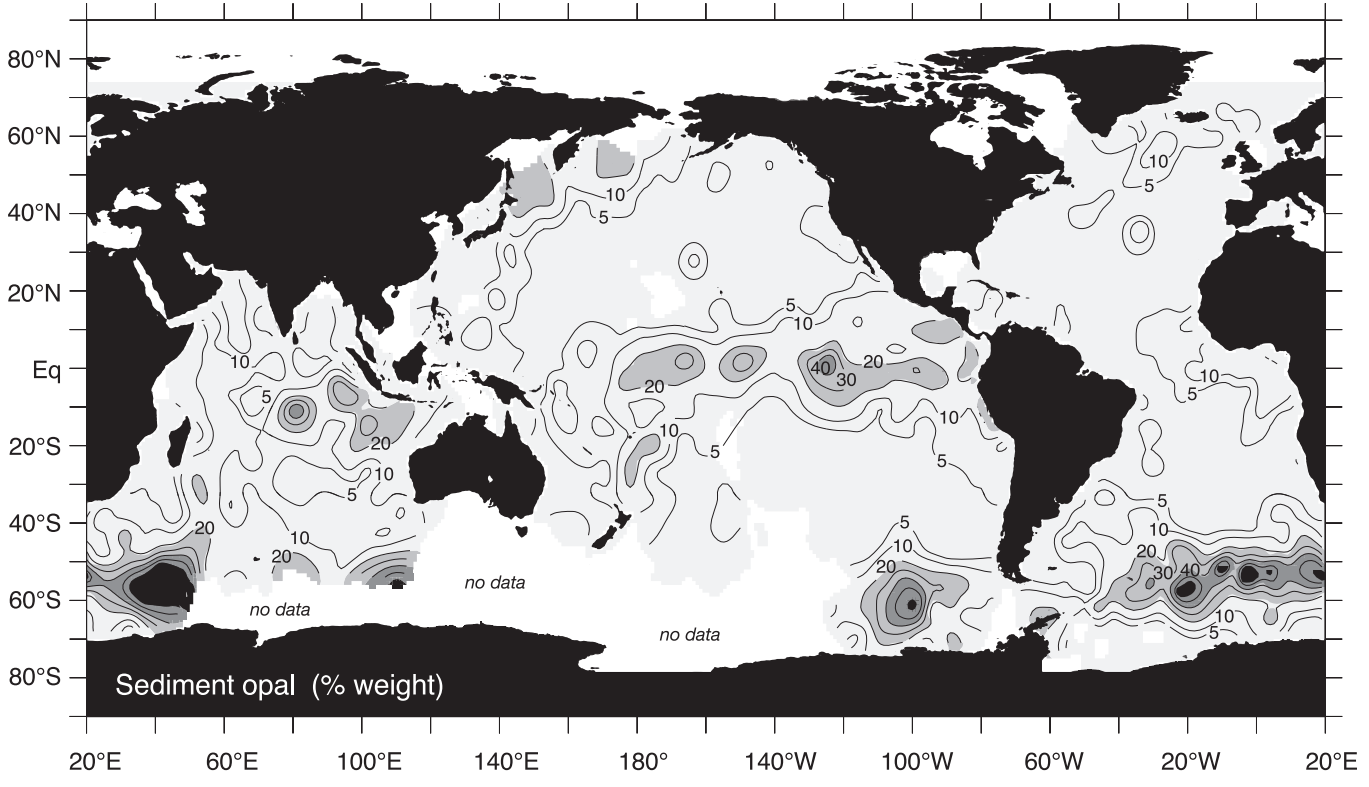

Figure 1.2 Global map of biogenic silica (opal) weight % in surface sediments of the oceans, from Sarmiento and Gruber (2006). Note the high concentrations of biogenic opal in the Southern Ocean and along the equatorial Pacific Ocean.

The structure of $bSiO_2$ is characterized by the absence of long-range order, and, due to its relatively low thermodynamic stability, its dissolution kinetics in water are orders of magnitude faster than those of framework silicate minerals (Alexandre et al., 1997; Iler, 1979). Because of the high recycling efficiency of $bSiO_2$, the biomineralization and dissolution of $bSiO_2$ dominate the global biogeochemical cycle of Si on time scales relevant to biological processes (Laruelle et al., 2008)

1.2 Production and preservation of biogenic silica in the ocean

The oceanic biogeochemical cycle of Si gained significant attention during the last few decades mainly because of the role of diatoms in the biological CO_2 pump (Dugdale et al., 1995; Nelson et al., 1995; Ragueneau et al., 2000; Tréguer et al., 1995). Diatoms are efficient exporters of organic matter from the surface ocean (Kemp et al., 2006; Kemp et al., 2000) and by far the single most important group of oceanic primary producers (Nelson et al., 1995). Unlike other algal species, however, diatoms are limited by the availability of dSi, which they require to synthesize their amorphous silica frustules.

Based on recent estimates (DeMaster, 2002; Nelson et al., 1995; Tréguer et al., 1995), biosiliceous production in today's ocean is in the order of 260 Tmol Si yr^{-1} (Fig. 1.1). Because the ocean is highly undersaturated with respect to $bSiO_2$ almost 90% of the global biosiliceous

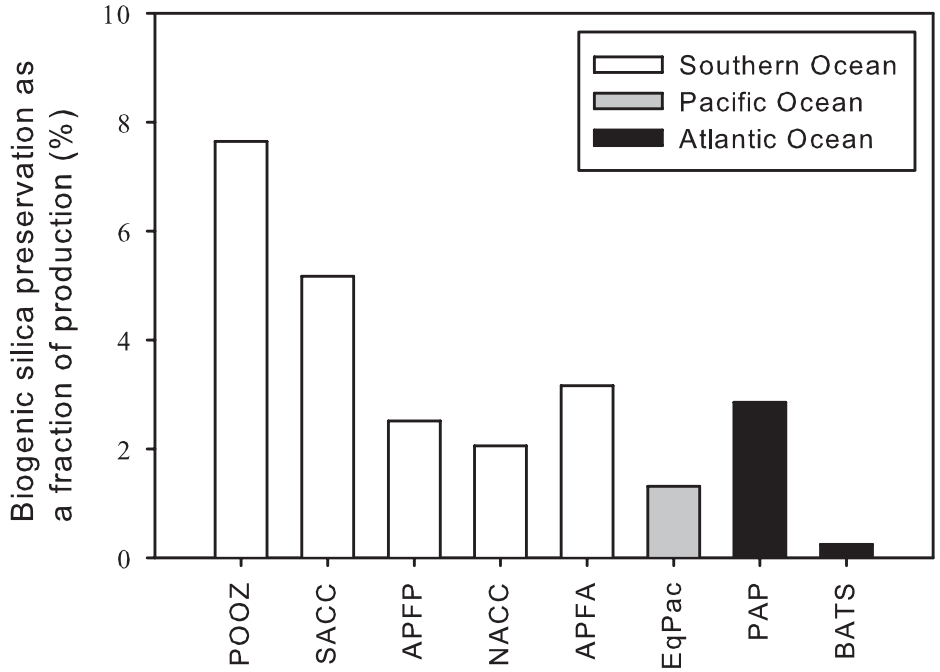

Figure 1.3 The ratio of $bSiO_2$ preservation to production in the Southern, Pacific, and Atlantic Oceans based on a review by Ragueneau et al. (2002). POOZ (Permanent Open Ocean Zone); SACC (Southern Antarctic Circumpolar Current); APFP (Atlantic sector of the Antarctic Polar Front); NACC (North Antarctic Circumpolar Current); APFA (Atlantic sector of the Antarctic Polar Front); EqPac (Equatorial Pacific); PAP (Porcupine Abyssal Plane); BATS (Bermuda Atlantic Time-Series Study) Oligotrophic Atlantic.

production is recycled within the water column. The remaining 10% reaches the bottom sediments, although only a small fraction (about 2%) of the biosiliceous production is permanently buried. The efficient recycling of $bSiO_2$ sustains the diatomaceous primary productivity in the ocean and therefore directly impacts the efficiency of the biological CO_2 pump.

The satial distribution of $bSiO_2$ in oceanic sediments is highly variable (Fig. 1.2), with the highest accumulation rates in the Southern Ocean and equatorial Pacific, and intermediate in equatorial Atlantic, North Atlantic and Indian Oceans. Although these areas correspond roughly to areas of high primary productivity, the ratio between biosiliceous production and preservation is characterized by high spatial and temporal variability (Nelson et al., 1995) (Fig. 1.3).

Since $bSiO_2$-rich sediments are distributed in a variety of depths and latitudes and across all climatic zones of the ocean (Fig. 1.2), biosiliceous fossils have a great potential as proxies for paleoproductivity (Ragueneau et al., 2000 and references therein). However, the great spatial and temporal inconsistencies between production, export and burial of $bSiO_2$ significantly hinder the interpretation of the sedimentary $bSiO_2$ record. The large variability in preservation efficiency reflects the great number of (interacting) biotic and abiotic processes involved in the recycling of $bSiO_2$ (Fig. 1.4). A sound knowledge of these processes is therefore essential to better understand the functioning of the Si cycle in the past, present, and future oceans.

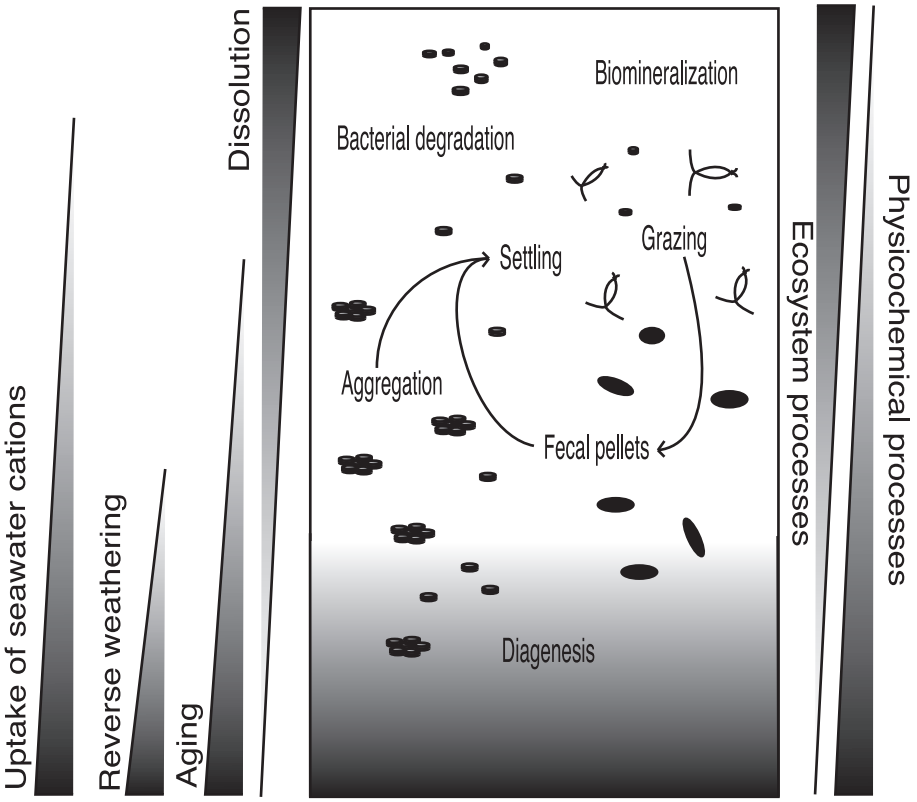

Figure 1.4 Physicochemical and ecosystem processes controlling the dissolution and ultimate preservation of diatomaceous silica in the oceans (see Chapter 2 for details).

1.3 Recycling of biogenic silica

1.3.1 Ecosystem processes in the water column

Part of the large variability in the recycling efficiency of diatomaceous silica reflects the large variety in frustule architecture and specific surface area (Fig. 1.5). Species-specific variations in frustule silicification and specific surface area can cause differences in dissolution efficiency of several orders of magnitude (Ryves et al., 2001). Furthermore, processes during biomineralization may lead to significant variations in silicification (Martin-Jezequel et al., 2000) and frustule morphology and architecture (Vrieling et al., 2000; Vrieling et al., 1999b) within the same diatom species.

Frustules of living diatoms are remarkably resistant to dissolution due to the presence of an organic matrix which acts as a protective barrier against hydrolysis of the silica (Lewin, 1961). Soon after the end of a diatom's lifecycle, colonization by bacterial assemblages and ectoproteases activity leads to the denudation of the organic matrix. The intensity of bacterial colonization controls the rate at which the organic matrix is removed, and therefore also the dissolution rate of $bSiO_2$ (Bidle and Azam, 1999; Bidle and Azam, 2001).

The effect of grazing on the recycling of $bSiO_2$ remains a subject of debate (Ragueneau et al., 2006). Diatoms processed through the digestive system of zooplankton undergo a series of transformations including digestion of the organic matrix, breakage of the frustules and encapsulation within fecal pellets. Some of these interactions enhance the dissolution efficiency of $bSiO_2$, while others reduce or even prevent it. The net result on the $bSiO_2$ recycling efficiency is highly variable and strongly depends on the grazer community structure (Schultes, 2004).

During blooms, aggregation of diatom cells in larger particles is facilitated by the excretion of dissolved polysaccharides which form a sticky substance known as TEP (Transparent Exopolymer Particles) (Passow, 2000). The role of aggregation can be critical to the fate of $bSiO_2$ in the ocean. Scientific opinions, however, are contradictory on whether aggregation enhances or slows down the recycling efficiency of $bSiO_2$ (Brzezinski et al., 1997; Moriceau et al., 2007; Passow et al., 2003). The dissolution of $bSiO_2$ within aggregates may be enhanced through intense bacterial activity (Brzezinski et al., 1997), although reduction of the diffusion rate of dSi inside the aggregates may slow down the dissolution kinetics of $bSiO_2$ (Moriceau et al., 2007).

1.3.2 Geochemical processes in the water column

After the disappearance of the organic matrix, the recycling efficiency of diatom frustules is controlled by the intrinsic physicochemical properties of the silica surface and the bulk solid, plus those of the solvent. It is generally accepted that the dissolution of silica polymorphs in aqueous solutions occurs via the hydrolysis of siloxane (>Si-O-Si<) bonds of the SiO_2 network exposed at the particle surface. Water molecules orient their electronegative oxygen towards the Si atom, leading to a transfer of electron density to the siloxane bond, thereby increasing its length and eventually breaking it. A series of such reactions leads to the release of hydrated Si atoms in the form of silicic acid, H_4SiO_4 (Fig. 1.6).

In the water column, the main physicochemical variables that affect the dissolution efficiency of settling diatoms are temperature and pressure. While the effect of temperature has been studied quite extensively (Hurd, 1972; Kamatani, 1982; Lawson et al., 1978; Van Cappellen and Qiu, 1997b), the effects of pressure on the dissolution kinetics and solubility of $bSiO_2$ remains largely unexplored. So far the dependence of $bSiO_2$ solubility on pressure has been estimated based on

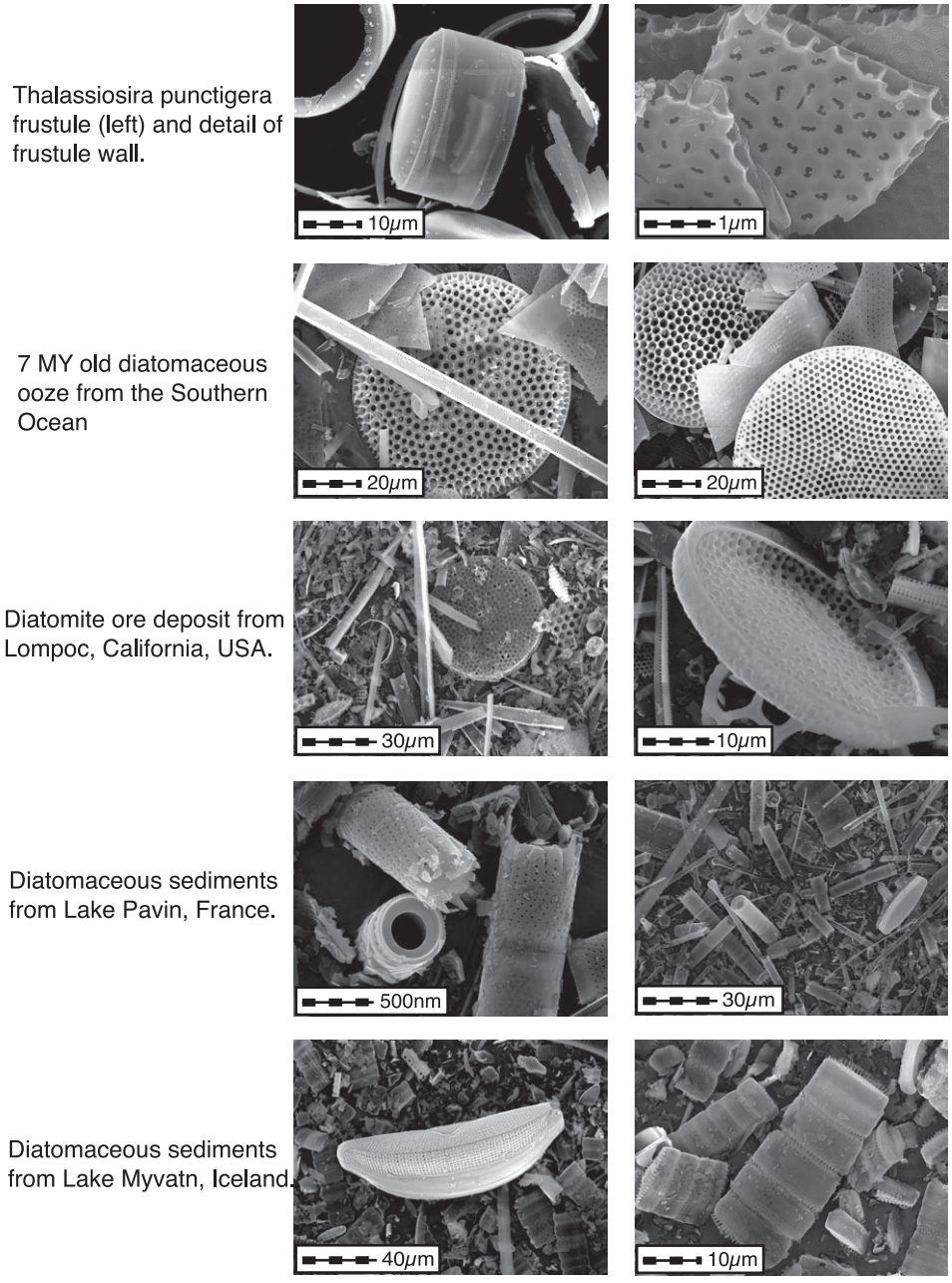

Figure 1.5 Various diatomaceous materials used in the experiments described in this thesis.

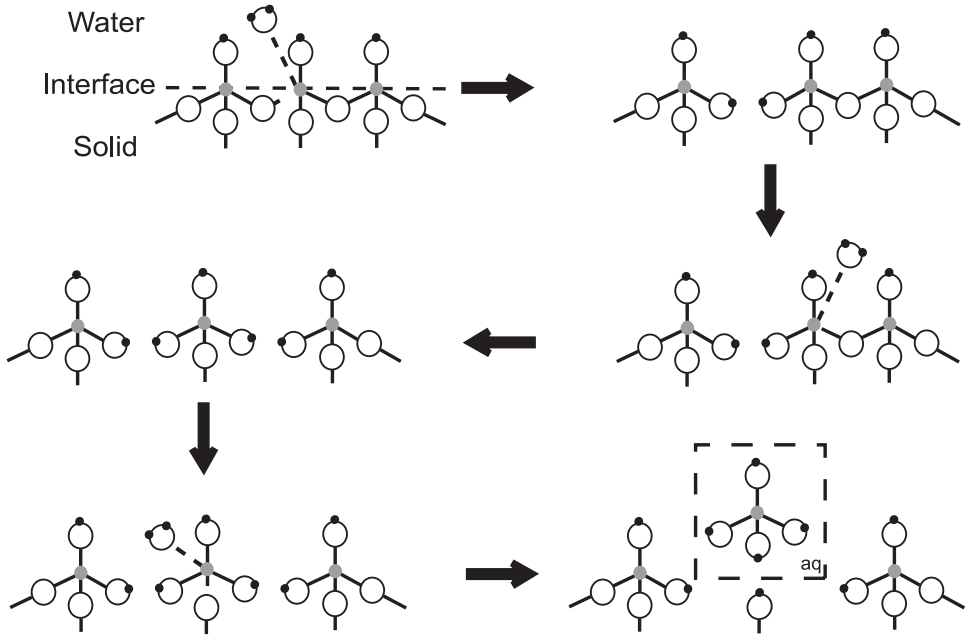

Figure 1.6 The hydrolysis reaction of silica in water under near-neutral pH. Adapted from Dove and Crerar (1990). White spheres represent O atoms, grey spheres Si atoms and black spheres H atoms.

laboratory experiments using synthetic amorphous silica (Willey, 1974). Field observations and recent experimental results, however, suggest that the dependence of the solubility of $bSiO_2$ on pressure may be significantly different than previously thought (see Chapter 3).

The progressive reduction in reactivity of $bSiO_2$ (ageing) from the ocean surface down to the seafloor suggests that interactions between seawater and diatom frustules significantly impact the recycling and preservation of $bSiO_2$ (Rickert et al., 2002). Combination of dissolution rate data and spectroscopic observations suggests that the apparent reduction in reactivity of $bSiO_2$ is associated with changes in the surface chemical structure, and in particular the progressive loss of reactive surface sites (Dixit and Van Cappellen, 2002; Schmidt et al., 2001).

Attempts to characterize the surface chemistry of $bSiO_2$ reveal significant variability in acid-base properties (Dixit and Van Cappellen, 2002). Surface charge densities reported for phytoliths even exceed the theoretical limit by several orders of magnitude (Fraysse et al., 2006b). Furthermore, the available data suggest that the acid-base properties of $bSiO_2$ departs from that of crystalline and synthetic amorphous silicas (Chapter 4), thereby complicating the relationship between dissolution rates and surface charge densities. Although a substantial body of work is dedicated to the dissolution kinetics of $bSiO_2$ (Barker et al., 1994; Fraysse et al., 2006b; Greenwood et al., 2001; Hurd and Birdwhistell, 1983; Kamatani, 1982; Kamatani and Riley, 1979; Kamatani et al., 1980; Koning et al., 1997; Lewin, 1961; Loucaides et al., 2008; Van Cappellen, 1996; Van Cappellen et al., 2002a; Van Cappellen et al., 2002b; Van Cappellen and Qiu, 1997b), the link with the acid-base properties remains to be elucidated.

1.3.3 Geochemical processes at the seafloor

Dissolution of $bSiO_2$ in marine sediments leads to an efflux of dSi to the water column. Typically pore water silicic acid concentrations increase downward until they level off at a quasi-constant value at depths of around 5-30 cm below the sediment-water interface. Asymptotic dSi concentrations measured throughout the ocean floor are highly variable, and often well below the solubility of fresh $bSiO_2$ (Gallinari et al., 2002; Koning et al., 1997; McManus et al., 1995; Rabouille et al., 1997; Van Beueskom et al., 1997; Van Cappellen and Qiu, 1997a). Explanations for the lower "apparent silica solubilities" measured in marine sediments fall within two fundamental categories: a) the apparent solubility represents the solubility of aged $bSiO_2$, which is significantly lower than that of fresh material, and b) the apparent solubility represents a kinetic equilibrium between the dissolution of $bSiO_2$ and the re-precipitation of authigenic silicate phases. Distinguishing between the two mechanisms is not at all straightforward. Experimental evidence, however, suggest that both mechanisms may be important (Dixit et al., 2001; Van Cappellen et al., 2002b; Van Cappellen and Qiu, 1997a; Van Cappellen and Qiu, 1997b).

Interactions between $bSiO_2$ and dissolved pore water aluminum (Al) have been proposed as an alternative diagenetic pathway, which leads to the formation of smectites and zeolites rather than opal-CT (Van Bennekom et al., 1989). Experimental evidence indicates that structural incorporation of Al (Gehlen et al., 2002) in the silica framework decreases the apparent solubility (Dixit et al., 2001) and reactivity (Van Cappellen et al., 2002b) of $bSiO_2$. In the open ocean, Al incorporation into $bSiO_2$ takes place at the seafloor, where Al is supplied by the slow dissolution of deposited lithogenic aluminosilicate minerals. Batch experiments with mixtures of diatomaceous silica and kaolinite or ground basalt lead to the conclusion that the increase in availability of dissolved Al ultimately results in the formation of authigenic aluminosilicate minerals (Dixit et al., 2001). The formation of authigenic aluminosilicate minerals from dSi produced by the dissolution of $bSiO_2$ may constitute a largely overlooked sink of silicon in the ocean. According to a recent estimate this sink may account for 11% of the total marine burial of reactive Si (Laruelle et al., 2008).

1.4 Biogenic silica transformation along the land-ocean continuum

Global scale studies have focused mainly on the oceanic biogeochemical cycle of Si (DeMaster, 2002; Ragueneau et al., 2000; Tréguer et al., 1995). Fixation of $bSiO_2$ by plants and aquatic organisms on the continents, however, has been proposed to be of similar magnitude as that by marine diatoms (Conley, 2002). Because of the large $bSiO_2$ production on land and its efficient recycling compared to silicate rocks, much of the reactive Si reaching the oceans has undergone prior biological cycling on the continents. A major fraction of dSi load of the world's rivers may in fact originate from the dissolution of phytoliths and freshwater diatoms rather than directly from silicate rocks (Derry et al., 2005). Furthermore, a significant portion of the riverine load of reactive Si may be in the form of $bSiO_2$ produced on the continents (Conley, 1997). Dissolution of this $bSiO_2$ may constitute an important source of nutrient Si for nearshore environments.

Although the global significance of the biogeochemical cycle of Si on land is now recognized, the vast majority of studies on $bSiO_2$ dissolution have focused on the marine environment (Gallinari et al., 2002; Hurd, 1972; Kamatani and Riley, 1979; Kamatani et al., 1980; Lawson et al., 1978; Lewin, 1961; Rickert et al., 2002; Van Cappellen and Qiu, 1997b). Nevertheless it has long been suspected that salinity may play a role on the dissolution efficiency of $bSiO_2$ at the land-

ocean transition (Anderson, 1986). To this day, however, there have been no systematic studies on the differences in the dissolution kinetics of $bSiO_2$ between freshwater and marine environments (Chapter 5).

Coastal and shelf environments represent a dynamic interface between the continents and the open ocean. Although they account for only 18% of all biological fixation of Si in the oceans, almost half of all marine $bSiO_2$ burial takes place in nearshore and shelf sediments (DeMaster, 2002; Laruelle et al., 2008). These sediments are also the main recipients of particulate matter originating from the continents, especially terrigenous clays. It has long been speculated that early diagenetic interactions involving terrigenous clays may produce new, authigenic clay minerals thus creating a sink for reactive Si but also for a number of other elements (the reverse weathering hypothesis, Mackenzie and Garrels, 1966). Available data indicate a close link between the precipitation of authigenic clays and the presence of $bSiO_2$, in which the latter provides not only the reactant (dSi), but also acts as a substrate for new mineral formation.

Although direct observation of reverse weathering reactions are limited to the sediments of the Mississippi and Amazon Deltas (Michalopoulos and Aller, 1995; Michalopoulos and Aller, 2004; Michalopoulos et al., 2000; Presti and Michalopoulos, 2008), early diagenetic processes altering $bSiO_2$ have also been invoked to explain variations in asymptotic pore water dSi concentrations and benthic dSi fluxes in the deep ocean (Dixit and Van Cappellen, 2003; King et al., 2000; McManus et al., 1995; Ragueneau et al., 2001). New evidence presented in this thesis (Chapter 6) shows that interactions between $bSiO_2$, seawater, and terrigenous minerals may be an ocean-wide phenomenon, whose role in the marine biogeochemical cycle of Si needs to be addressed.

1.5 Thesis outline

This thesis focuses on the biogeochemical processes, physicochemical variables (salinity, pH, and pressure) and material properties that affect the recycling efficiency of biogenic silica, in the water column, in marine sediments and along the land to ocean continuum. It provides an overview of the current knowledge on the subject, and presents novel findings based on laboratory and field experiments.

Chapter 2 is a review of the processes involved in determining the fate of $bSiO_2$ in the ocean. The first part of the chapter deals with processes that take place during, and shortly following, the life cycle of diatoms. Parameters known to affect the silicification of diatom frustules during biomineralization are briefly discussed. The important role of bacteria in initiating the chemical dissolution of $bSiO_2$ in the water column is highlighted, as well as those of aggregation and grazing. The second part of the chapter focuses on the geochemical aspects of $bSiO_2$ dissolution. It provides the theoretical background for the dissolution process and discusses different factors known to affect the dissolution kinetics and solubility of $bSiO_2$. Finally, the geochemical processes taking place in the water column during sinking, and in the sediments after deposition are reviewed.

Chapter 3 investigates the effect of pressure on the solubility of silica frustules of diatoms grown in laboratory cultures. The solubility experiments were performed in the laboratory using specially designed pressurized reactors. In addition, batch reactors were deployed at sea along mooring lines for 2 years. This chapter provides the first direct experimental evidence of the dependence of natural $bSiO_2$ solubility on pressure within the pressure range of 0-700 bar.

In **Chapter 4**, the acid-base properties of a range of marine and continental biosiliceous materials are investigated. We present an improved titration procedure, capable of producing accurate determinations of the build-up of electrical charge, which eliminates artifacts due to dissolution. The results of the acid-base titrations are interpreted using an equilibrium surface complexation model. The large variability in acid-base properties among the biosiliceous materials is explained by the existence of two pools of ionizable sites, at the surface and inside the $bSiO_2$ particle.

Chapter 5 focuses on the dissolution kinetics of $bSiO_2$ along a salinity and pH gradient representative of the estuarine freshwater to seawater transition zone. Based on a series of flow-through reactor experiments, we demonstrate that salinity and pH have significant effects on the dissolution kinetics of a range of biosiliceous materials. The faster dissolution kinetics in seawater compared to freshwater imply that the large amounts of continental $bSiO_2$ supplied by rivers could be an important, and so far overlooked, source of nutrients in coastal marine environments.

In **Chapter 6** we present results from long term laboratory and field incubations aimed to simulate diagenetic interactions between cultured diatom frustules, seawater and terrigenous clay-rich sediments. Based on chemical analyses (ICPMS) and microscopic observations (TEM/EDX) we present evidence of authigenic mineral formation and chemical alteration of the diatom frustules on the time scale of 1-2 years.

CHAPTER 2

Controls on the recycling and preservation of biogenic silica in the ocean: Biomineralization, settling and burial

Loucaides S., Roubeix V., Moriceau B., Van Cappellen P., Ragueneau O.

Manuscript in preparation

Abstract

The recycling of biogenic silica ($bSiO_2$) produced by diatoms is a vital process sustaining a significant fraction of primary production in the oceans. The efficiency with which $bSiO_2$ dissolves controls the availability of nutrient silicon in the water column, and modulates the export of organic carbon to the deep sea. Environmental conditions during biomineralization (temperature, nutrient availability, light, etc.) affect the silicification and weathering resistance of diatom frustules, while ecosystem processes, including grazing and aggregation, are determining factors for the recycling of $bSiO_2$ in the water column. Bacterial colonization of dead diatoms leads to the decomposition of the protective organic layers allowing for the dissolution of $bSiO_2$ to begin.

The dissolution rate of diatom frustules is a function of the physicochemical properties of both the silica (e.g., specific surface area, degree of hydration and condensation, impurities) and the aqueous medium (e.g., temperature, pH, pressure, electrolyte composition). In sediments, the dissolution of $bSiO_2$ is controlled by the presence of lithogenic minerals, aging processes and the build up of dSi in the pore waters. In particular, interactions between lithogenic silicate minerals and $bSiO_2$ may initiate rapid diagenetic alterations that favor the preservation of $bSiO_2$.

2.1 The oceanic Si cycle

The recycling of biogenic silica ($bSiO_2$) is a key biogeochemical process controlling the availability of nutrient Si in the global ocean (DeMaster, 1981; Ragueneau et al., 2000; Tréguer et al., 1995). Dissolved silicate (dSi) sustains a significant fraction of the oceanic primary production, which is carried out by diatoms (Nelson et al., 1995). Because of the close coupling between the Si and C cycles, substantial research has been conducted during the last few decades in order to better understand the biogeochemical cycling of Si in both aquatic and terrestrial environments (Conley, 2002; Ragueneau et al., 2006; Ragueneau et al., 2000).

The coupling of the marine Si and C cycles, however, is not a simple one. Rates of primary and biosiliceous productivity do not always match opal accumulation rates in the underlying sediments (Pondaven et al., 2000). For example, high rates of opal accumulation are observed in the Southern Ocean, despite relatively low biosiliceous and carbon production in the region. In comparison, high $bSiO_2$ productivity in the Northern Atlantic is accompanied by almost no opal preservation in the sediments. This phenomenon, commonly referred to as the "opal paradox", indicates that

the recycling efficiency of $bSiO_2$ exhibits significant spatial and temporal variability (Nelson et al., 1995). Variable $bSiO_2$ preservation efficiencies present a major obstacle when reconstructing past environmental conditions using sedimentary records (Abelmann et al., 1988; Barker, 1992; Koning et al., 2001; Lotter et al., 1997; McManus et al., 1995; Ragueneau et al., 2000; Rocha, 2006; Ryves et al., 2001).

Field studies and laboratory experiments have greatly advanced our understanding of how ecosystem processes, material properties and environmental conditions affect the recycling and preservation of $bSiO_2$ in the oceans and in terrestrial environments. The purpose of this chapter is to review some key facts about $bSiO_2$ dissolution in natural environments. Emphasis will be given to the dissolution of diatom frustules in the water column and the sediments of the ocean (Fig. 2.1).

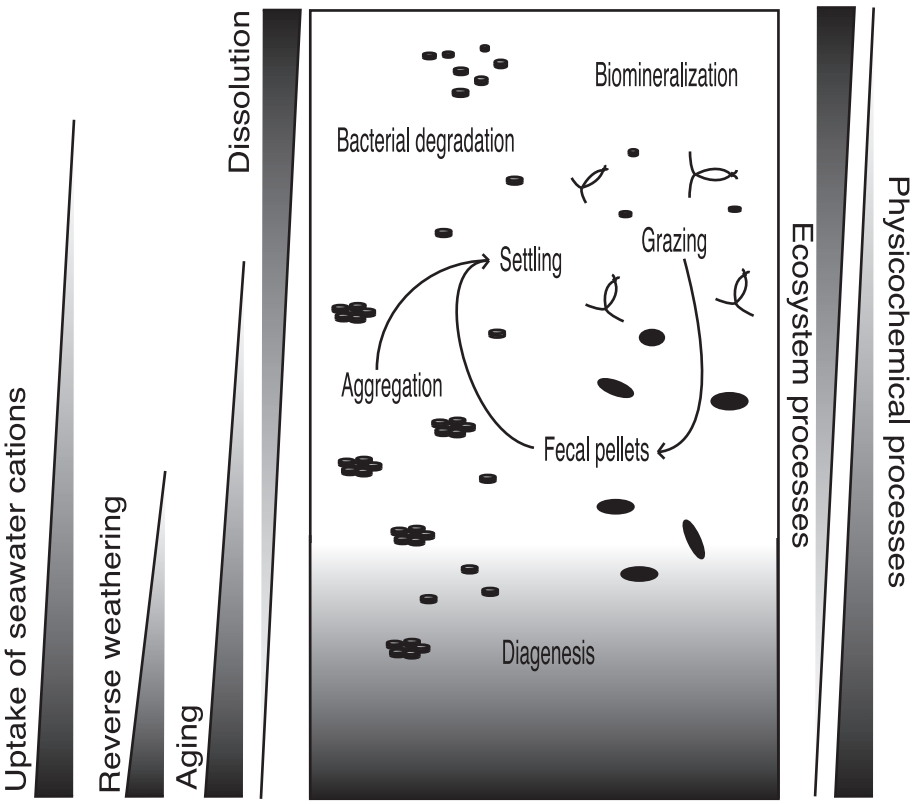

Figure 2.1 Schematic of the physicochemical and ecosystem processes that control the recycling efficiency of $bSiO_2$ from the surface waters to the bottom sediments. Several ecosystem processes are predominant in the upper water column while physicochemical forcings prevail in the sediments through the interaction of $bSiO_2$ with other mineral phases.

2.2 Biomineralization and the weathering resistance of diatom frustules

2.2.1 Cell growth and silicification

The rate at which $bSiO_2$ dissolves is in a large measure dependent on the intrinsic physicochemical properties of the amorphous silica material produced during biosynthesis. Genetic variations in diatom frustule silicification and morphology help explain the large variability in dissolution efficiency between different diatom species. Laboratory dissolution experiments have shown that the half life of diatom frustule counts (i.e. the time required for the number of frustules of a given species to decline by 50%) can vary by up to 30 orders of magnitude between different taxa (Ryves et al., 2001).

Frustule silicification can also vary significantly within the same diatom species. Studies indicate that the degree of silicification is a function of the cellular growth rate, and the ambient dSi concentration during biosynthesis (Martin-Jezequel et al., 2000). While during periods of Si limitation diatoms are able to maintain their division rates (Brzezinski et al., 1990; Nelson and Dortch, 1996; Paasche, 1973), they are forced to build less silicified frustules (Martin-Jezequel et al., 2000 and references therein). When Si is not limited, however, the degree of silicification is only a function of the cellular growth rate. Longer cell cycles during slow growth, allow for maximum uptake of dSi by diatoms while the contrary occurs during rapid growth.

Chaquin et al. (2002) monitored the growth rates and $bSiO_2$ content of diatoms (*Thalassiosira pseudonana*) cultured under light, nitrogen, and phosphorous limitation. They observed that the

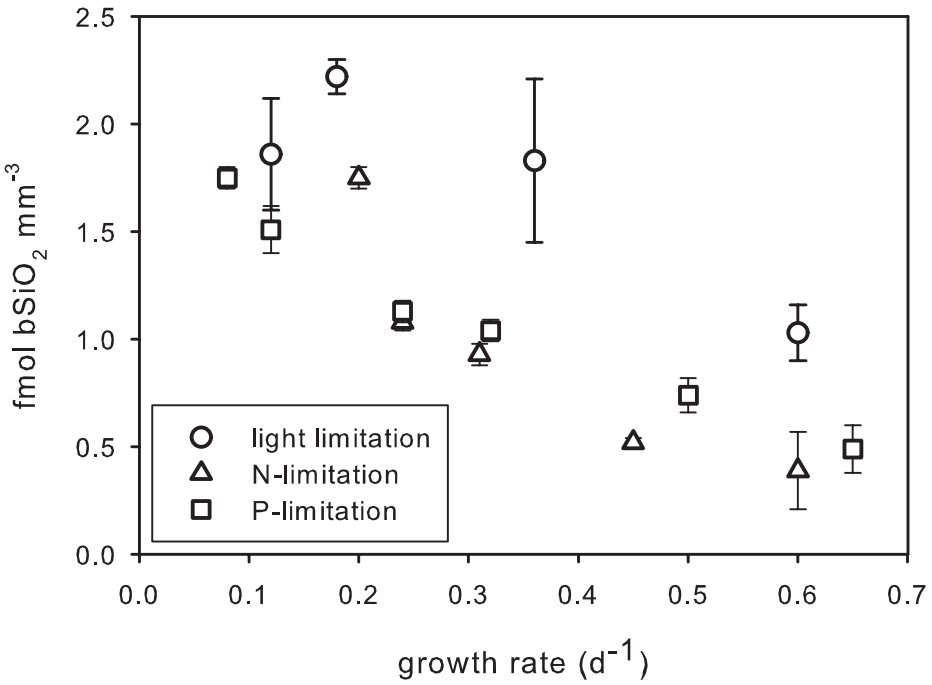

Figure 2.2 Change in the cellular $bSiO_2$ content of cultured diatoms (*Thalassiosira pseudonana*), normalized by cell volume, as a function of growth rate. The y-axis ultimately represents the thickness of the diatom frustules which decreases at faster growth rates. The diatoms were cultured under either light, nitrogen, or phosphorous limitation (Data from Claquin et al., (2002)).

$bSiO_2$ content of the cells decreased with increasing growth rates (Fig. 2.2), while the volume of the cells remained practically constant. Their results confirm that faster growth rates force diatoms to built thinner frustules. The growth rate of diatoms is a function of several environmental parameters, including light intensity (Davis, 1976; Taylor, 1985), temperature (Durbin, 1977; Paasche, 1980), and nutrient availability (Harrison et al., 1976; Harrison et al., 1977; Martin-Jezequel et al., 2000), therefore, these parameters indirectly control the silicification and weathering resistance of diatom frustules.

Marine environments tend to be more Si-limited than continental aquatic ecosystems. This may be one reason why marine diatoms exhibit up to one order of magnitude less silica mass per cell than freshwater diatoms, although different adaptation mechanisms between freshwater and marine species may also play a role (Conley and Kilham, 1989). Less silicified marine diatoms have higher buoyancy allowing them to stay longer in the photic zone. Sinking below the photic zone can be a fatal journey for marine diatoms, but in lacustrine environments resuspension and vertical mixing can lift the diatoms back to the photic zone after sinking into the hypolimnion. River environments are also more energetic, so positive buoyancy may not be as critical.

Although freshwater usually contains higher dSi concentrations, lower salinities may have a negative effect on the growth rate of diatoms (Vrieling et al., 1999b). Lower growth rates along with higher dSi levels could then partly explain why freshwater diatoms accumulate more silica per cell than their marine relatives. The effects of salinity on frustule micromorphology and architecture has been further investigated by Vrieling et al., (2000) using small and wide angle X-Ray scattering techniques. They found that diatom frustules grown in lower salinity medium exhibit smaller pores than diatoms grown in seawater.

The dissolution rate of diatom frustules is directly proportional to the surface area of the interface between the $bSiO_2$ and the solvent (water). The shape, weight, and morphology of a diatom frustule, define its specific surface area (SSA), which is equal to the ratio between the surface area and mass of the frustule. The SSA can also be a measure of the degree of silicification of diatom frustules. For a dissolving diatom frustule this property determines its recycling efficiency. For instance, diatom frustules of identical mass dissolve in rates that are proportional to their surface area (Van Cappellen et al., 2002b). Therefore, frustules with low specific surface area generally sink deeper into the water column before they completely dissolve.

Because of their complex surface morphology, diatom frustules are characterized by relatively large specific surface areas that can vary between species by as much as one order of magnitude, typically between 20 to 200 $m^2\ g^{-1}$ (Dixit et al., 2001). Due to the intricate surface morphology of diatom frustules, their true exposed surface area (as measured by gas absorption techniques) can often be orders of magnitude larger than the geometric surface area derived from the size of the frustule. Although evidence suggests that the geometric surface area of diatom frustules may vary depending on growth conditions (Brzezinski, 1985; Claquin et al., 2002; Martin-Jezequel et al., 2000), there is still a lack of knowledge on how the "true" surface area is affected. Spectroscopic evidence, however, suggest that the shape and size of micropores in diatom frustules is influenced by environmental conditions during biomineralization (Vrieling et al., 2000).

The production of less silicified frustules during non-limiting conditions has a negative impact on the $bSiO_2$ export but also the carbon export to the deep ocean. Diatoms grown during limiting conditions are more effective silicon and carbon exporters, and tend to predominate in the sedimentary record (Kemp et al., 2006; Kemp et al., 2000; Smetacek, 2000). On the contrary, the export of carbon during non-limiting conditions (i.e. algal blooms) may not be as significant

as previously thought, because the $bSiO_2$ and organic carbon are efficiently recycled within the upper ocean.

2.2.2 Aluminum incorporation during biomineralization

Diatoms may provide an important link between the marine silicon and aluminum cycles, by controlling the availability of dissolved Al in the surface ocean (Mackenzie et al., 1978). Although the exact role Al plays in the biological functioning of diatoms remains unclear, the assimilation of Al by diatoms seems to affect the development of diatom communities, as well as the physiology of individual cells (Gensemer, 1990; Menzel et al., 1963; Stoffyn, 1979; Vrieling et al., 2000). Culture studies show that Al has a limiting effect on the dSi assimilation by diatoms, although it has no effect on their division rates (Stoffyn, 1979). This suggests that Al availability enhances the silicification of diatom frustules (Gensemer, 1990) without, however, affecting their growth rates.

Aluminum incorporation into amorphous silica is known to reduce silica solubility and dissolution rates (Van Cappellen et al., 2002a; 2002b). However, even when diatoms are grown in Al-rich media the Al content of the diatom frustules does not exceed 0.8% (Van Beusekom, 1989; Vrieling et al., 1999a). In marine waters where Al concentrations are generally low (<0.1μM) Al:Si atomic ratios of diatom frustules remain well below 10^{-4} (Van Bennekom et al., 1991). These levels are generally too low to significantly affect dissolution kinetics or the solubility of diatom frustules (Van Cappellen et al., 2002b).

2.3 Early post-mortem processes: Si-C interactions

2.3.1 Organic coatings and bacteria

During the lifetime of a diatom, its frustule resists dissolution due to the presence of an external organic coating composed mainly of proteins and structural carbohydrates (Hecky et al., 1973). The protective role of the organic coating has been demonstrated experimentally. Diatom frustules, from which the organic matter has been removed, dissolve faster than frustules with the organic layer intact (Bidle and Azam, 2001; Kamatani and Riley, 1979; Rickert et al., 2002). After diatoms die, the organic layer is decomposed by bacteria and dissolution of the exposed silica can no longer be avoided (Bidle and Azam, 2001; Patrick and Holding, 1985). In shallow environments, due to the relatively short time frustules remain suspended, the bacterial-mediated destruction of the organic coating may be the limiting step in the recycling of $bSiO_2$.

Bacteria decompose the organic matter of diatom cells by producing proteases. The importance of bacterial proteases for the dissolution of fresh diatoms has been illustrated by Bidle and Azam (1999, 2001). They showed that the dissolution of diatom detritus was faster after addition of bacterial proteases under axenic conditions, and strongly reduced by the addition of protease inhibitors in the presence of bacteria. Moreover during the biodegradation of diatom detritus by bacteria, the bacterial ectoprotease activity was highest, compared to other enzymatic activity, and it correlated with the $bSiO_2$ dissolution rates. Particularly during the first days of diatom biodegradation, protease were found most active in detaching serin and glycin residues, the two most abundant amino acids in the organic coatings of diatoms (Hecky et al., 1973). Dense colonization by bacteria of the surface of diatom frustules may lead to the formation of microenvironments characterized by high concentrations of bacterial ectoenzymes which increase the decomposition of the organic coatings (Bidle and Azam, 1999).

The impact of bacteria on $bSiO_2$ dissolution likely depends on the nature of the bacterial community present in close proximity to the diatom cells, and on the environmental conditions controlling bacterial activity (e.g. temperature and nutrient availability). Species composition, ectoprotease profile, colonization dynamics, and the aggregating effect on diatom detritus are all ways by which the bacterial assemblage can modulate $bSiO_2$ dissolution (Bidle and Azam, 2001). In addition, the effects of various metabolic products accumulating in the bacterial microenvironment around diatom frustules on the dissolution of $bSiO_2$ still remain to be fully characterized (Roubeix et al., 2008).

2.3.2 Aggregation

Although aggregation seems to occur mainly under nutrient limiting conditions (Corzo et al., 2000; Drapeau et al., 1994), the processes controlling diatom aggregation are yet to be fully unraveled. What seems clear, however, is that diatoms can excrete polysaccharides that, after partial dissolution, become so-called transparent exopolymer particles (TEP) (Passow, 2002; Passow et al., 2003). This gel-like substance favors the cohesion between diatom cells after they collide, which then triggers diatom aggregation. Experimental observations indicate that grazing pressure (Malej and Harris, 1993), nutrient availability (Corzo et al., 2000; Drapeau et al., 1994), light intensity (Staats et al., 2000), and the presence of bacteria (Passow et al., 2001), affect TEP concentrations and adhesivity, which in turn control aggregation rates.

Aggregation influences the balance between recycling and preservation of $bSiO_2$ as aggregated diatoms sink faster (Alldredge and Gotschalk, 1988; Alldredge and Silver, 1988) than free suspended cells, leaving less time for dissolution. Furthermore, diatoms in aggregates also dissolve slower than free suspended cells (Moriceau et al., 2007). The decrease of the dissolution rate is due in part to the higher internal dSi concentrations inside the aggregates, but also to the higher proportion of diatom cells that remain alive in the aggregates. Other factors could play a role in retarding dissolution. For example, the pH inside aggregates has been shown to be lower (pH ~7) than typical seawater pH, possibly due to the respiratory activity of diatoms and bacteria (Alldredge and Cohen, 1987). (The effect of pH on $bSiO_2$ dissolution kinetics is described in section 5.3.2.) Bacterial densities and activities can also be higher in aggregates (Alldredge et al., 1990; Simon et al., 2002). Degradation of the organic coatings of diatom cells could then be controlled by the relative nutritional values of TEP and coatings to the bacteria.

2.3.3 Grazing and fecal pellets

Diatoms are at the basis of the oceanic food web, and the most important food source for zooplankton. For diatoms, the silica frustule does not only provide support and rigidity to the cells but also provides some protection against small grazers (Hamm et al., 2003). Even though once ingested most diatom frustules break, some remain intact even when the internal carbon has been digested (Turner et al., 2002), while some diatoms can even make it out of zooplankton guts alive (Fowler and Fisher, 1983; Platt et al., 1983).

Zooplankton fecal pellets can sink at rates of up to 2000-3000 m d^{-1} (Turner et al., 2002). Contrarily to aggregates, fecal pellets are very robust particles that cannot be easily destroyed. When diatoms are embedded into large fecal pellets they are essentially protected from dissolution mainly due to reduced contact between the $bSiO_2$ and seawater. Dissolution rates of $bSiO_2$ inside fecal pellets can be 2 to 10 times lower than dissolution rates of freely suspended diatoms (Schultes, 2004). Fecal pellets, however, are also subject to grazing by coprophages who can destroy the pellets and retrieve the broken diatom frustules. In that case the $bSiO_2$ dissolution rate increases

(Schultes, 2004). Grazing of freely suspended diatoms and aggregates also takes place at the bottom of shallow marine ecosystems by benthic organisms such as filter feeders. Silica dissolution rates measured in feces of the benthic filter feeder *Crepidula fornicata* show that $bSiO_2$ is protected from dissolution by the peritrophic membrane of the fecal pellets (Moriceau, unpublished). When the fecal pellets are destroyed the silica dissolution rates increase, because of the presence of broken frustules (and thus higher exposed surface areas) in the pellets (Moriceau et al., 2007).

2.4 Geochemical water column processes

2.4.1 Theoretical background

The process of silica dissolution, being of great interest to both material scientists and geochemists, has been studied extensively (Dove and Crerar, 1990; Heaney, 1994; Iler, 1979; Lasaga and Gibbs, 1990; Van Cappellen et al., 2002a). It is generally accepted that the dissolution of silica polymorphs is driven by the hydrolysis of the mineral surface through nucleophilic attack of water dipoles on the siloxane (>Si-O-Si<) bonds of the SiO_2 network. Water molecules orient their electronegative oxygen towards the Si atom, leading to a transfer of electron density to the siloxane bonds, thereby increasing their length and eventually breaking them. A series of such reactions leads to the release of hydrated Si atoms in the form of silicic acid, H_4SiO_4 (Dove and Crerar, 1990).

The general phenomenological rate expression for surface-controlled dissolution of silica is (Van Cappellen et al., 2002a):

$$R = \frac{1}{[bSiO_2]} \frac{d[H_4SiO_4]}{dt} = k_o \cdot g \cdot A_s \cdot f(\Omega) \tag{1}$$

where $[bSiO_2]$ is the mass of $bSiO_2$ per unit volume solution, k_0 is the rate coefficient, expressed in units of mass Si per unit surface area $bSiO_2$ per unit time, and is a measure of the intrinsic reactivity of the mineral surface depending primarily on the nature of the solid and temperature. The reactive surface area A_s is expressed in units of surface area per mass of solid, and is equal to the specific surface area S of the solid, in units of surface area per mass of solid, times the dimensionless term γ that represents the roughness of the surface:

$$A_S = \gamma \cdot S \tag{2}$$

The term g in Eqn. 1 is a dimensionless factor that accounts for all the solution-induced changes in the reactivity of the silica surface. In particular, g is a function of the pH and background electrolyte composition of the aqueous medium (see below).

The dissolution of silica is thermodynamically driven by the degree of undersaturation expressed as Ω in Eqn. 1. The degree of undersaturation Ω depends on the ratio between the concentration of dSi in solution (C) and the equilibrium solubility C_{eq} of the reacting solid according to:

$$\Omega = 1 - \frac{C}{C_{eq}} \tag{3}$$

The degree of undersaturation varies from a maximum value of 1 ($C = 0$) to a value of 0 for ($C = C_{eq}$), when the silica solid-aqueous solution reaches equilibrium. An important constraint on the function f in Eqn. 1 is that $f(\Omega)=0$ when $C=C_{eq}$. At $C > C_{eq}$, precipitation takes over and R represents the rate of silica precipitation.

The dissolution of biogenic silica is most commonly expressed by a linear relationship in which the dissolution rate R is linearly dependent on the degree of silica understaturation according to:

$$R = k\left(1 - \frac{C}{C_{eq}}\right) \tag{4}$$

where k is related to k_0 in Eqn. 1 according to Eqn. 5:

$$k = k_0 \cdot g \cdot A_S \tag{5}$$

The linear dissolution rate law, as expressed in Eqn. 4, has been justified on the basis of transition state theory (Rimstidt and Barnes, 1980; Van Cappellen and Qiu, 1997b). A discussion of this justification can be found in Van Cappellen et al. (2002a). Note, however, that because mineral dissolution is a complex multi-step process there is no *a priori* reason why the linear rate law should hold.

The empirical (Arrhenius) activation energy of biogenic silica dissolution is in the order of 60 kJ mol^{-1}, which is in the same range as those reported for dissolution of synthetic amorphous silica, quartz and cristobalite (Renders et al., 1995). These relatively high activation energies support a rate-limiting step controlled by the breaking of (strong) siloxane bonds at the solid to solution interface.

2.4.2 Measuring dissolution rates

In situ dissolution rates of $bSiO_2$ have been measured or estimated in various ways. For water column samples, Si isotopic tracer incubations provide the most direct rate determinations (Nelson and Brzezinski, 1997). Alternatively, mass balance calculations using concentration distributions of silicic acid and $bSiO_2$, or particulate settling fluxes during sediment trap deployments can yield estimates of net silica dissolution rates (Koning et al., 1997). In marine sediments, dissolution rates of $bSiO_2$ can be estimated from the net efflux of silicic acid from the sediments measured using benthic chambers (Jahnke and Jahnke, 2000; McManus et al., 1995), or derived from pore water dSi concentration gradients at the sediment-water interface (Dixit and Van Cappellen, 2003). Here we mainly concentrate on laboratory techniques used for measuring dissolution kinetics of $bSiO_2$.

2.4.2.1 Batch experiments

In the laboratory, dissolution rates of $bSiO_2$ have been measured under controlled conditions in closed or flow-through systems. Closed system or so-called batch reactor experiments have been most commonly used mainly due to their simplicity. Typically, a sample of siliceous material is suspended in a solution which initially contains no silicic acid. The concentration of silicic acid in the solution is then monitored until the concentration of dSi no longer changes with time. The final, steady dSi concentration is then usually assumed to represent the solubility of the dissolving $bSiO_2$.

Fig. 2.3a illustrates the evolution of dSi over time in two batch dissolution experiments with cultured diatom frustules (*Thalassiosira punctigera*) and a Pliocene age marine biosiliceous ooze

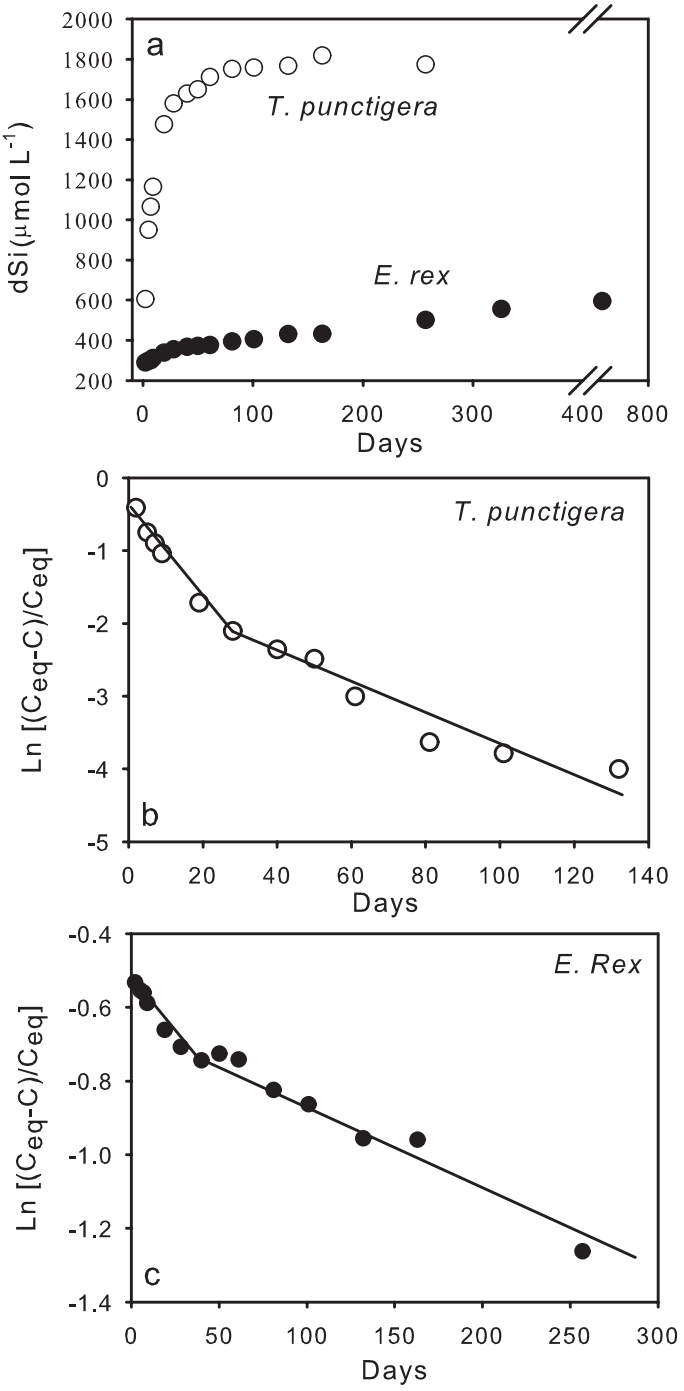

Figure 2.3 Dissolution data from two batch dissolution experiments with clean (organic matter removed) diatom frustules from cultures (*T. punctigera*), and diatomaceous ooze from the S. Ocean (*E. rex*), performed in 0.1mol L^{-1} NaCl at 25°C. The initial dSi concentration was 300µM. a) Build-up of dSi over time in the batch reactors. b & c) The same data plotted on log-linear plots where the slope of the line is equal to: $-(k \bullet [bSiO_2])/(C_{eq} \bullet V)$. Note that at high undersaturation, the kinetics deviate from the simple first order rate law.

sample, respectively. The ooze sample was obtained from a core from the Weddell Sea, within a layer consisting nearly exclusively of fragments of frustules from the diatom species *Ethmodiscus rex*. The difference in dissolution kinetics and solubility between the two biogenic silicas, under otherwise identical experimental conditions, demonstrates the dependence on the intrinsic material and surface properties of the different samples.

If the linear dissolution rate law holds (Eqn. 4), and provided that only a negligible fraction of the initial mass of $bSiO_2$ dissolves during the experiment, then the data should define a straight line when plotted on a log-linear plot, with a slope equal to $-(k \cdot [bSiO_2])/(C_{eq} \cdot V)$. The data shown in Fig. 2.3, however, cannot be fitted by a single rate constant k; rather, there is an initial stage of dissolution characterized by a higher apparent rate constant. This phenomenon has been described in several previous studies (Greenwood et al., 2001; Hurd and Birdwhistell, 1983; Kamatani, 1982; Kamatani and Riley, 1979; Kamatani et al., 1980; Tréguer et al., 1988; Van Cappellen et al., 2002b).

Hurd (1979) and Kamatani (1980) suggested that the deviation from linear kinetics at high degrees of undersaturation may represent the faster dissolution of a more reactive silica phase that is part of the frustule. A recent study presented a model demonstrating close fits to experimental dissolution data by assuming two separate silica phases of different reactivity with surfaces that exponentially decrease during dissolution (Truesdale et al., 2005). Using this model dissolution data are fitted by adjusting the ratio between the two $bSiO_2$ phases and the reactivity of each phase. To our knowledge, however, there is no direct evidence to suggest that the surface area of diatom frustules declines exponentially during dissolution, or that diatoms contain distinct $bSiO_2$ phases.

In fact, the faster initial dissolution kinetics are not only observed with "fresh" diatom frustules. The dissolution curve of the 5 m.y. old diatom ooze sample from the Southern Ocean (Fig. 2.3c) shows a similar change in slope in the log-linear plot. Scanning Electron Microscope (SEM) images show that the *E. rex* frustules that make up the diatomite have undergone a great deal of dissolution. All frustules are fragmented and most of the finer architecture has disappeared. If a more reactive silica phase once existed in the original frustules, it should have dissolved away long ago.

The two-stage dissolution kinetics are also observed with synthetic amorphous silica (Fig. 2.4). The solid used, Aerosil® OX50, is a well-characterized, single phase synthetic silica, of high physical uniformity and chemical purity. The high-resolution data from a batch dissolution experiment with Aerosil® OX50 show a distinct change of slope, similar to that observed with $bSiO_2$ materials. These results clearly show that enhanced initial dissolution kinetics do not necessarily indicate the presence of distinct silica phases. Rather they appear to be a feature inherent to batch dissolution experiments. Possibly they reflect a change in dissolution mechanism as the degree of undersaturation decreases in the reactor with advancing dissolution.

2.4.2.2 Flow through experiments

A major drawback of batch reactor systems is that the solution composition continuously changes with time. Furthermore, the introduction of a dry sample of $bSiO_2$ in an aqueous solution causes an initial readjustment of the chemical structure of the solid, which may affect the build-up of the dSi in solution and complicate the interpretation of the dissolution curves. These drawbacks can be avoided by using flow-through reactors. The use of mixed flow-through reactors for measuring the dissolution kinetics of $bSiO_2$ was originally introduced by Van Cappellen and Qiu (1997 a, b) and since then applied by a number of others (Dixit et al., 2001; Gallinari et al., 2002; Greenwood et al., 2001; Loucaides et al., 2008; Rickert et al., 2002; Schmidt et al., 2001; Van Cappellen, 1996; Van Cappellen and Qiu, 1997a; Van Cappellen and Qiu, 1997b).

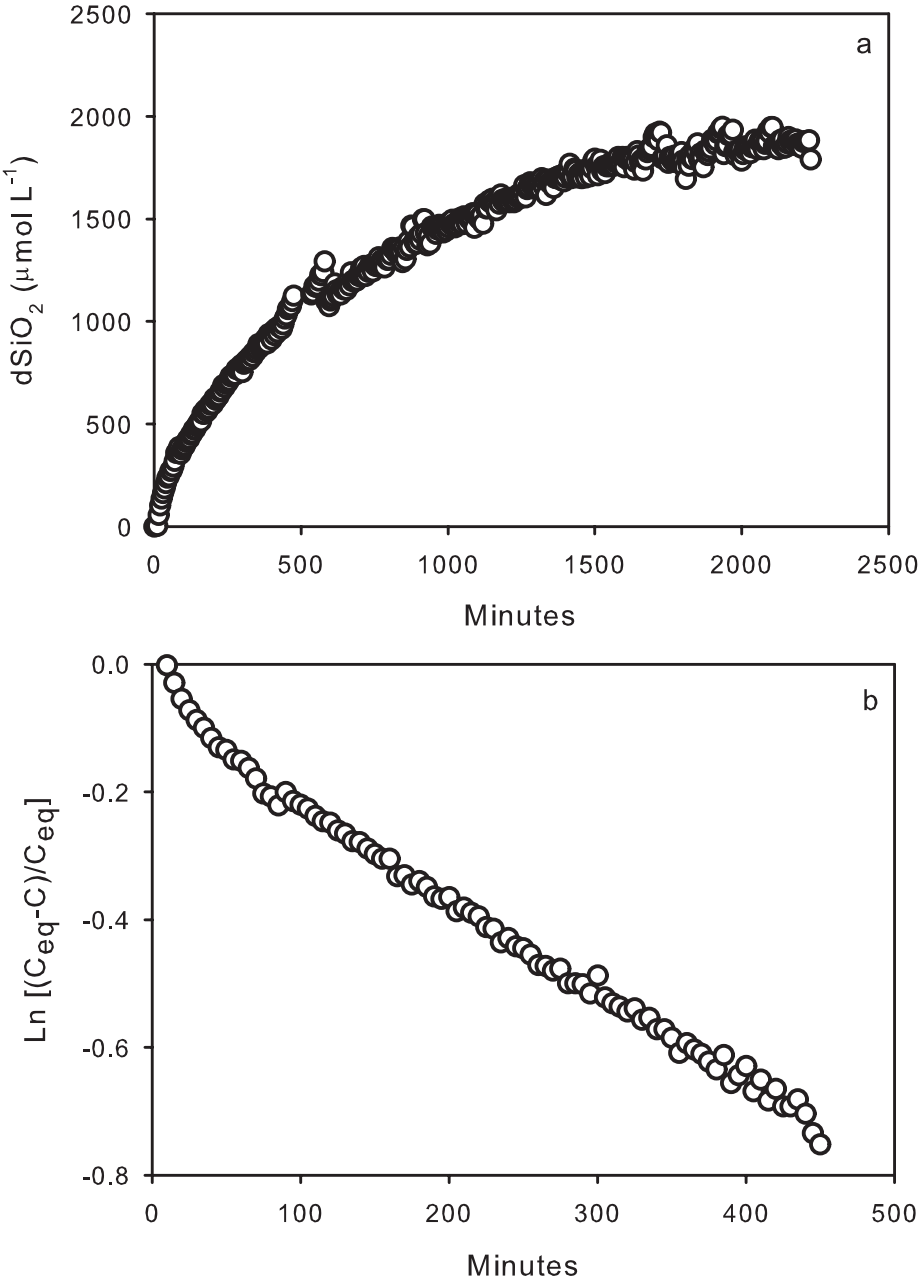

Figure 2.4 High resolution batch reactor experiment with a synthetic amorphous silica (Aerosil® OX50) in 0.1mol L^{-1} NaCl, at 25°C, and under pH-stat (pH 8). a) Buildup of dSi inside the batch reactor monitored in real time by a nutrient auto-analyzer connected online. b) The same data on a log-linear plot demonstrating the faster initial dissolution kinetics and deviation from the linear first order dissolution rate law.

The general approach consists in suspending a mass of siliceous material in the reactor cell, which is filled with solution. An input solution of known composition is then supplied at a constant flow rate to the reactor while output solution from the reactor flows out at the same rate. Filters at the inlet and outlet prevent solid material from escaping from the reactor cell. If the input dSi concentration is lower than the solubility concentration of the siliceous material in the reactor then dissolution takes place, and a higher dSi concentrations is measured in the output solution. When the output dSi concentration no longer changes (i.e. steady state is reached) the dissolution rate R is calculated as

$$R = \frac{1}{[bSiO_2]}\left(\frac{Q \cdot \Delta C}{V}\right) \tag{6}$$

where R is the steady state dissolution rate, [$bSiO_2$] is the concentration of $bSiO_2$ suspended in the reactor, Q is the volumetric flow rate through the reactor, ΔC is the difference in dSi concentration between outflow and inflow solutions, and V is the volume of the reactor cell. If both [$bSiO_2$] and ΔC are expressed in moles of Si per liter of solution, then R is the specific dissolution rate in units of inverse time. By changing the flow rate or the composition of the input solution the system is forced into a new steady state. In this manner, multiple steady states can be achieved using the same suspension of silica in the reactor.

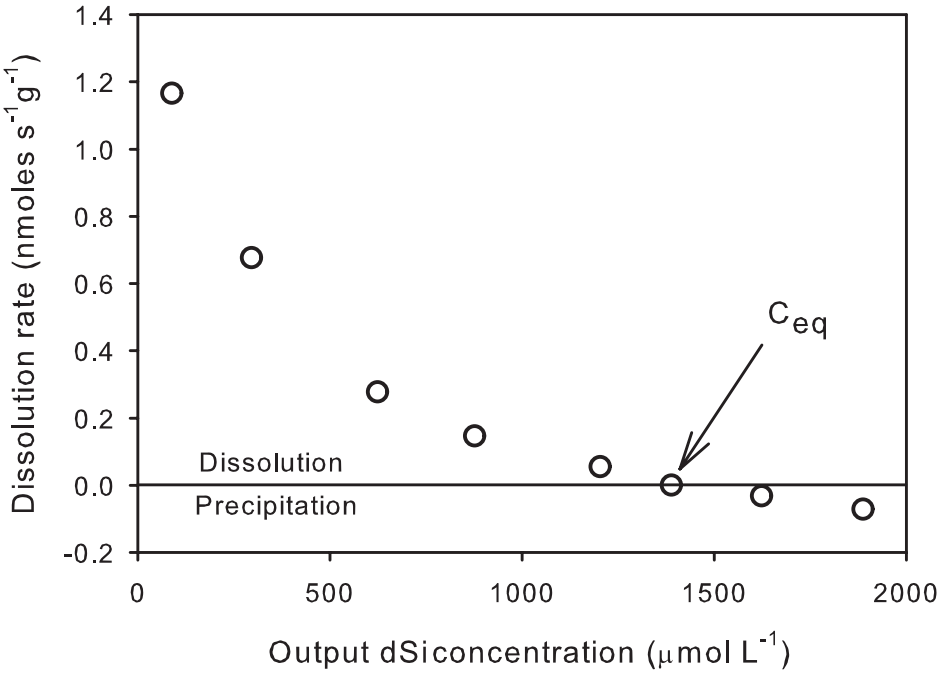

Figure 2.5 Dissolution rates of a coretop biosiliceous sediment sample from the S. Ocean measured at different background dSi concentrations in a flow-through reactor experiment by Van Cappellen and Qiu, (1997b). At dSi concentrations higher than the apparent solubility concentration of the sediment sample C_{eq}, dissolution seizes and precipitation takes over. Note that the dissolution rates don't appear to linearly depend on the degree of undersaturation as the simple first order rate law predicts.

Results of a flow-through reactor study of the dissolution kinetics of a biosiliceous ooze from the Southern Ocean is shown in Fig. 2.5. Each point in the figure represents a steady state rate reached for a particular saturation state of the solution inside the reactor. By providing both input solutions that are undersaturated and supersaturated, both rates of dissolution and precipitation can be measured. Based on the rates, the solubility of the silica sample in the reactor can then be estimated, as it corresponds to the input dSi concentration for which there is no net dissolution or precipitation (Fig. 2.5). This is a great advantage of this technique, since solubility concentrations in batch reactors may take months or years to achieve.

It can be seen in Fig. 2.5 that the dissolution rates do not correlate linearly with the degree of silica undersaturation, as predicted by the linear dissolution rate law. Because each point on Fig. 2.5 represents a dissolution rate measured at steady state, the non-linearity of the data is not due to a time-dependent change in the reactivity of $bSiO_2$. The non-linear dissolution kinetics have been interpreted to indicate a change in the reaction mechanism under variable degree of undersaturation (see Van Cappellen et al., 2002a for an in-depth discussion).

2.4.3 Environmental variables

2.4.3.1 Temperature

Temperature strongly affects both the dissolution kinetics and solubility of $bSiO_2$ (Kamatani, 1982; Kamatani and Riley, 1979; Kamatani et al., 1980; Lawson et al., 1978; Van Cappellen and Qiu, 1997a; Van Cappellen and Qiu, 1997b). Lawson et al. (1978) determined an experimental activation energy for the dissolution of natural diatom frustules in seawater of 58 kJ mol^{-1}. Kamatani (1982) reported near identical values (57-58 kJ mol^{-1}) for diatoms from cultures and natural assemblages. Dissolution rates of cultured diatom frustules (*Thalassiosira punctigera*) at 25°C, 50°C and 80°C measured in this study also yield the same activation energy of 58 kJ mol^{-1}. A number of Arrhenius activation energies reported for biogenic, synthetic and crystalline siliceous material are listed in Table 2.1. A value for the activation energy of $bSiO_2$ dissolution equal to 58 kJ mol^{-1} implies that the rate of dissolution is about 4 times slower at 4°C (average bottom ocean temperature) than it is at 21°C (average surface ocean temperature).

Table 2.1 Experimental activation energies Ea,ex for the dissolution of $bSiO_2$, synthetic amorphous silica, and quartz based on several experimental studies.

Ref.	Material	Temperature range °C	$Ea_{ex.}$ kJ mol^{-1}
1	Diatoms from cultures and natural assemblages	8-27	57-58
2	Natural diatom assemblages	7-28	58
3	Diatom culture T. punctigera	25-80	58
4	Arkansas quartz	200-300	71
5	Synthetic silica	25-250	74
6	Cristobalite	150-300	70

1. Kamatani (1982); 2. Lawson et al. (1978); 3. This study; 4. Dove and Crerar (1990); 5. Icenhower and Dove (2000); 6. Renders et al. (1995).

Because of the endothermic nature of the dissolution reaction, temperature has also a positive effect on the solubility of $bSiO_2$. Fig. 2.6 illustrates the relationship between the solubility of diatomaceous silica and temperature based on data from Lawson (1978), Kamatani and Riley (1979) and this study. The average linear relationship for all the data shown in Fig. 2.6, between 4.5˚C and 28˚C, is given by

$$C_{eq} = 23.8T + 936 \quad (6)$$

where T is the temperature in ˚C and C_{eq} is expressed in µM. This relationship predicts that a typical vertical temperature drop in the ocean from the surface (21˚C) to the bottom waters (4˚C) causes a drop in the solubility of $bSiO_2$ of over 30%.

2.4.3.2 Effect of pH

Although pH is rather constant throughout the ocean, in estuarine environments and in sediment pore waters it can vary significantly (Hurd, 1973; Jourabchi et al., 2005). As the point of zero surface charge (pH_{zpc}) of biogenic silica's ranges between 1.2-4 (Dixit and Van Cappellen, 2002; Fraysse et al., 2006b), the dissolution kinetics of $bSiO_2$ in most natural waters should increase with increasing pH. Increasing pH leads to the deprotonation of silanol groups ($> Si\text{-}OH^0 \Leftrightarrow Si\text{-}O^- + H^+$), further facilitating the breaking of bridging siloxane bonds ($>Si - O - Si<$), which are believed to be the rate limiting step of the dissolution process (Dove and Elston, 1992).

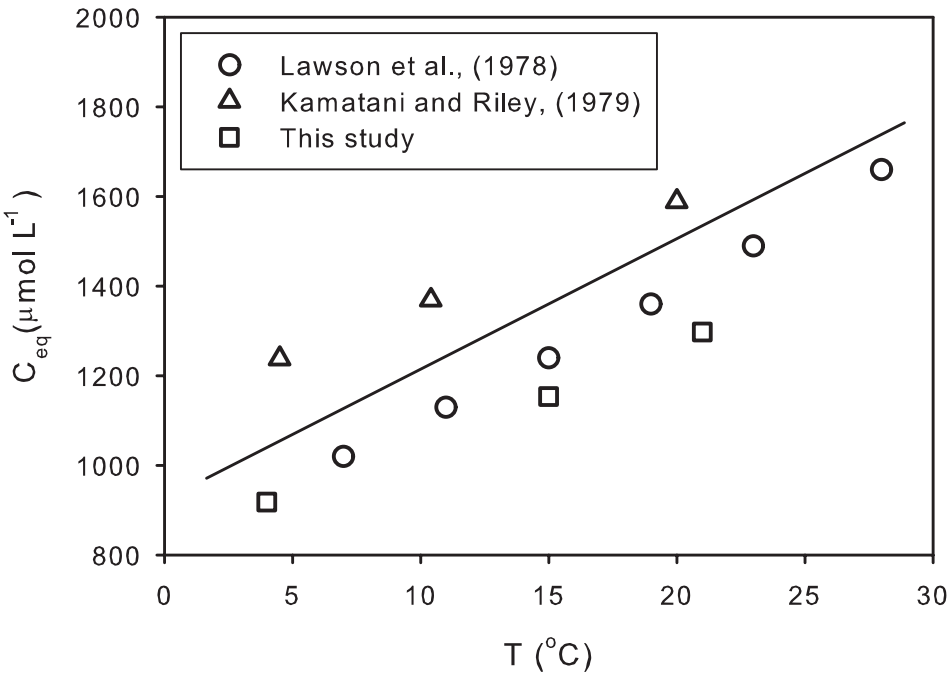

Figure 2.6 Temperature dependence of the solubility concentration C_{eq} of diatomaceous silica based on solubility measurements from Lawson et al. (1978), Kamatani and Riley, (1979) and this study. Solubilities in this study were determined in seawater using cultured diatoms (*T. punctigera*). The linear relationship is described by Eq. 6.

The catalytic effect of pH on the kinetics of silica dissolution has been demonstrated for quartz (Dove and Elston, 1992 and references therein), vitreous silica (Wirth and Gieskes, 1979), and biogenic silica (Fraysse et al., 2006a; Hurd, 1973; Loucaides et al., 2008; Van Cappellen and Qiu, 1997b). In a recent study, Loucaides et al. (2008) compared dissolution rates of a number of silica samples including phytoliths, cultured diatoms, biosiliceous lake sediments and synthetic silica, for a pH typical of seawater (pH 8.1) and an average riverwater (pH 6.3). They found that on average, dissolution rates double as pH increases from 6.3 to 8.1.

Experimentally estimating the effect of pH on the dissolution kinetics of $bSiO_2$ can be challenging since adjusting the pH of a solution usually requires the addition of a base or acid, which consequently alters the ionic speciation and electrolyte concentration of the solution. The dissolution kinetics of silica are sensitive to changes in the ionic concentration and composition of the solution (Dove and Nix, 1997; Loucaides et al., 2008), therefore special care must be taken in properly separating the dependence of dissolution kinetics on solution pH and electrolyte composition.

Solution pH has also been shown to affect the solubility of $bSiO_2$ (Hurd, 1973; Van Cappellen and Qiu, 1997a). Fig. 2.7 illustrates the dependence of $bSiO_2$ solubility on pH based on experiments by Hurd (1973) and Van Cappellen and Qiu (1997a). The latter authors found, using flow-through experiments, that the solubility of a siliceous ooze from the Southern Ocean increases by 10% between pH 6 and 8. At higher pH the effect on solubility is stronger; although in most oceanic and lacustrine environments pH values above 8.5 are uncommon. In some shallow-water ecosystems, however, benthic photosynthetic activity can lead to elevated pH values (pH>9) in the sediments.

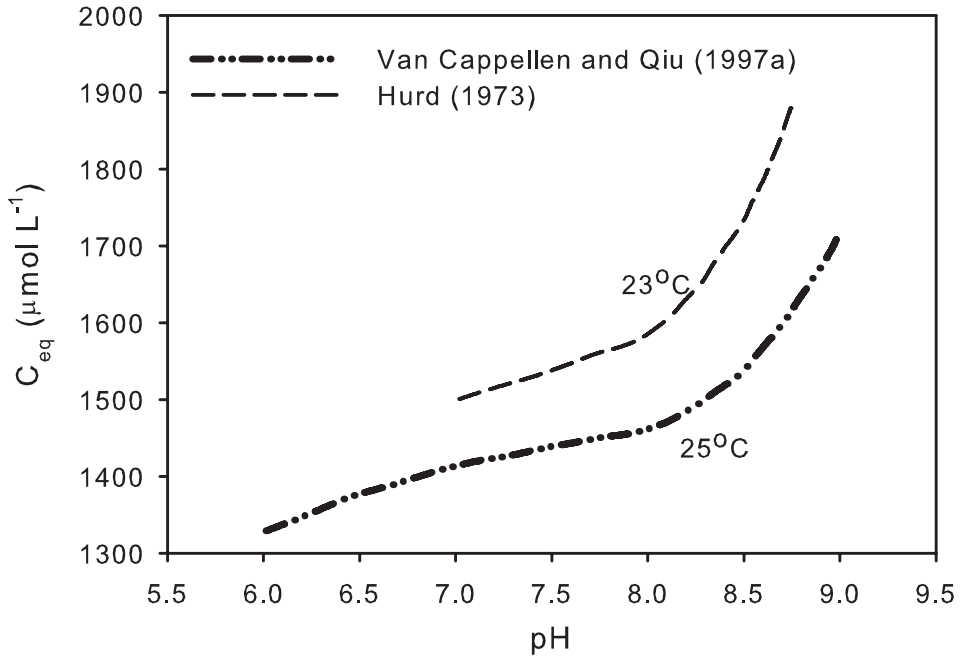

Figure 2.7 Apparent solubility concentrations C_{eq} of biosiliceous sediments from the S. Ocean and Central Equatorial Pacific as a function of pH, based on the experiments of Van Cappellen and Qiu, (1997a) and Hurd, (1973) respectively.

2.4.3.3 Pressure

The effect of pressure on the dissolution kinetics and solubility of $bSiO_2$ is of potential interest when oceanic settings are considered. To our knowledge, no experimental work has been published on the effect of pressure on the solubility and kinetics of $bSiO_2$. To this date, the pressure dependence of $bSiO_2$ solubility has been estimated based on experiments with synthetic amorphous silica (Willey, 1974).

Willey (1974) studied the solubility of amorphous silica at pressures up to 1240 bar. Her experiments showed that the solubility of synthetic silica increases with pressure. Below ~270 bar the solubility increases by ~0.70 μM bar^{-1} and between ~270 and 1240 bar by ~ 0.35 μM bar^{-1}. Willey's (1974) data suggest that the solubility at 400 bar (equivalent to an average oceanic water depth of 4000 m) is about 17% higher than at 1 bar. Recently, Koning et al. (Chapter 3) studied the solubility of diatom frustules, at pressures between 1 and 700 bar, in laboratory and field experiments. In contrast with the work of Willey (1974) their results showed that the solubility of diatom frustules decreases when pressure increases from 1 to ~200 bar. Around 200 bar, however, their data imply a reversal in the pressure dependence and a gradual increase in solubility with pressure to 700 bar. According to their results, the solubility of diatom frustule at 400 bar is about 15% higher than at atmospheric pressure. This estimate is within experimental error of that by Willey (1974).

The available data indicates that the effect of pressure on the solubility of $bSiO_2$ should not be ignored. Considering an average oceanic water depth of 4000 m, however, a typical drop in temperature of about 20°C can have a far more significant effect on solubility than an equivalent 400 bar increase in pressure. Nevertheless the anomalous dependence of $bSiO_2$ solubility on pressure suggests that further experimental work is necessary in order to understand the effect of pressure on the recycling efficiency of $bSiO_2$.

2.4.3.4 Electrolyte composition

It has been well documented that dissolution rates of quartz are significantly enhanced by the presence of alkali salts (Dove, 1999; Dove and Crerar, 1990; Dove and Elston, 1992; Dove and Nix, 1997; Kamiya and Shimokata, 1976; Van Lier et al., 1960). The exact mechanism by which the presence of these salts enhances the dissolution process is not yet fully understood. Dove (1999) proposed that the presence of alkali cations enhances the nucleophilic properties of water, thus increasing the frequency of hydrolysis attacks at the silica surface. Recently, Loucaides et al. (2008) found that the dissolution rates of a number of $bSiO_2$ samples were on average 5 times higher in seawater than in freshwater (Fig. 2.8). They also observed an increase in dissolution rates in freshwater that was augmented with alkali salts (NaCl, KCl, $MgCl_2$ and $CaCl_2$), thus confrming the catalyzing effect of alkali and earth alkali cations on silica dissolution.

The catalytic effect of salts on the dissolution of $bSiO_2$ may explain the generally more efficient recycling of $bSiO_2$ in marine environments, compared to continental aquatic environments. Furthermore it points to the need to reevaluate the role of estuaries and coastal embayments in the global $bSiO_2$ cycle. In these environments, favorable conditions lead to high biosiliceous productivity that contributes to a significant fraction of the world's $bSiO_2$ production (Lemaire et al., 2002; Ragueneau et al., 2002), while at the same time they serve as filters for $bSiO_2$ produced on land (Conley, 1997; Roubeix et al.). Salinity enhanced dissolution along the land to ocean transition zone may be an important source of nutrient Si to the global coastal ocean that has to date been underestimated.

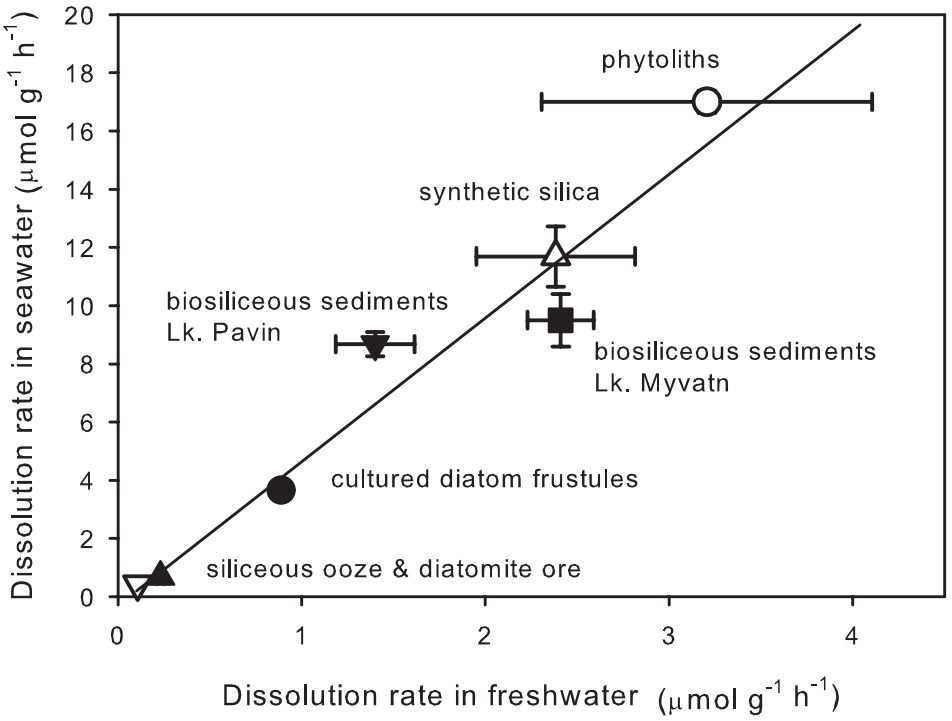

Figure 2.8 Dissolution rates in seawater versus dissolution rates in freshwater at 25°C of several siliceous materials. The strong linear relationship (r^2=0.95) indicates on average 5 times higher dissolution rates in seawater. (Figure adapted from Loucaides et al., 2008).

2.5 Below the sediment-water interface

Biogenic silica that survives dissolution in the water column is deposited at the seafloor and slowly becomes buried. Dissolution continues in the sediments leading to an efflux of dSi to the bottom waters. Typically pore water silicic acid concentrations increase downward until they level off at a quasi-constant value at depths of around 5-30 cm below the sediment-water interface (Gallinari et al., 2002; Hurd, 1973; Koning et al., 1997; McManus et al., 1995; Rabouille et al., 1997; Van Beueskom et al., 1997; Van Cappellen and Qiu, 1997a; van der Weijden and van der Weijden, 2002). This quasi-constant or asymptotic dSi concentration has often been interpreted as the equilibrium concentration of the biogenic silica buried in the sediments. This interpretation, however, poses the following problems: a) there is considerable spatial variation in the asymptotic dSi concentration between various sediments, b) the asymptotic dSi concentrations found in the sediments are well below solubility values measured directly on $bSiO_2$ (Dixit et al., 2001; Hurd and Birdwhistell, 1983; Kamatani et al., 1980; Lawson et al., 1978; Loucaides et al.,; Van Bennekom et al., 1991), and c) solubility values of $bSiO_2$ collected in sediment traps can be considerably higher than asymptotic dSi values measured in the underlying sediments (Gallinari et al., 2002). Similarly, when pore water dSi profiles are fitted to early diagenetic models, the resulting dissolution rate constants are highly variable and orders of magnitude lower than dissolution rate constants measured on cleaned biogenic opal (Boudreau, 1990; Khalil et al., 2007).

2.5.1 Opal-detrital interactions

Early diagenetic reactions involving $bSiO_2$ and lithogenic constituents in sediments have been invoked to explain the observed variations in asymptotic pore water dSi concentrations and benthic dSi fluxes in the deep and coastal ocean (Dixit and Van Cappellen, 2003; King et al., 2000; McManus et al., 1995; Michalopoulos and Aller, 2004; Presti and Michalopoulos, 2008; Ragueneau et al., 2001). Dixit et al. (2001) found that the build-up of dSi, in batch experiments where $bSiO_2$ and either kaolinite or ground basalt were suspended together in 0.7 M NaCl solution, decreased systematically as the mass ratio of the lithogenic constituent to $bSiO_2$ increased. This inverse relationship is reminiscent of that observed between the asymptotic pore water dSi concentration and the abundance of lithogenic mineral compounds, relative to that of $bSiO_2$, in deep-sea sediments of the Southern Ocean (Van Cappellen and Qiu, 1997b), the Equatorial Pacific and the North Atlantic (Gallinari et al., 2002), as well as the Atlantic sector of the Southern Ocean (King et al., 2000).

Van Cappellen and Qiu (1997a) suggested that asymptotic dSi concentrations obtained from heterogeneous samples in flow-through or batch experiments, should be treated as "apparent" saturation levels and not as the actual solubility of the biogenic fraction. Similarly in marine sediments, asymptotic porewater dSi concentrations represent weighted averages of the solubilities of the various silicate phases present.

2.5.2 Aluminum-$bSiO_2$ interactions

Previous studies dealing with variations of pore water dSi concentrations and $bSiO_2$ preservation in marine sediments have stressed the role of Al uptake by biosiliceous debris (Dixit et al.,

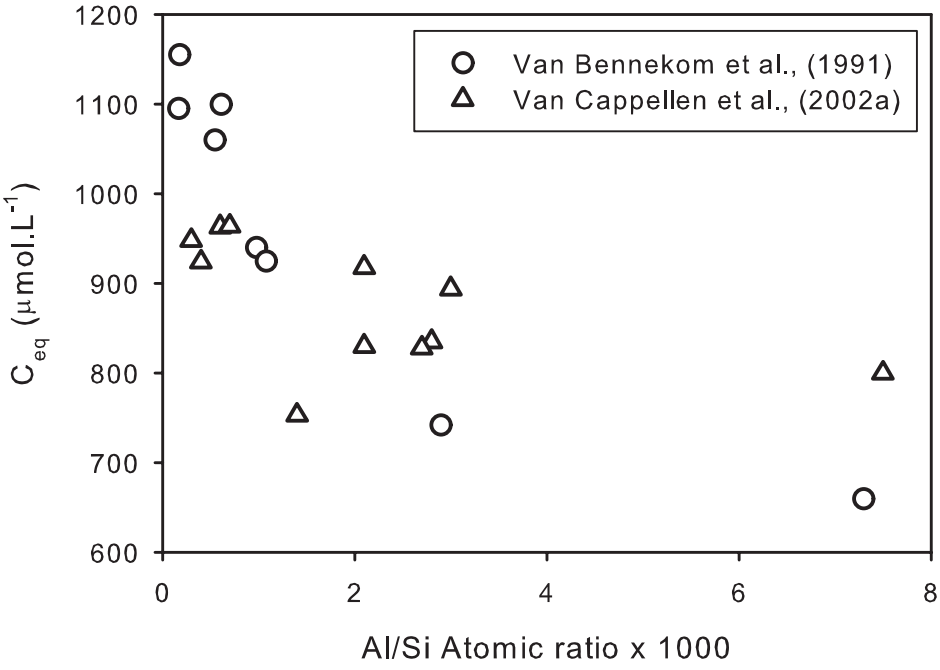

Figure 2.9 Relationship between $bSiO_2$ solubility C_{eq} and its aluminum content expressed here as the Al/Si atomic ratio. Data from Van Bennekom et al., (1991) and Van Cappellen et al., (2002a).

2001; Van Bennekom et al., 1989; Van Bennekom et al., 1991; Van Cappellen and Qiu, 1997b). Diatom frustules retrieved from Congo Fan sediments have clearly shown that $bSiO_2$ can take up significant amounts of Al during early diagenesis (Van Bennekom et al., 1989). Results from experimental studies further demonstrate that sorption of aluminum reduces both the solubility and dissolution kinetics of $bSiO_2$ (Iler, 1979; Van Bennekom et al., 1989; Van Bennekom et al., 1991). Fig. 2.9 presents results from two studies (Van Bennekom et al., 1991; Van Cappellen et al., 2002b) where bulk solubilities of diatom frustules (cultured diatoms, open ocean diatoms, core sediments) were measured in batch reactors. Both studies demonstrate the negative effect of Al sorption on the solubility of $bSiO_2$.

In the water column, because of the low levels of dissolved Al, Al to Si atomic ratios of natural plankton assemblages don't exceed 10^{-4}, while higher ratios are generally found in diatoms buried in the sediments (Dixit et al., 2001; Van Bennekom et al., 1991; Van Cappellen et al., 2002b). Therefore, Al sorption mostly takes place in the sediments where Al concentrations are higher due to the dissolution of terrigenous aluminosilicate minerals. The net result is that Al uptake results in a slower rate and extent of silica dissolution, thereby increasing the preservation of reactive Si in the sediments.

Gehlen et al. (2002) presented direct evidence of structural association of Al with diatoms from cultures and pelagic assemblages. Based on the results of a number of spectroscopic techniques (XAS, XANES, EXAFS) the authors found that Al was present within the silica framework in tetrahedral coordination. The authors proposed that Al was probably incorporated within the frustules during biomineralization. In a later study, Koning et al. (2007) cultured diatoms in Al-enriched seawater, and for comparison incubated clean (organic matter removed) diatom frustules in Al-rich seawater for several weeks. The authors found that the Al in seawater did not affect the Al content of the live diatoms. In contrast, the Al/Si atomic ratio of the clean diatom frustules incubated in the Al-rich seawater significantly increased with time. These results suggest that Al sorption takes place after diatoms die (secondary uptake) rather than during biosynthesis. In line with the results of Gehlen et al. (2002), the authors found that Al was present in the incubated frustules mostly in tetrahedral coordination. Furthermore, results from N_2 BET analyses suggest that the incubation of the frustules in Al-rich seawater results to significant changes in the frustules surface area and porosity. Based on these results, the authors proposed, that Al was incorporated, not in the frustule itself, but in an aluminosilicate layer formed on the surface of the frustules. As proposed by Van Cappellen and Qiu (1997b), Al uptake by $bSiO_2$ exhibits a continuum from adsorption of Al^{3+} ions to surface sites to incorporation into newly formed phases associated with the frustules.

2.5.3 Reverse weathering in continental margin sediments

The main sink for reactive Si in the oceans is burial in marine sediments, about half of which occurs in nearshore and continental shelf sediments (DeMaster, 2002; Laruelle et al., 2008). These sediments are also the main recipients of particulate matter originating from the continents, especially terrigenous clays. It has long been suspected that early diagenetic interactions in continental margin sediments exert a major control on the biogeochemical cycle of Si and, ultimately, on the siliceous productivity of the oceans (Mackenzie and Garrels, 1966).

Michalopoulos et al. (2000) discovered diatom frustules in deltaic sediments of the Amazon River that were partly or fully converted into authigenic K-rich and Fe-rich aluminosilicate material. The authors demonstrated through laboratory incubations that the conversion of diatom frustules into clays can be completed in less than 23 months. Loucaides et al. (submitted; see

Chapter 6) incubated cultured diatom frustules in suspensions of terrigenous sediments from the Mississippi River Delta and the Congo River Fan. The incubations were carried out in the laboratory and deployed along mooring lines at sea for 1 to 2 years. Chemical and microscopic analyses of the incubated frustules at the end of the experiments revealed the transfer of chemical elements from seawater (e.g., Mg, K) and from the clay-rich sediments (e.g., Al, Fe, Mn) to the frustules. The latter resulted in the formation of a variety of new mineral precipitates, including alumino-silicate and magnesian silicate phases, deposited on the surfaces of the frustules. In experiments performed under oxic conditions, phosphate-rich ferric iron oxyhydroxides also formed.

Interactions between biogenic silica, seawater and lithogenic minerals enhance the removal of reactive silicon from the ocean system through sedimentary burial. Previous estimates of burial of reactive Si in river deltas may have been biased by the commonly used leaching techniques for $bSiO_2$, which fail to measure the diagenetically altered material. Recent estimates based on improved leaching techniques suggest that river deltas may be a far more important marine sink of reactive Si than previously thought (Michalopoulos and Aller, 2004; Presti and Michalopoulos, 2008). In addition, uptake by biogenic silica and the precipitation of secondary mineral products may affect the biogeochemical cycles of other key biological (e.g., Fe, P) and geochemical (e.g., Mg, Al) elements. While some of these processes have long been recognized, they are rarely considered in budgets and model studies of biogeochemical cycles.

2.6 Surface reactivity and "aging" of $bSiO_2$

The dissolution rate of $bSiO_2$ dissolution is directly related to the surface area of the solid-solution interface. Differences among species and environmental conditions during growth are responsible for large inter and intra-species variations in specific surface areas (see section 3.1). Hurd and Theyer (1974) found that BET specific surface area values of $bSiO_2$ extracted from sediments of the Central Equatorial Pacific, declined from about 250 $m^2 \cdot g^{-1}$ to less than 50 $m^2 \cdot g^{-1}$ in a period of 40 million years (~2100 cm below sediment/water interface). Since net dissolution of $bSiO_2$ in deep sea sediments is limited to the topmost few centimeters (Van Cappellen, 1996) according to the results of Hurd and Treyer (1974) the specific surface area does not significantly change enough to affect solubility or dissolution kinetics.

Van Cappellen (1996), however, observed that even though the BET surface area of bulk $bSiO_2$-rich Southern Ocean sediments was practically constant down to 30 cm depth, the reactivity of the $bSiO_2$ steadily declined. Since elemental and microscopic analyses showed no changes in mineral composition or any diagenetic alterations throughout the sediment cores, the author proposed that the gradual loss of reactivity with depth was due to the reduction of the specific reactive surface area of $bSiO_2$ (not to be confused with the BET specific surface area). He further proposed that the reactivity of $bSiO_2$ decreases with depth in the sediments due to a progressive loss of reactive sites, which he defined as "aging". Later experiments on the same sediment samples demonstrated that the decrease in adsorption capacity for exchangeable Co^{+2} ions (which correlates with the number of adsorption sites on the silica surfaces) with depth, correlated positively with that of the measured dissolution rates (Van Cappellen and Qiu, 1997b).

Reactive site densities of $bSiO_2$ have also been measured using acid-base titrations (Dixit and Van Cappellen, 2002; Fraysse et al., 2006b; Loucaides et al., 2009). Dixit and Van Cappellen (2002) found that reactive site densities were systematically lower for biosiliceous material found

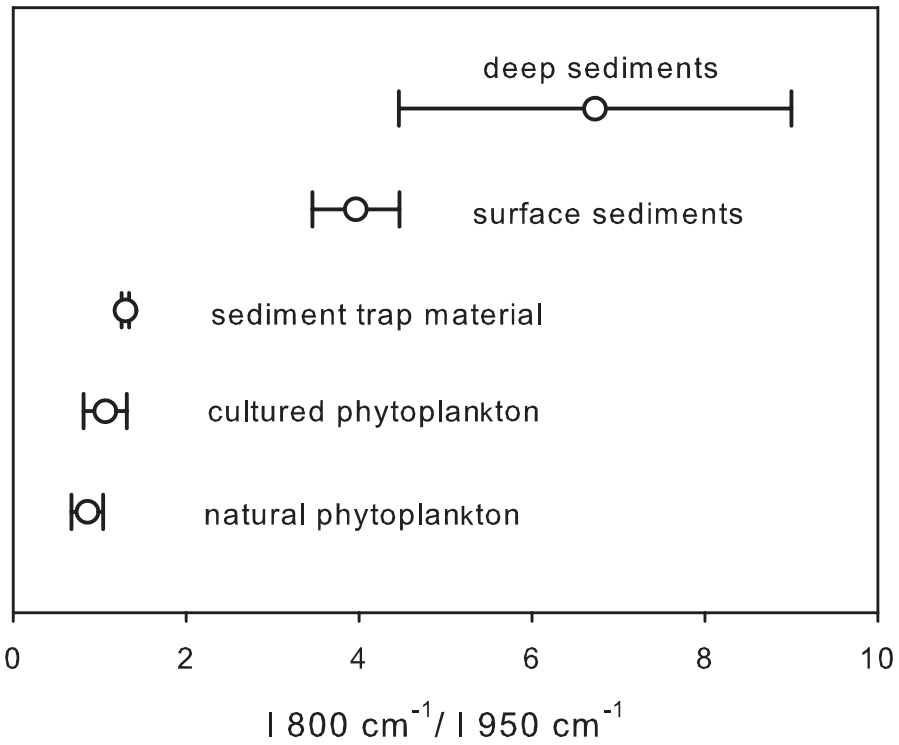

Figure 2.10 Ratio between peak intensities at 800cm^{-1} and 950cm^{-1} that correspond to (>Si-O-Si<) and (<Si-O) groups respectively as measured by FTIR spectroscopy (Schmidt et al., 2001).

in marine sediments than cultured or planktonic diatoms. Loucaides et al. (2009) observed similar a pattern when comparing the surface charge density of freshly cultured diatoms and plant phytoliths with that of lacustrine and marine biosiliceous sediments.

The progressive alteration (aging) of bSiO_2 in the water column and oceanic sediments has also been proposed based on spectroscopic evidence (Rickert et al., 2002; Schmidt et al., 2001). Schmidt et al. (2001) used FTIR spectroscopic analyses to estimate the ratio between siloxane (>Si-O-Si<) and silanol (>Si-OH) groups. FTIR spectra of silica show peaks at both 800cm^{-1} and 950cm^{-1} corresponding to silanol and siloxane bonds respectively. The ratio between the integrated intensities of the 800 and 1100 cm^{-1} ($A_{800\ cm\text{-}1}/A_{1100\ cm\ -1}$) absorption bands can be used as an indication of the degree of organization or ordering of the SiO_2 framework (Gendron-Badou et al., 2003). The authors performed the analysis on a variety of biosiliceous samples including natural phytoplankton, cultured diatoms, sediment trap material, surface sediments, and biosiliceous material from deeper sediments. As illustrated in Fig. 2.10, their analyses showed that the intensity ratio between siloxane and silanol peaks increased systematically with the age of the sample (i.e. fresh diatoms< sediment trap diatoms<surface sediments<deep sediments) suggesting that aging starts as soon as the silica is exposed to seawater after death of the organism. In a related study, Rickert et al (2002) demonstrated that the decrease of reactive silanol density observed by Schmidt et al. (2001) corresponded to a reduction of dissolution rates by more than two orders of magnitude.

2.7 Summary and Perspectives

The dissolution of $bSiO_2$ sustains a significant fraction of the oceanic primary productivity by controlling the availability of nutrient Si in the ocean. Diatoms, limited by the availability of dSi, are an important link between the marine Si and C cycles. The apparent spatial and temporal variability in the dissolution efficiency of $bSiO_2$ is most likely responsible for the so called "opal paradox". This work suggests that this variability, is controlled by a number of geochemical and ecosystem processes both during biosynthesis and after diatoms die.

Environmental conditions during biomineralization (i.e. temperature, light, nutrient availability) significantly affect the silicification of diatoms by controlling their growth rates. Frustule silicification is enhanced when growth rates are low but also when dSi concentrations are high. On the contrary, fast growth rates during diatom blooms generally lead to the production of less silicified frustules. While dSi limitation doesn't significantly affect growth rates, it has a negative effect on the silicification of diatom frustules.

Because of their higher resistance to weathering, highly silicified diatoms are regarded as more efficient exporters of Si but also C to the deep. During diatom blooms, enhanced utilization of CO_2 through high primary productivity may not inherently correspond to higher carbon export. Instead, CO_2 uptake under these conditions may only be temporary, since lightly silicified diatoms are physically incapable of transferring the carbon below the photic zone. On the contrary, during fast diatom growth, carbon export to the deep ocean may be exclusively controlled by grazers who prefer smaller and more lightly silicified diatoms and through the formation of fecal pellets can efficiently transfer C and Si to the deep ocean.

Immediately after death, the fate of diatom frustules depends on the efficiency in which bacteria can consume the protective organic coatings. In the open ocean, bacteria have ample time to break down the organic layer while diatoms are sinking. In shallow waters, however, it's possible that some diatoms can reach the sediments with the organic layer intact. Since the dissolution of diatom frustules is limited by the presence of the organic layer, in such shallow environments the efficiency in which bacteria can consume the organic layer can be critical.

Sinking velocities of diatom frustules are enhanced when single cells aggregate together into larger and less buoyant particles. Aggregation is enhanced by the presence of TEP which it's production and adhesivity can be a function of several parameters including grazing pressure, nutrient availability, light intensity, and bacterial activity. During diatom blooms, C and Si export can be significantly enhanced by aggregation, which along with grazing (and the formation of fecal pellets) can be the main processes responsible for the Si and C flux to the deep ocean.

Once free from organic matter, the dissolution efficiency of diatom frustules is mainly controlled by the physicochemical properties of both the mineral's surface as well as the aqueous medium. The dissolution rates of sinking diatom frustules are strongly controlled by the changing temperature and pressure throughout the water column. Similarly along the land to ocean transition, dissolution rates change significantly as a function of salinity and pH.

In the sediments, recycling of $bSiO_2$ continues although interactions with pore water constituents (mainly Al), build-up of dSi, and aging processes reduce the rate of dissolution. Interactions between $bSiO_2$ and elements released from the sediments play an important role in the global Si cycle by providing diagenetic pathways of silica preservation that can be far more rapid than the classic opal-A>opal-CT>quartz recrystallization generally considered. Relatively recent evidence suggest that diatoms deposited in clay-rich sediments can be completely transformed to authigenic clays in less than 3 years, while in other cases diatom frustules provide the substrate

for the formation of aluminosilicate coatings that can protect the frustules from dissolution. It has been proposed that the interaction between $bSiO_2$ and Al can lead to alternative diagenetic pathways, with smectites or zeolites as intermediates.

Better knowledge of the possible interaction between $bSiO_2$ and other elements is vital in order to better characterize links between different elemental cycles but also identify elemental sinks that to date have been overlooked. A substantial amount of research has been conducted, studying the interactions of Al and Si in the sediments but also in the water column during biomineralization. To our knowledge, however, little work has been done on the effect of other elements on the preservation of $bSiO_2$, even though evidence suggests that such interactions could exist.

Recent spectroscopic evidence suggest that aging mechanisms can reduce the reactivity of $bSiO_2$ even during sinking. These mechanisms still remain unknown but recent advances in spectroscopic and analytical techniques may be able to detect minor changes in the chemical structure and surface chemistry of amorphous silica. Laboratory aging experiments with cultured diatom frustules combined with spectroscopic techniques have the potential to elucidate these early diagenetic transformations of $bSiO_2$.

This chapter presents the great complexity involved in the recycling of $bSiO_2$ in the ocean. Biomineralization, dissolution, and preservation processes are dependent on a variety of physical, chemical, and biological factors that together define the relationship between $bSiO_2$ production and preservation. Environmental parameters including, temperature and nutrient availability can affect the fate of $bSiO_2$ in many levels from biomineralization to burial. Aware of this complexity we have to realize that simple interpretations of the sedimentary record based on diatom taphonomy can be a risky and misleading while instead, a better understanding of each forcing factor must be carefully evaluated. Most importantly, due to the fact that the recycling efficiency of $bSiO_2$ is closely coupled to the cycle of C, good knowledge of the dynamics involved is vital to better understand the significance and functioning of the biological pump.

CHAPTER 3

The effect of pressure on the silica solubility of diatom frustules in the oceans: Results from long-term laboratory and field batch experiments

Erica Koning#, Socratis Loucaides,#, Erik Epping, and Philippe Van Cappellen

Manuscript in preparation

[#] Both authors contributed equally to the research presented

Abstract

The oceanic cycle of silicon (Si) has been studied extensively due to its close coupling to the oceanic C cycle and the biological pump of CO_2. The oceanic Si cycle is dominated by the uptake of dissolved silicate by planktonic organisms, predominantly diatoms, who use it to synthesize siliceous frustules. As oceanic waters are undersaturated with respect to biogenic silica ($bSiO_2$) the frustules dissolve after death of the organisms, thereby regenerating dissolved silicate. Because the dissolution rate of $bSiO_2$ depends on the degree of undersaturation, the thermodynamic solubility of $bSiO_2$ is a key parameter controlling the recycling efficiency of nutrient Si in the water column and sediments. While an extensive body of data exists describing the dependence of $bSiO_2$ solubility on temperature, the effect of pressure has never been measured directly using natural diatom frustules. In this study, we conducted long-term (up to 22 months) laboratory and field equilibration experiments to determine the solubility of cleaned frustules of a cultured marine diatom (*Thalassiosira punctigera*) in seawater, for pressures between 1 and 700 bar, and temperatures between 2 and 21˚C. According to our results, the solubility of the diatom frustules gradually decreases by about 10% from 1 to ~200 bar. At 200 bar, the pressure dependence reverses and, at 700 bar, the solubility is about 15% higher than at atmospheric pressure. Integrated over an average oceanic water depth of 4000 m, a drop in temperature of 15-20˚C has a far more significant effect on the solubility of $bSiO_2$ than a corresponding 400 bar increase in pressure.

3.1 Introduction

The oceanic silicon cycle is driven by the production of biogenic silica ($bSiO_2$) by marine organisms, primarily diatoms (Brzezinski et al., 2003; Dugdale et al., 1995; Tréguer et al., 1995). The siliceous organisms expend metabolic energy to extract dissolved silicate from seawater and precipitate amorphous silica, which is thermodynamically unstable under conditions encountered in the water column. Undersaturation of seawater with respect to amorphous silica causes dissolution of the silica hard parts following death of the organisms, thereby recycling most of the dissolved silicate

(Hurd, 1972; Nelson et al., 1995; Tréguer et al., 1995). Small amounts of $bSiO_2$, however, escape dissolution and are buried in marine sediments. Over geological time, the burial flux of $bSiO_2$ exerts a major control on the biosiliceous productivity of the oceans (DeMaster, 1981; DeMaster, 2002; Ragueneau et al., 2002; Van Cappellen et al., 2002a; Van Cappellen et al., 2002b).

Many studies have been devoted to the recycling and ultimate preservation of $bSiO_2$ in the oceans. Surface water productivity, rain rate, water depth, sediment accumulation rate, temperature, bottom water chemistry, and sediment composition have all been invoked as playing a role in the efficiency by which $bSiO_2$ is recycled (Archer et al., 1993; Dixit et al., 2001; McManus et al., 1995; Rabouille et al., 1997; Rickert et al., 2002; Schink et al., 1974). Because dissolution depends on the degree of disequilibrium between the silica solid and the surrounding solution, the silica solubility represents a key thermodynamic parameter controlling $bSiO_2$ dissolution in the water column and at the seafloor.

The solubility of diatom frustules is a function of the physicochemical properties of the solid material, including the degree of condensation and order of the silica framework, the water and impurity contents, and the specific surface area (Beck et al., 2002; Dixit and Van Cappellen, 2002; Gehlen and Van Raaphorst, 2002; Hurd and Birdwhistell, 1983; Lewin, 1961; Willey, 1980). Because these properties vary substantially between different biosiliceous materials, silica solubilities measured under identical conditions exhibit a large variability. At 25°C and 1 bar, reported solubilities of diatomaceous silica in seawater vary anywhere from 200 to 1600 μM (Hurd, 1972; Hurd and Theyer, 1974; Kamatani et al., 1980; Lawson et al., 1978; Loucaides et al., 2008; Van Bennekom et al., 1991; Van Beusekom, 1989). The highest values generally correspond to fresh diatom frustules grown in open ocean seawater.

The solubility of $bSiO_2$ is a function of the ambient temperature and pressure. An extensive body of data exists describing the dependence of $bSiO_2$ solubility on temperature (Hurd, 1972; Hurd, 1973; Kamatani, 1982; Lawson et al., 1978; Lewin, 1961). Between 0 and 30°C, the solubility of fresh diatom frustules increases roughly by a factor of 2, making temperature an important environmental variable affecting the marine recycling efficiency of silica (Kamatani, 1982; Kamatani and Riley, 1979; Lawson et al., 1978). In contrast, no work has been done on the effect of pressure on the solubility of $bSiO_2$. To this date, the control of pressure on $bSiO_2$ solubility has been estimated based on experiments with synthetic amorphous silica (Willey, 1974).

In the present study, $bSiO_2$ solubilities were determined by equilibrating diatom frustules in the laboratory using pressurized reactors, and at sea by deploying batch reactors down to 2500 m water depth along mooring lines. Preliminary experiments were carried out to define the contact time and solid to solution ratio required for the frustules to reach equilibrium with seawater. The pressure range covered by the experiments was 1-700 bar.

3.2 Materials and methods

3.2.1 Siliceous materials

Frustules of the marine diatom *Thalassiosira punctigera*, a species widely distributed throughout the oceans (Hasle, 1983) were used in the experiments. The frustules have been previously characterized in terms of their microstructure, specific surface area, acid-base properties, dissolution kinetics and solubility (Loucaides et al., 2009; Loucaides et al., 2008; Van Cappellen et al., 2002b; Vrieling et al., 2000). The diatoms were grown in large batch cultures at the Royal Netherlands Institute of Sea Research (NIOZ), in low-nutrient natural seawater. After harvesting the cells, organic matter was

Table 3.1 Field and laboratory batch experiments and experimental conditions. TP = T. punctigera frustules; AE = Aerosil® OX 50

Series	Material	Pressure* (bar)	Temperature (°C)	Incubation time (days)	Solid/solution ratio (g/L)
Field experiments					
A	TP	50	10	660	0.25, 0.5, 1, 2.5, 3.75, 5
	TP	90	6	660	0.25, 0.5, 1, 2.5, 3.75, 5
	TP	150	4	660	0.25, 0.5, 1, 2.5, 3.75, 5
	TP	200	3	660	0.25, 0.5, 1, 2.5, 3.75, 5
	TP	250	2	660	0.25, 0.5, 1, 2.5, 3.75, 5
B	TP	50	10	660	1
	TP	125	5	660	1
	TP	200	3	660	1
	AE	50	10	660	1
	AE	125	5	660	1
	AE	200	3	660	1
Laboratory experiments					
C	TP	1	4	365	25
	TP	1	15	226	5
	TP	1	21	365	25
D	TP	1	15	70	0.25, 0.5, 1, 2.5, 3.75, 5
	TP	200	15	70	0.25, 0.5, 1, 2.5, 3.75, 5
E	TP	100	5	80	5
	TP	300	5	42	5
F	TP	300	4	365	25
	TP	500	4	365	25
	TP	700	4	365	25
	TP	300	21	365	25
	TP	500	21	365	25
	TP	700	21	365	25

* For the field experiments, pressure is estimated assuming that pressure increases by 1 bar for every 10 meters of depth.

removed by low-temperature ashing. Details on the culturing conditions and ashing protocol can be found in Koning et al. (2007). Aerosil® OX50, a synthetic, non-porous silica, well characterized in terms of dissolution kinetics and solubility (Loucaides et al., 2008) as well as surface properties (de Keizer et al., 1998; Gun'ko et al., 2005), was used as a non-biogenic reference material in a limited number of experiments.

3.2.2 Field experiments

Diatom frustules were weighted and transferred to 4 mL polyethylene vials filled with filtered seawater. The vials were placed in steel cages and attached to mooring lines deployed at the narrowest section of the Mozambique Channel during oceanographic cruises in the Mozambique Channel as part of the LOCO (Long-term Ocean Circulation Observations) program (Ridderinkhof and Quartly, 2006). The seawater in the vials was collected on site from a water depth of about 1250 m.

In one set of deployments (Series A, Table 3.1), the diatom mass to solution ratio in the vials was varied from 0.25 to 5 g L^{-1}, and the vials were deployed at 500, 900, 1500, 2000 and 2500 m water depth. The vials were recovered after 22 months. Upon recovery, each vial was sampled immediately. The samples were diluted with deionized water and subsequently filtered through 0.45 μm pore size cellulose acetate filters. In a second set of deployments, vials with 1 g L^{-1} of

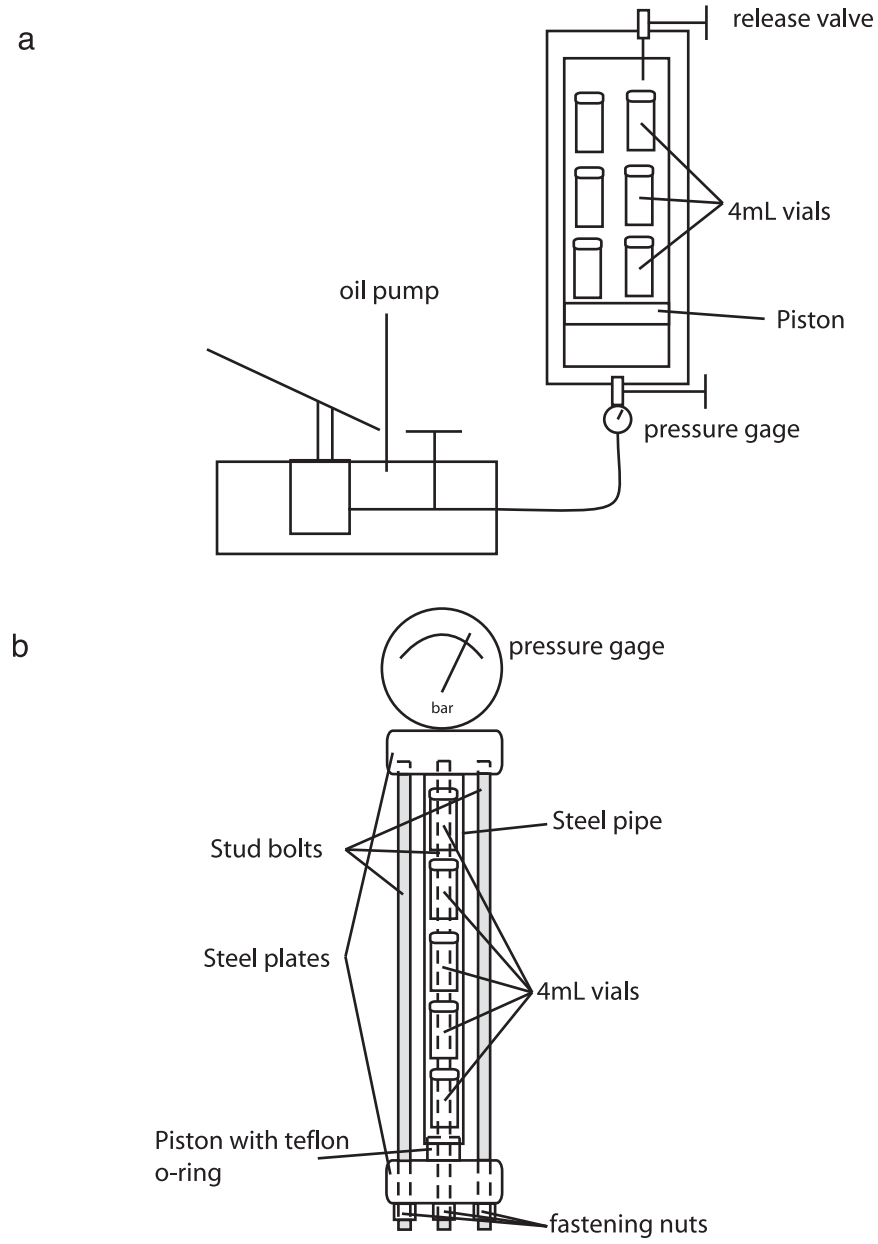

Figure 3.1 Pressure reactors used in the laboratory experiments.

diatom frustules or 1 g L^{-1} of Aerosil® OX50 were deployed at 500, 1250, and 2000 m depth (Series B, Table 3.1).

3.2.3 Laboratory experiments

Two types of pressurized reactors were used (Fig. 3.1). The first type was used for pressures up to 300 bar and consisted of a 50 x 10 cm stainless steel cylinder filled with water that could hold several 4 mL batch reactors (Fig. 3.1a). The water was pressurized hydraulically by a piston inside the cylinder. For pressures ≥300 bar, a 25 x 3 cm stainless steel tube, which could hold up to five 4 mL polyethylene vials in water was used (Fig. 3.1b). One end of the tube was sealed with a steel plug and a Teflon o-ring while the other end was fitted with a steel piston. The plug and the piston were held together by two metal plates attached to each other by 3 stud bolts and locknuts. Tightening the locknuts forced the piston into the tube thereby pressurizing the water. Pressures up to a maximum of 800 bar could be reached and maintained for extended periods of time.

Laboratory incubations were performed using seawater from the oligotrophic central part of the North Atlantic (dSi ~ 2 μmol L^{-1}, pH 8.1) filtered through 0.45 μm pore size filters. For the low pressure range experiments (≤ 300 bar), diatom frustules were weighted and transferred into 4 ml polyethylene vials filled with seawater, in solid to solution ratios ranging from 0.25 to 5 g L^{-1} (Series D, Table 3.1). The experiments at 200 bar were performed at 15°C for a duration of 70 days. Otherwise identical control experiments were run in parallel at atmospheric pressure. In another set of experiments, diatom frustules were incubated at 5°C, at 100 or 300 bar pressure (Series E). In the latter experiments, the buildup of dissolved silicate (dSi) was monitored periodically for total periods of 42 (300 bar) and 80 days (100 bar).

In the high pressure range experiments (≥300 bar, Series F) 100 mg of diatom frustules were suspended in 4mL polyethylene vials filled with filtered seawater. The vials were pressurized to 300, 500, and 700 bar and kept in thermostated rooms at 4 and 21°C for the duration of the experiments (1 year). Otherwise identical control experiments were also performed at atmospheric pressure (Series C).

3.2.4 Analytical

All samples were diluted with deionised water and immediately filtered through 0.45 μm pore size cellulose acetate filters. Dissolved silicate concentrations in the filtrates were determined colorimetrically with a BRAN & LUEBBE TRAACS 800 auto-analyzer. Calibration standards were prepared by diluting silicate stock solutions in the same seawater as used in the laboratory experiments. Each calibration run had a correlation coefficient for the standards of at least 0.999. Within a single run, the relative standard deviation of the analytical method was less than 0.1%.

3.3 Results

3.3.1 Field experiments

Concentrations of dissolved silicate measured after 22 months in the vials with variable diatom mass to seawater ratios (Series A, Table 3.1) are shown in Fig. 3.2a. Below 2 g L^{-1}, the concentrations were dependent on the amount of solid in the vials: the concentrations decreased progressively with decreasing mass of frustules. However, at solid to solution ratios higher than 2 g L^{-1}, the silicate concentrations at a given depth no longer varied significantly with the solid to solution ratio. When only considering the results from the vials with diatom frustules in excess of

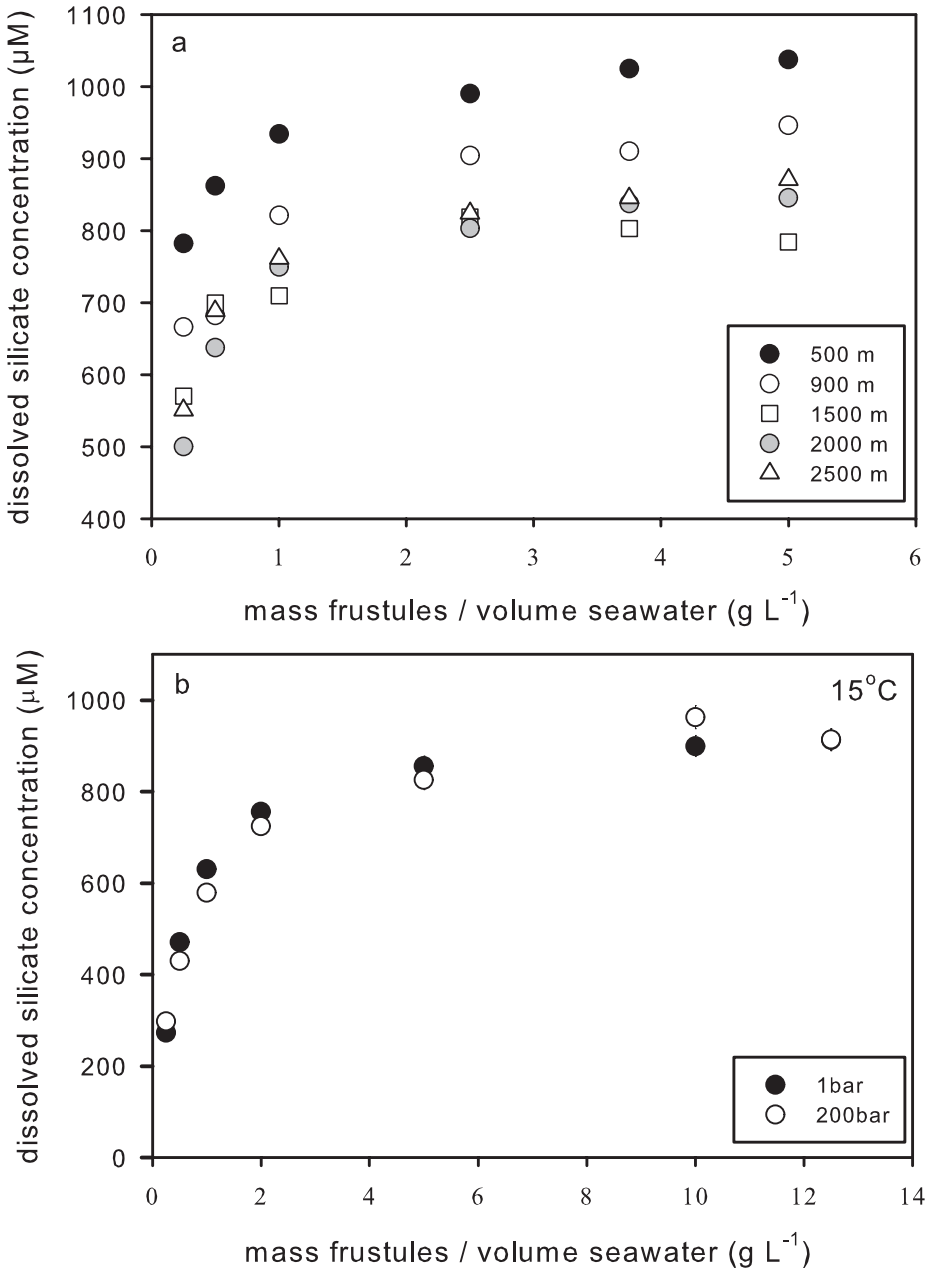

Figure 3.2 a) Dissolved silicate concentrations measured after 22 months in the batch reactors along the mooring line (Series A) and b) after 70 days of incubation at 15°C in the laboratory (Series D). The experiments were performed with variable initial masses of frustules in the reactors.

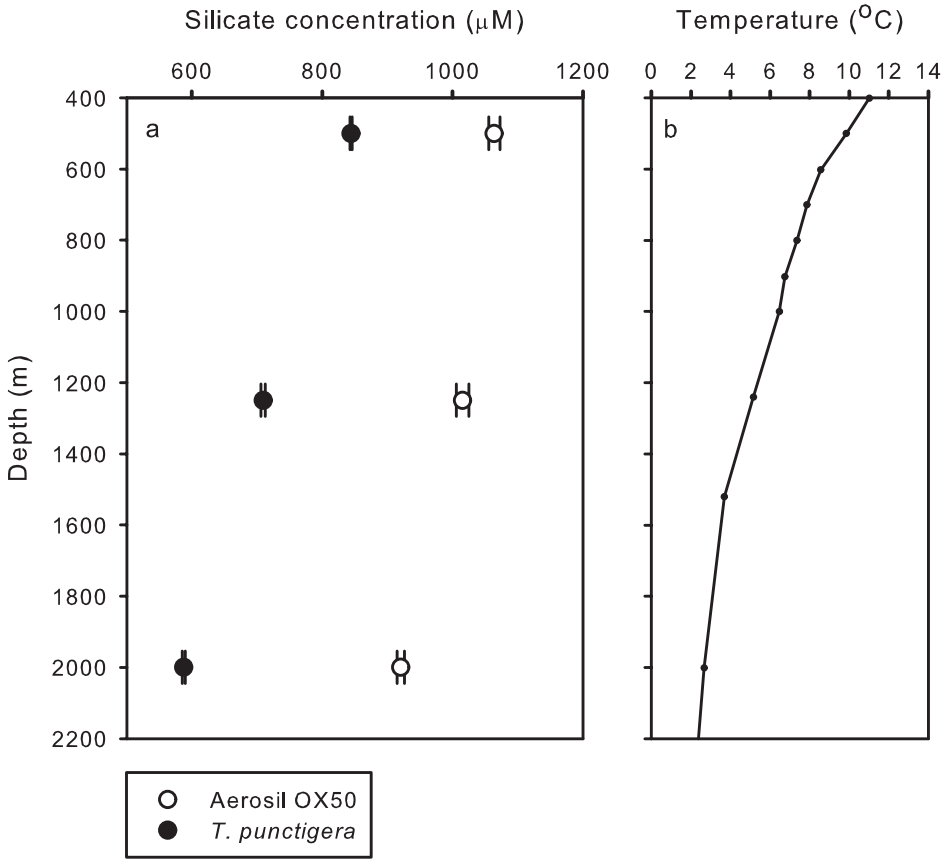

Figure 3.3 a) Dissolved silicate concentrations in batch reactors incubated on the mooring lines for 22 months with *T. punctigera* frustules and Aerosil OX50 (Series B). The error bars represent the standard deviation between 4 replicate samples taken from each reactor. b) Temperature profile measured with a CTD instrument at the location of the mooring line at the time of recovery.

2 g L^{-1}, a clear drop in the dissolved silicate concentration from 1020 ± 20 μM to 800 ± 20 μM was observed between 500 and 2000 m. At 2500 m, the corresponding dissolved silicate concentration was 830 ± 20 μM.

The dissolved silicate concentrations in the 1 g L^{-1} suspensions of diatom frustules and Aerosil® OX50 incubated at 500, 1250, and 2000 m water depth (Series B, Table 3.1) exhibited decreasing trends with depth (Fig. 3.3a). For the frustules, the dissolved silicate concentration was 30% lower at 2000 m than at 500 m depth, while for the synthetic silica it was 14% lower. Fig. 3.3b shows the corresponding temperature depth profile at the location of the mooring line.

3.3.2 Laboratory experiments

Dissolved silicate concentrations measured after the 70-day incubations of frustules in the laboratory (Series D, Table 3.1) exhibited a dependence on the solid to solution ratio of the suspensions similar to that observed in the field experiments (compare Fig. 3.2a and 3.2b). As can

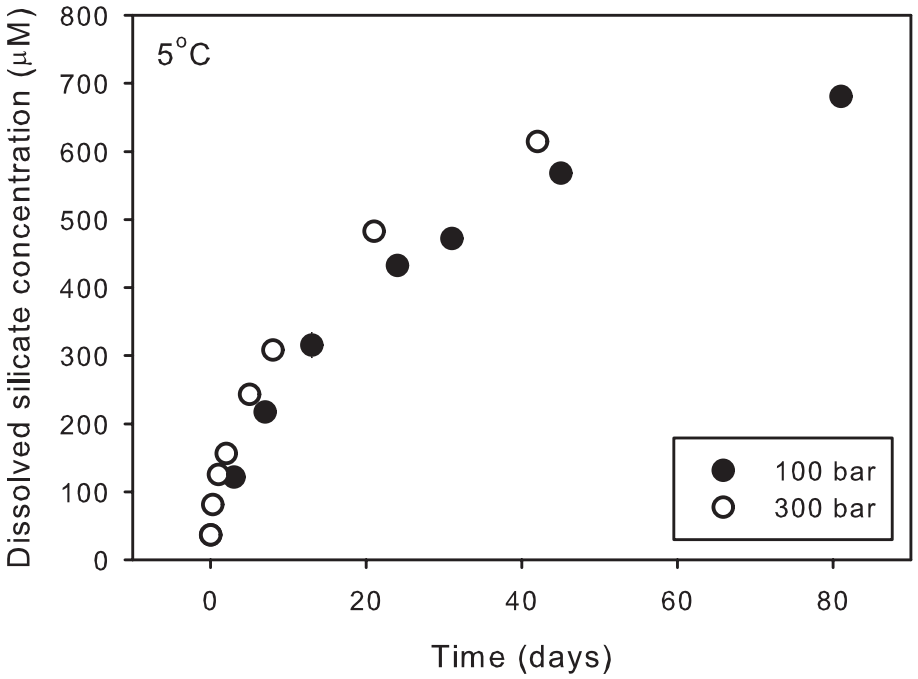

Figure 3.4 The buildup of dissolved silicate over time in batch reactors incubated at 100 and 300 bar in the laboratory (Series E). The solid to solution ratio of the suspensions was 5 g L^{-1}.

be seen in Fig. 3.2b, the dissolved silicate concentrations at 200 bar were practically identical to those measured at atmospheric pressure.

The dissolved silicate concentration measured as a function of contact time in the batch reactors incubated at 100 and 300 bar at 5°C (Series E, Table 3.1) are shown in Fig. 3.4. The continued build-up of dissolved silicate implied that even after 80 days equilibrium had not been reached. The time series data also indicated systematically higher dissolved silicate concentrations in the 300 bar incubations, compared to those at 100 bar.

The dissolved silicate concentrations in the suspensions of frustules incubated for 1 year at atmospheric pressure in the laboratory (Series C, Table 3.1) were 920 ± 4 and 1300 ± 30 μM at 4 and 21°C, respectively. The dissolved silicate concentrations in the higher pressure range experiments (Series F, Table 3.1) increased with pressure (Fig. 3.5). At 4 and 21°, the concentrations at 700 bar were 1070 ± 10 and 1510 ± 10 μM, respectively.

3.4 Discussion

The results from the laboratory and field incubations indicate that in order to reach solubility equilibrium, the mass of diatom frustules to seawater ratio and the contact time must be sufficient (Fig. 3.2 and 3.4). Not only are the kinetics of $bSiO_2$ dissolution relatively slow under in situ temperature conditions, the thermodynamic driving force of dissolution also decreases with time as the dissolved silicate concentration progressively builds up in batch reactor systems. As shown

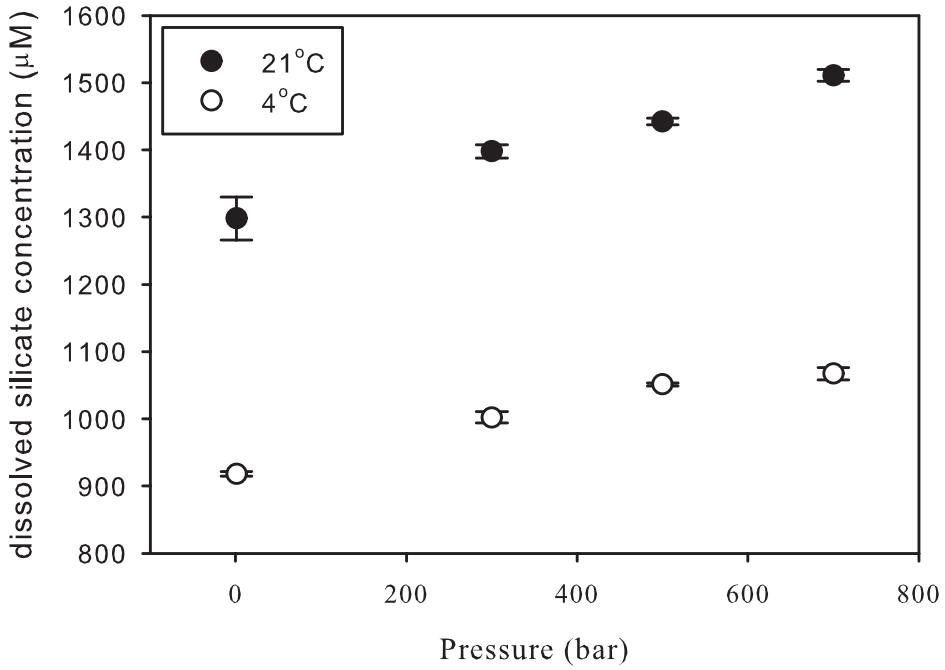

Figure 3.5 Dissolved silicate concentrations of suspensions of *T. punctigera* frustules incubated in the laboratory for one year at 4 and 21°C (Series F). The frustule mass to solution ratio was 25g L^{-1}.

in Fig. 3.2a, even after 22 months of deployment at sea, the dissolved silicate concentrations in the incubations with less than 2 g L^{-1} of frustules remain below the equilibrium solubility values. The laboratory experiments run at 15°C show a similar pattern after 70 days of incubation: the mass of frustules must exceed 5 g L^{-1} for the dissolved silicate concentrations to approach constant values (Fig. 3.2b). Therefore, for the temperature range considered here (2-21°C), we assume that only suspensions of at least 2 g L^{-1} of frustules incubated for periods of one year or longer represent true equilibrium conditions.

Many $bSiO_2$ solubilities reported in the literature were determined in short-term (days) batch experiments with solid to solution ratios well below 2 g L^{-1}. For example, Kamatani and Riley (1979) measured maximum concentrations of dissolved silicate on the order of 120 µM at 20°C, in suspensions with initial masses of frustules as low as 0.007 g L^{-1}. The authors proposed that these low dissolved silicate concentrations represent the solubility of a residual and insoluble fraction of the frustules (note: due to the low amounts of silica, only about 10% of the frustules remained after 15 days of equilibration time). In light of the results presented here, however, it seems equally possible that thermodynamic equilibrium was never reached in these experiments.

The trend of decreasing dissolved silicate concentrations with depth illustrated in Fig. 3.3a for the reactor vials deployed along the mooring lines is, to a large degree, caused by the drop of temperature with depth (Fig. 3.3b). To separate the effects of temperature and pressure, the in situ solubilities are therefore corrected using the temperature dependence of the solubility of *T. punctigera* frustules measured at 4, 15 and 21°C, under atmospheric pressure (Fig. 3.6). Note that these solubilities were obtained on suspensions of frustule suspensions in excess of 5 g L^{-1}, incubated for longer than 7 months. The temperature relationship predicts that the silica solubility

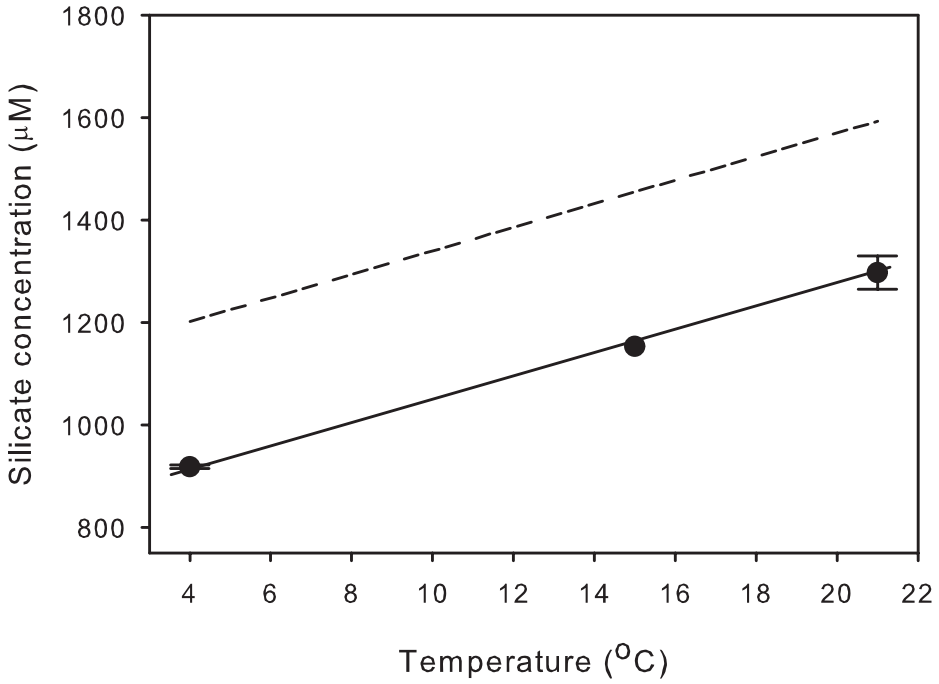

Figure 3.6 Temperature dependence of the solubility of *T. punctigera* frustules at 1 bar in seawater. Solubilities were determined in long-term laboratory batch experiments with high solid to solution ratios (Table 3.1, Series C). The error bars (4 and 21°C) represent the standard deviation between 3 replicate experiments. The dashed line represents the temperature dependence of the solubility of Aerosil OX 50 between 4 and 21°C (Loucaides S., unpublished).

of the frustules increases by 22±2 μM for each 1°C increase in temperature, which is consistent with previous work on diatom frustules (Lawson et al., 1978) and diatomaceous sediments (Van Cappellen and Qiu, 1997a).

The silica solubilities of the diatom frustules derived from the 22-month field incubations, after correction to a common temperature of 4°C, are shown in Fig. 3.7 (filled circles). Note that for this figure, only the dissolved silicate measurements from incubations with frustules in excess of 2 g L^{-1} were used. Between 0 and 2000 m water depth the results imply a drop in the silica solubility as pressure increases. At 4°C, the solubility is slightly over 10% (110±20 μM) lower at 2000 m depth than at the surface for the same temperature. The 4°C silica solubility derived form the field incubations at 2500 m water depth (Fig. 3.7), as well as the laboratory experiments performed at 300, 500 and 700 bar (Fig. 3.5), imply a reversal in the pressure dependence of the solubility of the diatom frustules at a pressure around 200 bar. According to the trend in Fig. 3.5, the solubility of the frustules at an average ocean depth of 4000 m should be about 10% higher than in the surface ocean.

The drop in solubility of the diatom frustules between 0 and 2000 m water depth is more pronounced than observed for the (non-porous) silica gel Aerosil® OX50 (Fig. 3.3a). In fact, when accounting for the temperature dependence of the solubility of Aerosil® OX50 (23 μM per °C; see

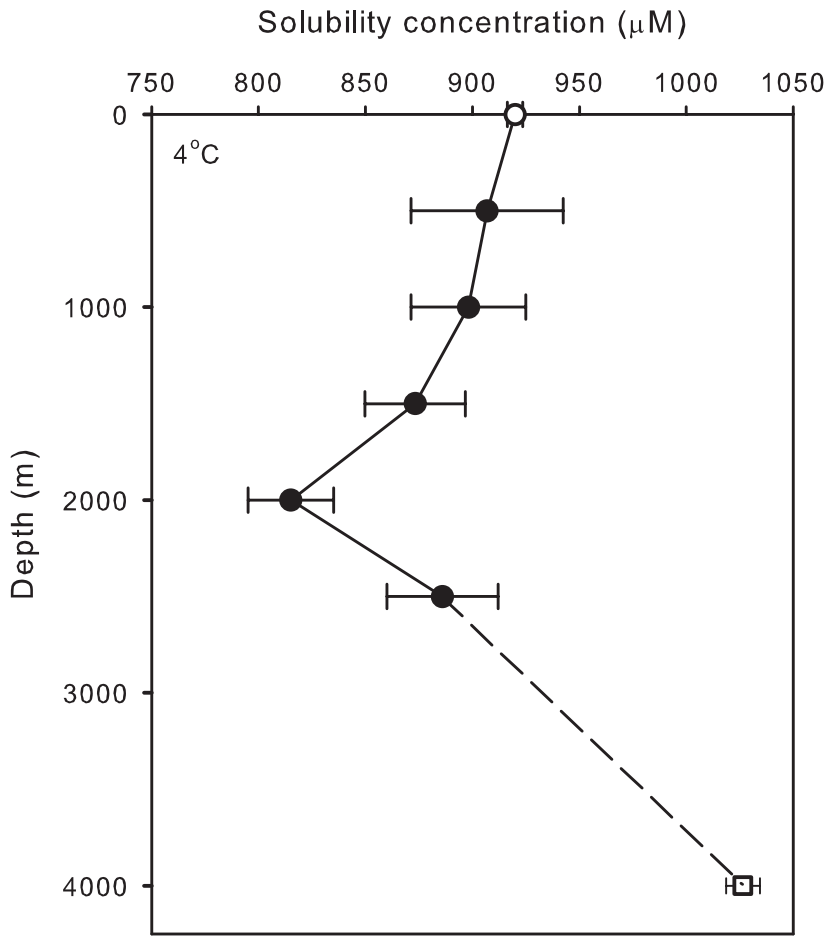

Figure 3.7 Silica solubility of *T. punctigera* frustules as a function of depth, from the sea surface to an average ocean depth of 4000 m. The open circle at 0 m water depth corresponds to the solubility measured in the laboratory at 1 bar and 4°C (25 g L^{-1}, 1 year equilibration time). The filled symbols correspond to the silicate concentrations measured in batch reactors deployed for 22 months along a mooring line, corrected to a common temperature of 4°C, using the relationship shown in Figure 3.6. Only dissolved silicate concentrations measured in suspensions containing frustules in excess of 2 g L^{-1} were used. The open square at 4000 m water depth corresponds to the solubility at 400 bar interpolated from the solubility measurements obtained at 4°C in the laboratory experiments at 300 and 500 bars (25 g L^{-1}, 1 year equilibration time). Error bars represent the range of dissolved silicate concentrations measured in replicate reactors.

Fig. 3.6), the measured dissolved silicate concentrations imply that, in the range 1-200 bar, pressure actually has a positive effect on the solubility of the synthetic silica gel. This is in agreement with Willey (1974), who found a monotonic increase of the solubility of synthetic silica with pressure, from 1 up to 1240 bar.

To date, effects of pressure on the solubility of $bSiO_2$ in seawater have been accounted for by assuming a behavior identical to that of synthetic amorphous silica (Dixit et al., 2001; Gallinari

et al., 2002), using the experimental data of Willey (1974). The inverse relationship between the solubility of the diatom frustules and pressure in the range 1-200 bar, however, does not agree with that of synthetic silica gel. Overall, our results indicate that the pressure dependence of synthetic silicas may not provide an adequate analogue for that of diatomaceous silica. Possibly this may be related to the micro-porous nature of the silica frustules of the diatoms. Confinement of water in nanopores is known to significantly alter the thermodynamic properties of porous materials (Wang et al., 2003).

Further work will be needed to refine the pressure dependence of diatomaceous silica observed in this study. In particular, it would be interesting to compare the pressure dependencies of various biogenic silicas, from fresh diatom frustules to siliceous remains buried in sediments. Several studies have demonstrated that the solubility of $bSiO_2$ decreases with time due to aging processes (Loucaides et al., 2009; Rickert et al., 2002; Schmidt et al., 2001). The latter include condensation of the silica framework, which, by changing the nanoporosity, may change the responses of the solubility to pressure.

3.5 Concluding remarks

The silica solubility of diatom frustules shows a complex dependence on pressure. From 1 to 200 bar, the solubility drops with increasing pressure, while above 200 bar the opposite trend is observed. Our observations imply that the pressure dependence of diatomaceous silica deviates from that observed for synthetic, non-porous amorphous silica. We speculate that the deviating behavior of biogenic silica may be related to the presence of water confined in its porous structure, although this will have to be confirmed by further studies.

From the ocean surface to an average water depth of 4000 m, the solubility of the diatom frustules used in this study varies by about ±10%. That is, pressure changes should have a relatively minor, but not negligible, effect on the biogenic silica solubility in the oceans. For comparison, a typical temperature gradient between the ocean surface and the deep-sea of, say, 20°C, causes a drop in solubility by nearly 50%.

The results presented in this study also draw attention to the need to critically evaluate the various solubility determinations of biogenic silica that have been reported in the literature. For batch reactor experiments, reaction times and solid to solution ratios must be sufficiently large in order for thermodynamic equilibrium to be reached. We recommend that when determining solubilities in the temperature range relevant to marine environments, suspensions of at least 2 g L^{-1} are left to incubate for periods of 1 year or longer.

CHAPTER 4

Reactivity of biogenic silica: surface versus bulk charge density

Socratis Loucaides, Thilo Behrends, and Philippe Van Cappellen

Submitted to *Geochimica et Cosmochimica Acta*
October, 2008

Abstract

Acid-base titrations were carried out at three different ionic strengths (0.01, 0.1 and 0.7 M NaCl)) on a range of marine and continental biosiliceous materials. The large variability in electrical charging behavior of the various materials is consistent with the existence of two pools of ionizable groups, namely silanols on the outer surface of and within the silica particles. The relative amounts of internal and external silanols were estimated by fitting a two-site complexation model to excess proton *versus* pH curves obtained at different ionic strengths. For fresh diatom frustules and phytoliths, as well as recently deposited biosiliceous sediments, the abundance of internal silanols was of the same order of magnitude as, or exceeded, that of silanols on the external surface. Older biosiliceous materials exhibited lower proportions of internal groups, while a decrease in the relative amount of internal silanols was also observed for diatom frustules artificially aged in seawater. The existence of internal ionizable functional groups explains measured charge densities of biogenic silicas that largely exceed the theoretical site density of silica surfaces. Variations in the relative abundance of internal *versus* surface silanols further explain the non-uniform dependence of electrical charging on ionic strength, the lack of correlation between total charge density and dissolution kinetics, and the variable 950 cm^{-1} peak intensity in the infrared spectra of biogenic silicas. Dissolution rate constants correlated positively with the external charge, rather than the total charge build-up, as expected if dissolution only involves the removal of silicate units from the outer surfaces of the particles. The progressive reduction with time of the internal *versus* external silanol concentration ratio represents one of the mechanisms altering the material properties that affect the recycling and preservation of biogenic silica in earth surface environments.

4.1 Introduction

Diatoms are responsible for up to 40% of the annual oceanic uptake of CO_2 from the atmosphere (Tréguer et al., 1995), and represent one of the most important agents of organic carbon export to the deep ocean (DeMaster, 1981; Dugdale and Wilkerson, 1998; Rabouille et al., 1997). Diatom productivity, however, strongly depends on the availability of dissolved silicate, which the organisms use to synthesize their amorphous silica frustules (Spencer, 1983). Since seawater is strongly undersaturated with respect to biogenic silica ($bSiO_2$), diatom frustules readily dissolve after the organisms die. The dissolution of biogenic silica is therefore a key process controlling nutrient silicon cycling in the ocean.

Fixation of silica by land plants, mainly in the form of phytoliths, has been proposed to be of comparable magnitude to that by marine diatoms (Conley, 2002). Because of the relatively fast dissolution of $bSiO_2$ in soils compared to the chemical weathering of silicate rocks (Alexandre et al., 1997; Derry et al., 2005), a significant fraction of the reactive Si reaching the oceans may have undergone prior biological cycling on land. Recent estimates further indicate that a significant portion of the reactive Si load in rivers may be under the form of $bSiO_2$ produced by land plants and freshwater diatoms (Conley, 1997; Laruelle et al., 2008). Dissolution of land-derived $bSiO_2$ may thus constitute an important, but so far overlooked, source of nutrient Si to the world ocean (Loucaides et al., 2008).

Because the recycling of $bSiO_2$ exhibits significant temporal and spatial variability in the oceans, a considerable number of studies during the last decades have been dedicated to the dissolution of diatomaceous silica. The variability in dissolution efficiency does not only challenge our predictive understanding of the oceanic Si cycle, but also presents a hurdle when sedimentary $bSiO_2$ is used as a proxy for reconstructing past oceanic productivity, climate, and chemistry (Berger and Herguera, 1992; Birks et al., 1990; Fritz et al., 1991; Lisitzin, 1985). The accurate interpretation of these records requires a proper understanding of the material properties and environmental factors affecting the dissolution kinetics of $bSiO_2$ (Van Cappellen et al., 2002b).

Dissolution of $bSiO_2$ first requires the removal of any organic materials protecting the silica surfaces, a process often carried out by heterotrophic microorganisms (Bidle and Azam, 2001; Kamatani and Riley, 1979; Rickert et al., 2002). Once exposed, the dissolution kinetics of $bSiO_2$ particles are intimately linked to the chemical structure of the solid-aqueous solution interface (Van Cappellen et al., 2002a). In the presence of water, hydrolysis of siloxane bonds (>Si-O-Si<) on a silica surface produces silanol (Si-OH) groups which may lose or gain protons depending on the pH of the solution (Sverjensky and Sahai, 1996). Schematically:

$$SiOH^0 + H^+ \Leftrightarrow SiOH_2^+ \quad (1)$$

$$SiOH^0 \Leftrightarrow SiO^- + H^+ \quad (2)$$

Because of the relatively low point of zero charge of silica, $pH_{zpc} \approx 2\text{-}3.5$ (Sverjensky and Sahai, 1996), reaction (2) predominates around neutral pH and reaction (1) can be neglected.

It is generally accepted that the dissolution of silica at near-neutral pH is due to the nucleophilic attack of water molecules that cause the breaking of siloxane bonds at the surface (Dove and Crerar, 1990). At pH values higher than the pH_{zpc} the surface exhibits a net negative charge due to the presence of deprotonated silianol groups ($>SiO^-$) (see equation 2). The negatively charged surface enhances the nucleophilic character of water molecules at the solid/solution interface, thereby facilitating the hydrolysis reaction and the breaking of additional siloxane bonds (Dove, 1994 and references therein). The pH dependent surface charging thus implies a strong pH dependence of the dissolution kinetics, as experimentally demonstrated for quartz (Dove and Elston, 1992), vitreous silica (Wirth and Gieskes, 1979), and biogenic silica (Fraysse et al., 2006b; Van Cappellen and Qiu, 1997b). Dove and Elston (1992) developed an isothermal model (25°C) explicitly expressing the silica dissolution rate in terms of the pH-dependent surface speciation.

Dissolution rates of diatom frustules and phytoliths have been measured under a wide range of experimental conditions (Barker et al., 1994; Fraysse et al., 2006b; Greenwood et al., 2001; Hurd and Birdwhistell, 1983; Kamatani, 1982; Kamatani and Riley, 1979; Kamatani et al., 1980; Koning et al., 1997; Lewin, 1961; Loucaides et al., 2008; Van Cappellen, 1996; Van Cappellen et

al., 2002a; Van Cappellen et al., 2002b; Van Cappellen and Qiu, 1997b). In contrast, little work has been done on the acid-base properties of biogenic silicas in aqueous solutions (Dixit and Van Cappellen, 2002; Fraysse et al., 2006b). The limited amount of data available demonstrates significant variability in the electrical charging behavior of $bSiO_2$ (Dixit and Van Cappellen, 2002). Furthermore, the surface charge densities reported for phytoliths by Fraysse et al. (2006) exceed the allowable site densities of silica surfaces by many orders of magnitude, but no satisfactory explanation for this observation has been proposed so far.

The purpose of this work is to better characterize the charging behavior of $bSiO_2$ as a function of pH and solution electrolyte concentration. Based on the results, we propose that silanol groups participating in (de)protonation reactions are not restricted to the external surface of $bSiO_2$ particles. Unlike crystalline and non-porous synthetic amorphous silicas, $bSiO_2$ contains ionizable silanol groups located beneath the external surface. The existence of varying proportions of ionizable groups located on and below the external surface of $bSiO_2$ particles helps explain the observed variations in charging behavior among different biogenic silicas, as well as the apparent lack of correlation between the electrical charge density and the dissolution kinetics of $bSiO_2$.

4.2 Materials and methods

4.2.1 Biosiliceous Materials

Acid-base titration experiments were carried out with a range of continental and marine biosiliceous materials (Table 4.1). These include frustules of cultured marine and euryhaline diatoms, phytoliths extracted from land plants, a siliceous lake sediment, a siliceous ooze from the Southern Ocean, and a diatomite ore deposit. The non-siliceous fractions of the natural samples were removed as much as possible with the treatments described below. Afterwards the samples were rinsed several times with deionised water and freeze-dried, prior to being used in the dissolution experiments.

The marine diatoms (*Thalassiosira punctigera*) were cultured at the Royal Netherlands Institute for Sea Research (NIOZ) in central North Atlantic seawater containing low nutrient and trace metal levels. After harvesting the cells, organic matter was removed by low-temperature ashing. Descriptions of the culturing conditions and ashing protocol are given in Koning et al. (2007). A fraction of the cleaned diatom frustules were used as such (TP in Table 4.1), while another fraction was aged in a flow-through reactor through which filtered low-nutrient seawater was flown continuously for 5 weeks at 15°C (Koning et al., 2007). After the aging period the remaining material was recovered, rinsed several times with deionized water and subsequently freeze-dried before use in the experiments (TP_{AGED} in Table 4.1).

The euryhaline diatoms (*Cyclotella meneghiniana*) were isolated from the Scheldte estuary (NW Europe, Baeyens et al., 1997) and grown in diluted artificial seawater enriched with culture medium. At the end of the exponential growth phase the culture was concentrated by centrifugation and subsequently dried at 40°C. The organic matter was removed by means of low-temperature ashing. Details of culturing conditions are given in Roubeix et al. (2008). Phytoliths were extracted from grass horsetail (*Equisetum arvense*), a known silicon accumulating plant, by heating the plant material for 6 hours at 450°C.

Core-top sediments were collected from Lake Myvatn, a shallow lake located in Iceland. The lake experiences seasonal diatom blooms, which cause the accumulation of biosiliceous sediments (Einarsson, 2004). The marine biosiliceous ooze is of Pliocene age; it was obtained from a core

Table 4.1 Siliceous materials used in the experiments.

ID	Material	Origin/description	Composition*	Further information
TP	Fresh diatom frustules	Monoculture of marine diatom Thalassiosira punctigera grown in open ocean surface water	Very low impurity levels Al/Si<0.001	Dissolution kinetics (Loucaides et al., 2008; Van Cappellen et al., 2002); ultrastructure (Vrieling et al., 2000)
TP_{AGED}	Artificially aged TP	TP aged in natural seawater for 5 weeks.	Very low impurity levels Al/Si<0.001	See above
CY	Fresh diatom frustules	Monoculture of euryhaline diatom Cyclotella meneghiniana grown in diluted artificial seawater	Very low impurity levels Al/Si<0.001	Dissolution kinetics (Roubeix et al., 2008)
EQ	Fresh phytoliths	Oxidative extraction of whole plant horsetails (Equisetum arvense)	Very low impurity levels Al/Si<0.001	Morphology, surface chemistry and dissolution kinetics (Fraysse et al., 2006; Loucaides et al., 2008)
LM	Biosiliceous lake sediment	Lake Myvatn: upper 2 centimeters of sediment core collected at 31 m water depth	Al/Si = 0.008 Fe/Si = 0.009 K/Si = 0.001	Environmental setting/ecology (Einarsson, 2004); dissolution kinetics (Loucaides et al., 2008)
ER	E. Rex Biosiliceous ooze sample	Weddell Sea: sample from 1 m thick diatomaceous layer in core collected at 3550 m water depth	Al/Si=0.003	Core location, dating, formation, environmental setting (Abelmann et al., 1988); dissolution kinetics (Loucaides et al., 2008)
DI	Diatomite ore	Miocene diatomaceous earth deposit from a mine in Lompoc, California (USA)	Al/Si = 0.029 Fe/Si = 0.007 K/Si = 0.005	Paleoenvironment and species composition (Moyle et al. 2002); dissolution kinetics (Loucaides et al., 2008)
AE	Aerosil® OX50 Synthetic amorphous silica	Pyrogenic, non-porous amorphous silica	Very pure; well characterized physico-chemical properties	Surface physicochemical properties (Gun'ko et al., 2005; Wang and Wunder, 2000; Wells et al., 2000); dissolution kinetics (Loucaides et al., 2008)

* Atomic ratios are based on ICP-MS analyses after total destruction of the samples.

from the Weddell Sea, within a layer consisting nearly exclusively of fragments of frustules from the diatom species *Ethmodiscus rex*. Descriptions of the core and the *E. rex* layer sampled are given in Abelmann et al. (1988). The diatomite was obtained as untreated ore material from a commercial mine in Lompoc, California, and dates from the Miocene. Details on the depositional setting and composition of the diatomite are summarized in Moyle and Dolley (2002). The various sediment samples were homogenized and air-dried prior to cleaning. Organic matter was removed by low-temperature ashing, by placing the samples for 4 hours in a Plasmaprep 300 plasma oven (<40°C). Subsequently, they were washed in 1 mol L^{-1} HCl overnight, in order to remove traces of $CaCO_3$.

A non-porous, fumed silica (Aerosil® OX50, Degussa GmbH) of high chemical purity was used as a synthetic reference material. Its specific surface area (50 m^2 g^{-1}) falls within the typical range

of diatom frustules and plant phytoliths (Dixit et al., 2001; Fraysse et al., 2006b). The material was used as received in the experiments.

The specific surface areas of the biosiliceous materials were determined by the conventional N_2-BET method using a Micromeritics Tristan 3000 analyzer. Samples were heated overnight at 90 °C and for one hour at 150 °C prior to analysis. The 8-point BET surface area was calculated from the N_2 absorption isotherm in the relative pressure range 0.07-0.20. The BET measurements were performed at NIOZ.

4.2.2 Acid-Base Titrations

Potentiometric titrations of silica suspensions were carried out in pH range 4-9 using 0.02M HCl and NaOH titrant solutions. The experiments were conducted at 25 ± 0.5° C in a 250 mL Teflon® reactor equipped with a Teflon® floating magnetic stirring bar. The suspension was continuously purged with purified argon gas. Acid and base were added at a maximum rate of 0.01 mL min^{-1} via two Metrohm Titrino® automated titrators. Each solid was titrated using 0.5 to 5 g L^{-1} suspensions in 0.01M, 0.1M, or 0.7M NaCl. The solid to solution ratio was adjusted according to sample availability and charge density (i.e. if the maximum excess proton concentration was low compared to the experimental error, the titration was repeated at a higher solid to solution ratio).

Preliminary results indicated that dissolution of the suspended silica at high pH caused hysteresis between the acid and base titrations. To minimize the impact of dissolution, dissolved silicate was added to the suspensions under the form of concentrated (6M) Na_2SiO_3 solution. By trial and error, it was found that addition of 600 µM dissolved silicate eliminated the hysteresis in the titration curves.

The "background" concentration of protons $[H^+]$ was determined by titrating the electrolyte plus dissolved silicate solution, prior to the addition of the solid, in both directions (i.e. with base and acid addition respectively). Each titration was performed in 30, 9 mV steps between -90 and 180 mV. At the end of each step, equilibrium was assumed once the potential remained constant for longer than 5 minutes. Next the solid was added to the electrolyte solution, and the suspension was kept at pH 4 for a minimum of one hour and until the pH was constant for at least 5 minutes. The suspension was then titrated in both directions with base and acid, respectively, as previously described.

Based on the assumption that under the experimental conditions, acid consumption by the silica suspensions was due to the protonation of $>SiO^-$ groups, the concentration of deprotonated sites was given by the excess proton concentration $[H^+]_{XS,}$ calculated as

$$\left[H^+\right]_{XS} = C_A - C_B + \left[H^+\right]_{INI} - \left(\frac{10^{-pH}}{\gamma_{H^+}} + \frac{10^{-pKw+pH}}{\gamma_{OH^-}}\right) - \left[H_4SiO_4\right]_T \cdot \left(\frac{10^{-pH}\gamma_{H_3SiO_4^-}}{K_a} + 1\right)^{-1} \quad (3)$$

where C_A and C_B are the concentrations of added acid and base, respectively. The initial proton concentration $[H^+]_{INI}$ in the reactor after addition of the solid was calculated from the measured solution pH, assuming that $[H^+]_{XS}$ was equal to zero at pH 4. The activity coefficients of H^+ and OH^- (γ_{H^+}, γ_{OH^-}) were calculated for the appropriate ionic strength using the Pitzer model (Pitzer, 1973), while the acid dissociation constant of silicic acid (pKa) and activity coefficient $\gamma_{H_3SiO_4^-}$ were taken from Millero (1995). The total dissolved silicate concentration $[H_4SiO_4]_T$ was set to $6x10^{-3}$ M. Dividing the volumetric concentration of $[H^+]_{XS}$ by the mass of silica or the N_2-BET surface area, $[H^+]_{XS}$ was expressed per gram of solid, or per m^2 of BET surface.

The second part of equation 3 represents the background proton concentration $[H^+]_{BGR}$ in the electrolyte solution:

$$[H^+]_{BGR} = \left(\frac{10^{-pH}}{\gamma_{H^+}} + \frac{10^{-pKw+pH}}{\gamma_{OH^-}} \right) - [H_4SiO_4]_T \cdot \left(\frac{10^{-pH}\gamma_{H_3SiO_4^-}}{K_a} + 1 \right)^{-1} \quad (4)$$

Equation 4 was fitted to the background titration curve by finely adjusting the slope and intercept of the pH calibration curve (Fig. 4.1). Changes in slope and intercept never exceeded 0.0005% and 0.05% respectively. Fitting equation 4 to the background titration curve was then used to calculate $[H^+]_{XS}$ at each of the 30 end points of a given titration (Fig. 4.1).

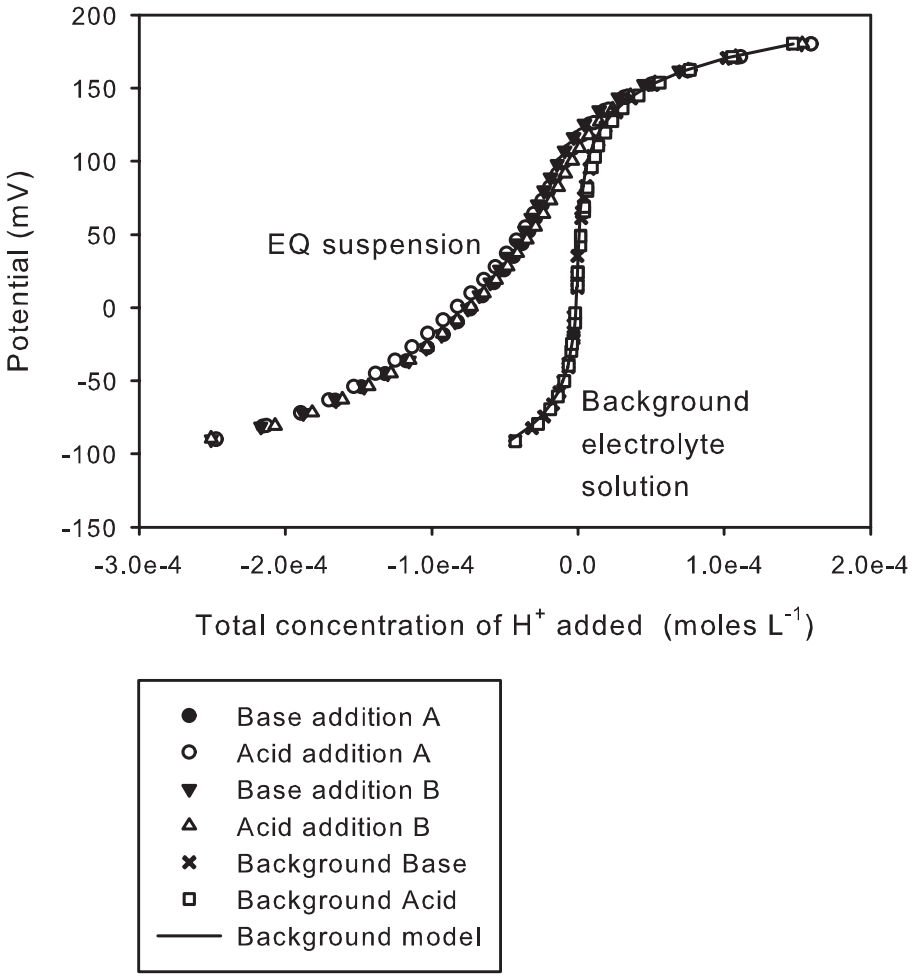

Figure 4.1 Total concentration of H^+ versus potential measured at 25° C during the titration of EQ in 0.1 M NaCl. The solid to solution ratio was equal to 0.7 g L^{-1}. The background titration was performed once in both alkaline and acid directions. After the addition of the solid the suspension was titrated twice in each direction (additions A and B). The solid line represents the model fit to the background titration data (see Eq. 4). The difference between the background curve and the suspension titration curve is equal to excess proton concentration $[H^+]_{XS}$ of the silica.

4.2.3 Surface Complexation Modeling

The working hypothesis is that silanol groups exist in two distinct regions of a $bSiO_2$ particle: namely on the external surface of the particle (outer region), and within the particle (inner region). The external surface of the particle is in direct contact with the electrolyte solution, hence the surface potential for a given surface charge is dependent on the composition and concentration of the background electrolyte. In contrast, silanol groups in the inner region are not in direct contact with the outside solution, and their protonation-deprotonation should therefore be less sensitive to changes in the electrolyte composition.

To account for the existence of the two populations of silanol groups the classical surface complexation model was adapted using the software Visual MINTEQ_v. 2.53. The acid- base properties of the outer region were simulated using the diffuse double layer model (DDL), which accounts for electrostatic interactions at the surface due to the presence of electrolyte ions. The external surface area was obtained from the N_2-BET measurements, while the surface site density (i.e. the concentration of silanol groups on the external surface) was fixed at 4.6 silanol groups per nm^2, a value widely accepted for amorphous silicas (Zhuravlev, 1993). The acid-base chemistry of the inner region was modeled using the constant capacitance model (CCM), assuming that the capacitance is independent of the ionic strength of the bulk electrolyte solution. Its value was arbitrarily set equal to 1.5 Fm^{-2}. The site density of the silanol groups within the bulk solid was treated as a fitting parameter.

4.2.4 FTIR Spectroscopy

Infrared spectra were collected with a Jasco FTIR 470*plus* spectrometer. Silica samples were mixed with spectroscopic grade KBr in a ratio of 1/100 and pressed into tablets. The tablets were analyzed in transmission mode with a resolution of 0.5 cm^{-1}. The absorption bands at 800, 950 and 1100 cm^{-1} were integrated by the instrument's software.

4.3 Results

4.3.1 Acid-Base Titrations

The large differences in negative charge ($>SiO^-$) build-up among the various siliceous materials is illustrated in Fig. 4.2. In Fig. 4.2a, $[H^+]_{XS}$ is expressed in moles per m^2 of BET surface area, and in Fig. 4.2b per gram of $bSiO_2$. The results show that with increasing pH the $bSiO_2$ particles became increasingly negatively charged and that complete deprotonation of ionizable groups did not take place within the experimental pH range. Figures 4.2a and 4.2b suggest a general trend in which the negative charge density declined from the "fresh" cultured diatoms (TP and CY) to the older Southern Ocean sediment (ER) and diatomite (DI) samples. The two fresh diatom samples (CY and TP) exhibited significantly higher negative $[H^+]_{XS}$ than all other materials, particularly when normalized to the BET surface areas (Fig. 4.2a). Furthermore, the $[H^+]_{XS}$ values at high pH yielded surface densities of silanol groups close to an order of magnitude higher than those expected for silica surfaces, which is around 4.6 sites nm^{-2} (Zhuravlev, 1993).

While for synthetic AE and a number of the biosiliceous materials the excess proton concentrations were dependent on the ionic strength of the electrolyte solution, this was not systematically the case (Fig. 4.3). In particular, the negative charging of the "fresh" diatom samples TP and CY with increasing pH was practically identical in 0.01M, 0.1M, and 0.7M NaCl. The TP frustules aged in seawater for 5 weeks (TP_{AGED}), however, showed systematically higher negative

$[H^+]_{XS}$ with increasing ionic strength of the electrolyte. The relative effect of ionic strength on the negative charge build-up of the silicas declined in the order AE>EQ>LM>TP_{AGED}>TP=CY. For AE, EQ, LM, and TP_{AGED}, the negative $[H^+]_{XS}$ at pH 8 was higher by 230%, 93%, 63%, and 28%,

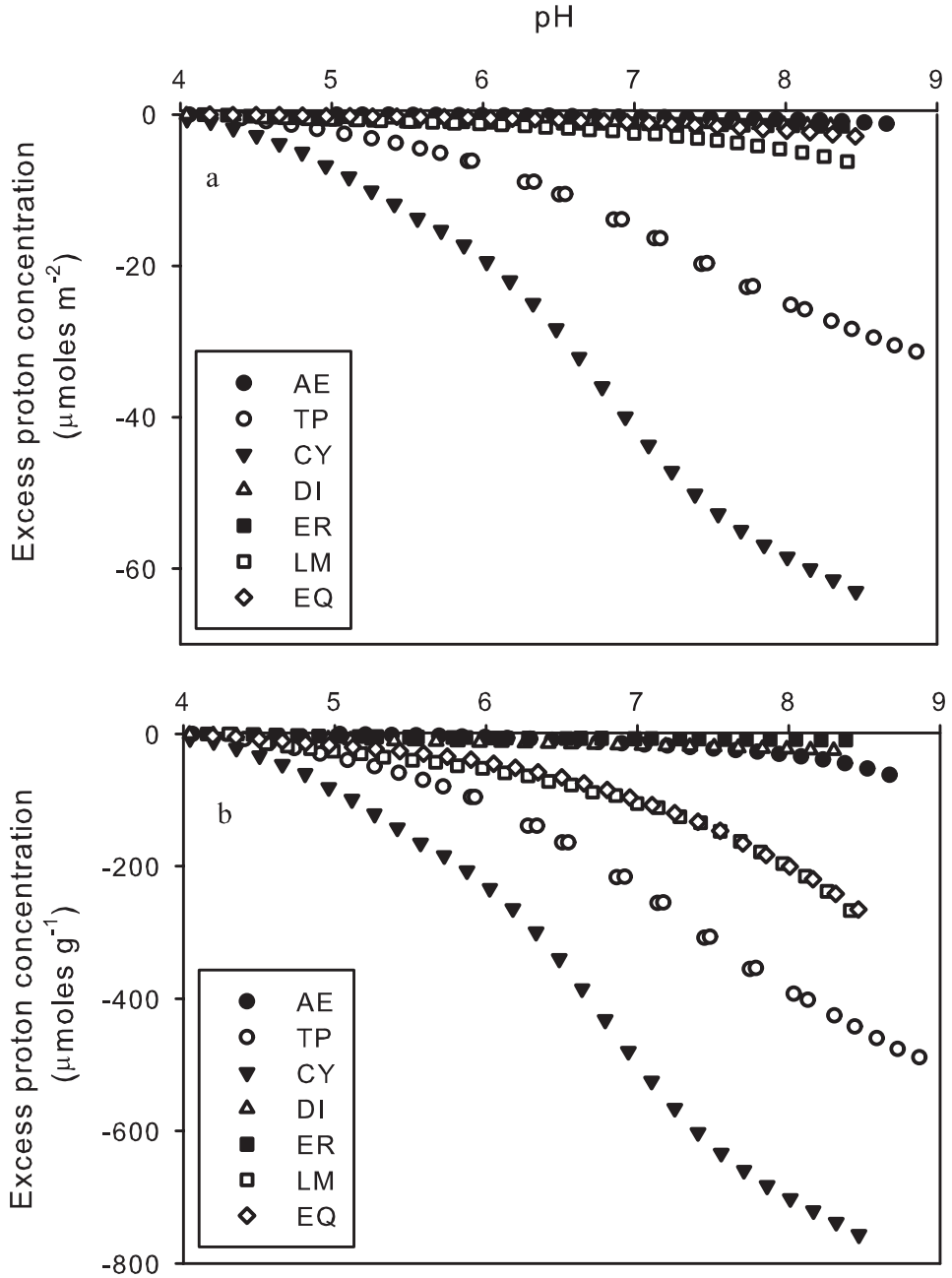

Figure 4.2 Excess proton concentrations normalized to BET surface areas (a) and silica mass (b). Results shown are from acid-base titrations in 0.1M NaCl and 25°C. See Table 4.1 for the identification of the siliceous materials.

in 0.7M NaCl than in 0.01M NaCl. Because of the limited availability and relatively low $[H^+]_{XS}$ of the fossil biogenic silicas (ER, DI), we were unable to accurately determine the effect of ionic strength on the charging of the materials. For this reason, the titration results for ER and DI were not included in the modeling part of the study.

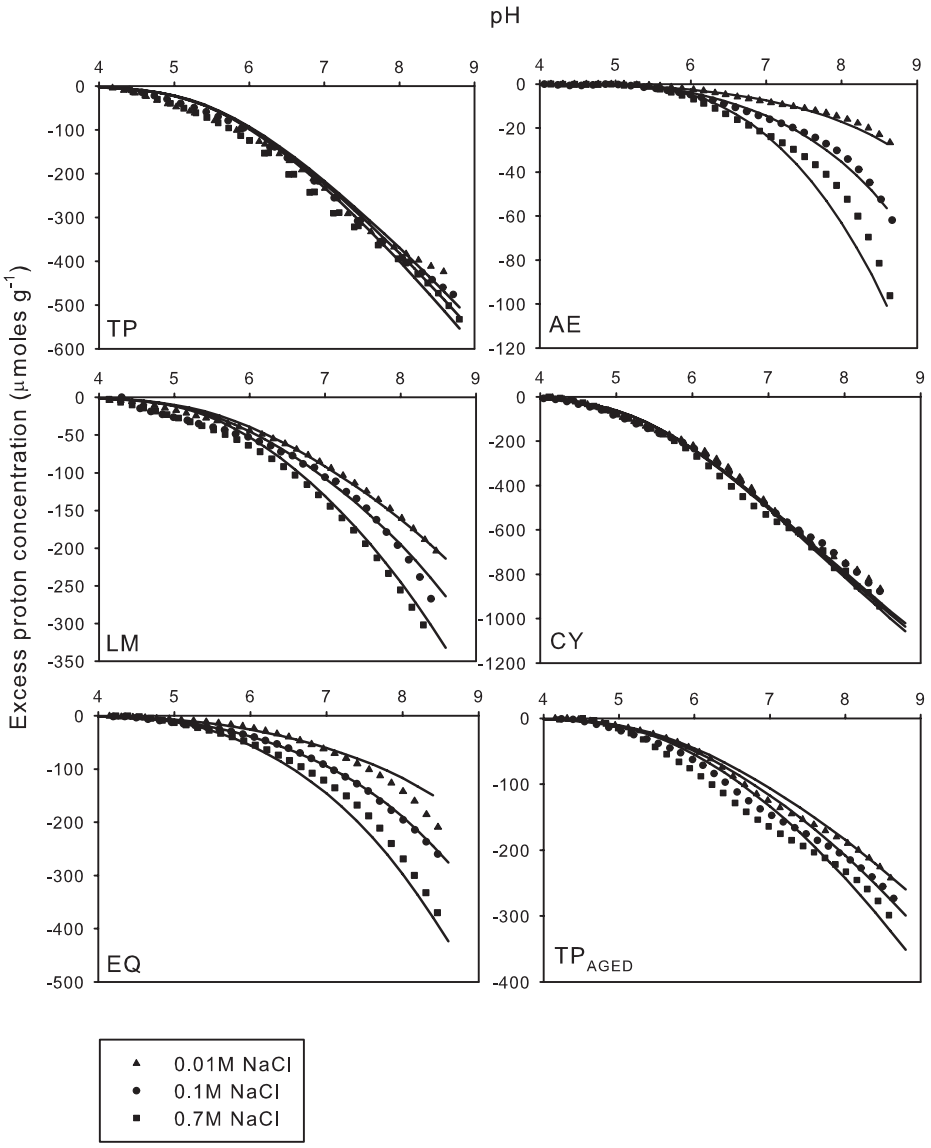

Figure 4.3 Excess proton concentrations derived from acid-base titrations (symbols) in 0.01, 0.1, and 0.7M NaCl at 25° C. Solid lines represent model fits to the data. Corresponding model parameters are listed in Table 4.2. Note the differences in vertical scales. See text for complete discussion.

4.3.2 Surface Complexation Modeling

Model fits are shown in Fig. 4.3 along with the experimental $[H^+]_{XS}$ versus pH curves data. The specific surface area of each material measured by N_2 BET (Table 4.2) was imposed as the outer surface area. The site density of the outer surface was assumed equal to 4.6 sites nm^{-2} in all simulations. This site density value has been experimentally and theoretically validated for amorphous silica (Iler, 1979; Sahai and Sverjensky, 1997; Zhuravlev, 1993). For all biogenic materials reasonable model fits could be obtained by using the same acid dissociation constant (pKa_{int}=6.8) for the outer silanol groups. For AE a higher pKa_{int} value of 7.8 was required to reproduce the shape of the $[H^+]_{XS}$ versus pH curve. Note that the values of the deprotonation constants used fall within the range reported for $bSiO_2$ and synthetic amorphous silicas (Dixit and Van Cappellen, 2002).

The model was fitted to the experimental data by adjusting the site density of the inner region. Fig. 4.4 shows an example of model results for the phytoliths (EQ) at 0.01M, 0.1M, and 0.7M NaCl. The site density of the inner region was kept constant for the three ionic strengths. Note that in the model simulations the electrostatic effects are entirely due to the response of the outer silanol groups. In other words, the sensitivity of $[H^+]_{XS}$ to the ionic strength of the solution depends on the relative importance of outer and inner silanol group densities. For the fresh diatom frustules (TP and CY), very high internal silanol densities were needed to reproduce the high negative charge build-up. In addition, because of the large excess of inner sites the model-predicted charging of the silica particles was not sensitive to changes of the ionic strength of the bulk electrolyte.

Based on the model fits, the inner site density increased from zero for the (non-porous) synthetic amorphous silica (AE) to $2.1x10^{21}$ sites per gram for the fresh CY diatom sample, in the order AE<EQ≤LM<TP_{AGED}<TP<CY (Table 4.2). The contributions of surface sites (outer region) to the total number of ionizable sites (inner and outer regions) were equal to 100%, 75%, 35%, 23%, 7%, and 2.6% for AE, EQ, LM, TP_{AGED}, TP, and CY respectively.

4.3.3 FTIR Spectra

Generally, FTIR spectra of amorphous silica exhibit four vibration bands (Iler, 1979; Legrand, 1998). The two main bands at 1100 and 471 cm^{-1} are attributed to the stretching and bending vibration modes of the SiO_4 tetrahedron respectively. The band at 800 cm^{-1} is attributed to the

Table 4.2 Model-derived site densities for the external surface (outer) and bulk (inner) regions of different siliceous materials. The acid-base chemistry of the external surface was modeled using the diffuse double layer model, that of the inner region using the constant capacitance model. The deprotonation constant pKa_{INT} for the silanol groups of the biosiliceous materials was 6.8 and for the synthetic silica (AE) 7.8. The capacitance of the inner region was fixed at 1.5 Fm^{-2}. The specific surface areas (SSA) reported were determined by the N_2-BET method.

Material	SSA (m^2g^{-1})	Site density (OH g^{-1})	
		Surface	Bulk
TP	16	$7.4x10^{19}$	$1.0x10^{21}$
TP_{aged}	30	$1.4x10^{20}$	$4.6x10^{20}$
LM	43	$2.0x10^{20}$	$3.7x10^{20}$
AE	50	$2.3x10^{20}$	0
CY	12	$5.5x10^{19}$	$2.1x10^{21}$
EQ	93	$4.3x10^{20}$	$1.4x10^{20}$

bending vibration mode of inter-tetrahedral Si-O-Si bonds, while, the band around 950 cm $^{-1}$ represents the Si-O stretching of Si-OH groups (Fig. 4.5). The ratio between the integrated intensities of the 800 and 1100 cm^{-1} ($A_{800\ cm\text{-}1}/A_{1100\ cm\ -1}$) absorption bands can be used as an

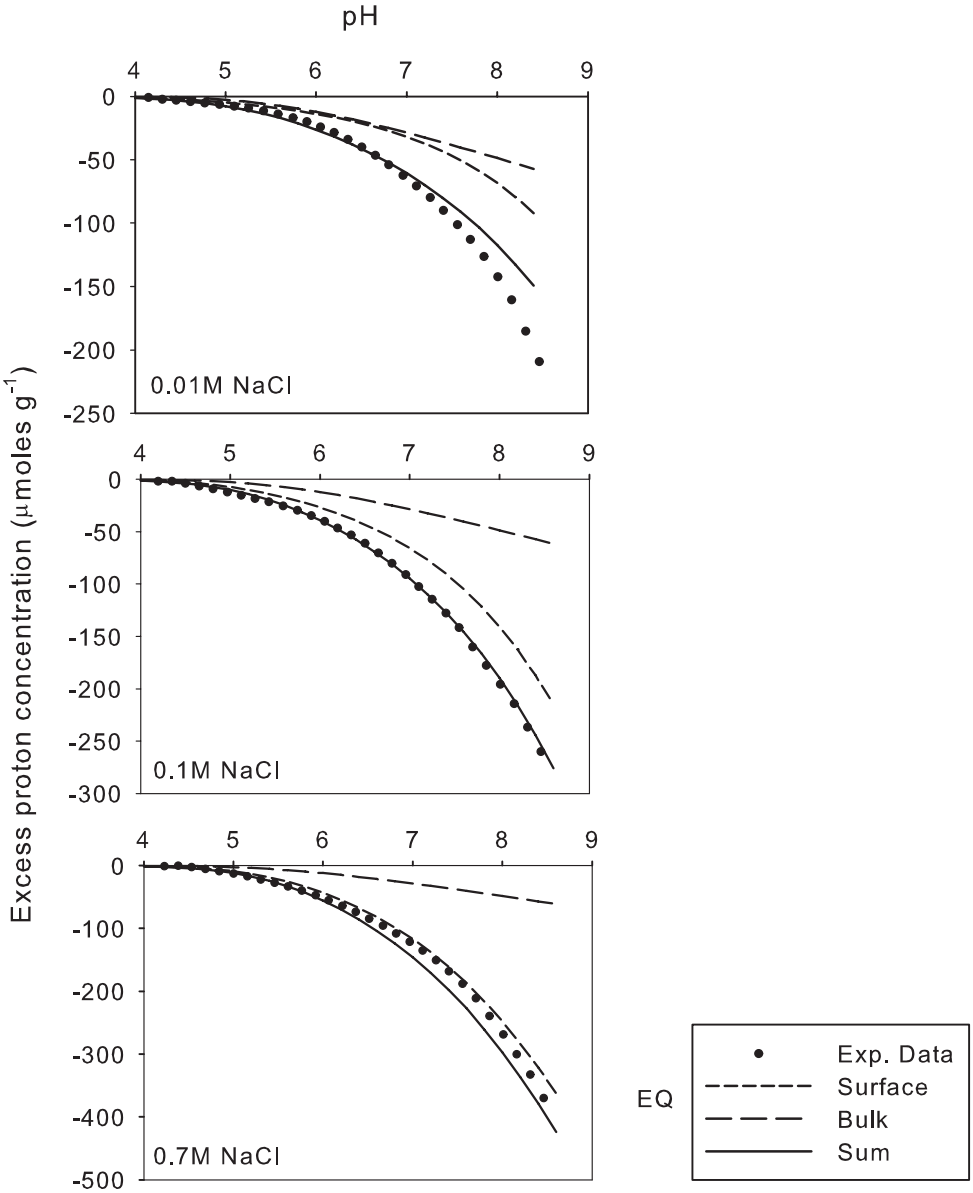

Figure 4.4 Excess proton concentrations of fresh phytoliths (EQ) measured in acid-base titrations (symbols) at 0.01, 0.1, and 0.7 M NaCl. The short dashed line represents the internal excess proton concentration calculated using the constant capacitance model and the long dashed line the external (surface) excess proton concentration calculated using the diffuse double layer model. Solid lines are the sum of the internal and external excess proton concentrations. Note the differences in vertical scales. See Table 4.2 for corresponding model parameters.

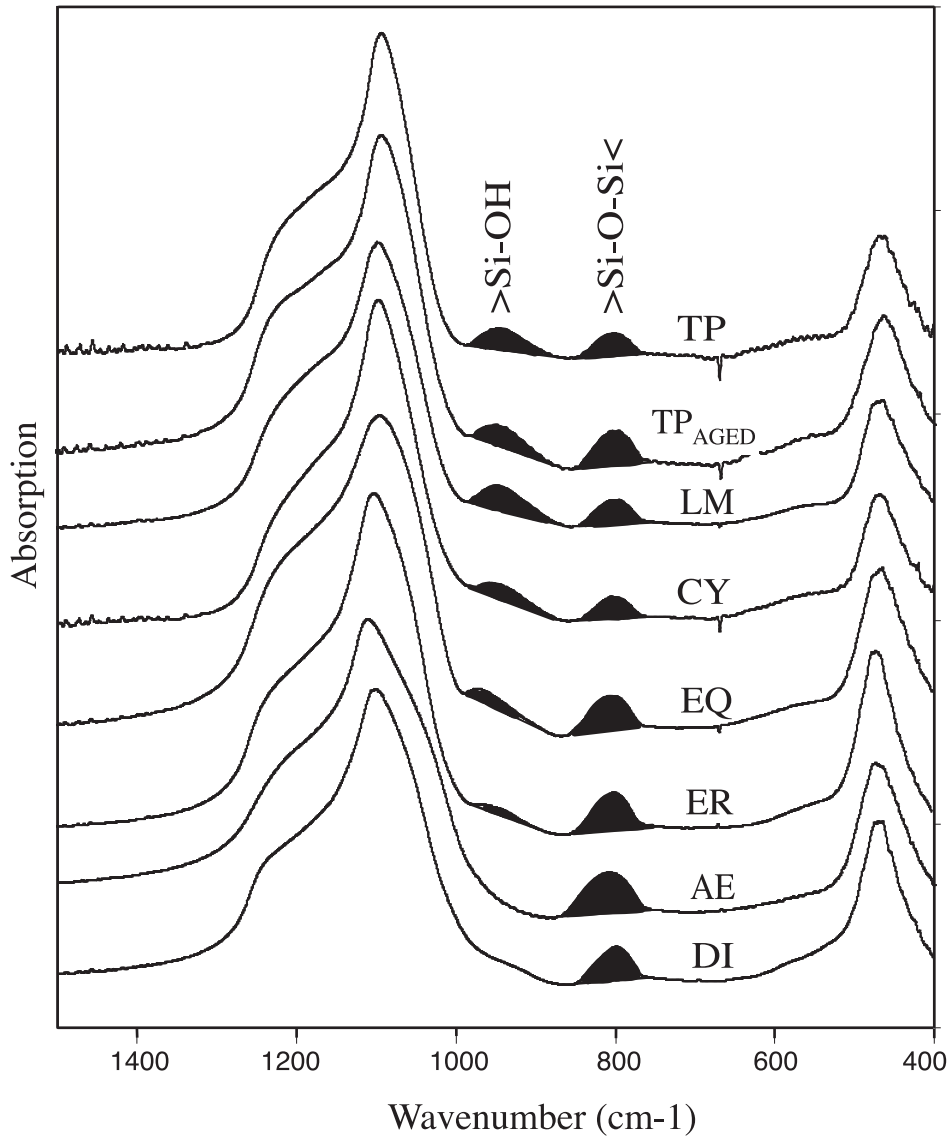

Figure 4.5 Fourier Transform Infrared (FTIR) absorption spectra of the siliceous materials used in this study (see Table 4.1 for identification of the materials). Integrated band ratios A_{950}/A_{800} provide a measure of the relative abundances of silanol groups in the silica samples, while A_{800}/A_{1100} ratios are an indication of the ordering of the amorphous SiO_2 network.

indication of the degree of organization or ordering of the SiO_2 framework (Gendron-Badou et al., 2003). The ratio between the integrated intensities of the 950 and 800 cm^{-1} ($A_{950\ cm\text{-}1}/A_{800\ cm\ -1}$) absorption bands accounts for the relative abundance of silanol groups in the SiO_2 network (Schmidt et al., 2001). While the ($A_{800\ cm\text{-}1}/A_{1100\ cm\ -1}$) ratios were comparable among the different materials, the ($A_{950\ cm\text{-}1}/A_{800\ cm\ -1}$) ratio varied significantly (Table 4.3). The absorption band at

Table 4.3 Band intensity ratios for the FTIR spectra shown in Fig. 4.5. The A_{800}/A_{1100} ratio is a measure of the degree of ordering of the SiO_2 framework, while the A_{950}/A_{800} ratio is a measure of the relative abundance of silanol groups.

Material	A_{800}/A_{1100}	A_{950}/A_{800}
TP	0.03	0.98
TP_{AGED}	0.04	0.55
LM	0.03	0.97
ER	0.04	0.12
DI	0.04	~0
AE	0.05	~0
CY	0.03	0.63
EQ	0.03	0.30

950 cm^{-1} was strongest for the fresh diatom and phytolith samples (TP, CY, EQ, LM), while it dropped for the older fossil samples (Fig. 4.5). Note also that the 950 cm^{-1} band was undetectable on the AE spectra.

4.4 Discussion

4.4.1 Acid-Base Titrations

The titration procedure used in this study yields reproducible and consistent acid and alkaline titration curves for biogenic and synthetic amorphous silicas. The addition of dissolved silicate to the background electrolyte avoids hysteresis between consecutive acid and base titrations caused by dissolution of the reactive solid (Karlsson et al., 2001; Osthols, 1995). Titration of the electrolyte solution prior to adding the solid further eliminates uncertainties that arise when the background proton concentration $[H^+]_{BGR}$ is measured separately, or when it is estimated theoretically. Fitting of the electrolyte titration curve also allows one to fine-tune the pH electrode calibration, thereby increasing the accuracy of the estimation of the initial proton concentration ($[H^+]_{INI}$, see equation 3).

The $[H^+]_{XS}$ versus pH curves in Fig. 4.2 show the characteristic electrical charging behavior of silicas, in which significant deprotonation takes place above pH 5-6, that is, well beyond the pH of zero charge (pH 2-3) (Iler, 1979; Legrand, 1998). Even beyond pH~8.5 the negative excess proton concentration $[H^+]_{XS}$ continues to increase implying that at relatively high pH some silanol groups remain protonated. The general shapes of the titration curves in Fig. 4.2 and 4.3 agree with those of amorphous and crystalline silicas observed in previous studies (de Keizer et al., 1998; Prelot et al., 2002; Riese, 1982; Sonnefeld, 1996; Sonnefeld et al., 2001; Wells et al., 2000). The $[H^+]_{XS}$ of AE in 0.1M NaCl and at pH 8 equals -6.5 x 10^{-7} moles m^{-2} which corresponds to a surface charge density σ of -0.05 C m^{-2}. This value is in close agreement (± 0.005 C m^{-2}) with values reported for other synthetic amorphous silicas (de Keizer et al., 1998; Prelot et al., 2002; Sonnefeld, 1996), but also for quartz (-0.07 C m^{-2}, Riese 1982) measured under comparable conditions.

The charge build-up of the biosiliceous materials varies by several orders of magnitude (Fig. 4.2). Large variations in the electrical charging of $bSiO_2$ have also been reported in the few published studies (Dixit and Van Cappellen, 2002; Fraysse et al., 2006b). This is true whether the measured negative charge is normalized by the BET surface area or the mass of the solid. Fig. 4.2a and b

suggest a trend in which the negative excess proton concentration declines with the sample's age. The freshly cultured diatom frustules CY and TP show significantly higher negative $[H^+]_{XS}$ values than the sediment material LM, DI, and ER. Dixit and Van Cappellen, (2002) observed a similar pattern when comparing the surface charge density of freshly cultured diatoms and that of a biosiliceous ooze collected from the seafloor.

The BET surface area normalized $[H^+]_{XS}$ versus pH plots of Fig. 4.2a illustrate one obvious problem. Based on theoretical considerations and extensive experimental data (Zhuravlev, 1993), the total number of silanol groups on silica surfaces should be on the order of 8 μmoles m^{-2}. Fig. 4.2a, however, shows that for several $bSiO_2$ samples $[H^+]_{XS}$ under alkaline pH exceeds this value, in the case of CY and TP by several orders of magnitude. Unrealistically high surface charge densities have been previously reported for porous synthetic silicas (de Keizer et al., 1998) and for plant phytoliths (Fraysse et al., 2006b). In the case of porous synthetic silicas, de Keizer et al. (1998) suggest that the measurement of the specific surface area by N_2-BET is biased by the size and shape of the pores which are inaccessible to the relatively large N_2 molecule. Furthermore, micropores are likely to contain surface bound water that is not removed by the BET drying procedure, thereby preventing N_2 molecules from entering the pores.

Diatom frustules are characterized by an intricate architecture and elaborate pore structure with pore diameters on the order of a few nanometers (Vrieling et al., 2000). It is thus reasonable to assume, especially in the case of "fresh" diatom frustules, that a large fraction of the site density measured through acid-base titrations corresponds to silanol groups present in confined pore spaces inaccessible to N_2 molecules. Thus, we hypothesize that differences in microporosity between different $bSiO_2$ samples explain the variations in charge densities reported in the literature (Dixit and Van Cappellen, 2002; Fraysse et al., 2006b), and observed in this study.

The titration data of Fig. 4.3 present yet another intriguing feature of biogenic silicas. In the case of the fresh diatom frustules (CY and TP), the $[H^+]_{XS}$ measured through acid-base titrations is largely independent of the ionic strength of the electrolyte solution. According to the Gouy-Chapman theory, however, the surface charge density of an oxide mineral should be a function of the ionic strength of the electrolyte solution. A higher concentration of electrolyte ions leads to a reduction of the double layer thickness and an increase of the surface charge density of the oxide (Stumm, 1992). The acid-base properties of AE exhibit this expected behavior (Fig. 4.3). Some of the biosiliceous materials, e.g. LM and EQ, also exhibit the expected dependence of surface charging on electrolyte concentration. Aging of fresh frustules in aqueous solution further induces the appearance of a dependence of surface charging on ionic strength (compare TP and TP_{AGED} in Fig. 4.3).

The acid-base titration data obtained in this study present a unique acid-base behavior of $bSiO_2$ that, to our knowledge, has not been previously documented. Our results further indicate that for the "fresh" diatom frustules, the exceptionally high negative $[H^+]_{XS}$ and the lack of dependence of electrical charging on the ionic strength of the electrolyte solution are likely interrelated phenomena. Comparing Fig. 4.2a and Fig. 4.3, it becomes apparent that a negative correlation exists between the magnitude of $[H^+]_{XS}$ (in sites m^{-2}) and the sensitivity of $[H^+]_{XS}$ to the electrolyte concentration. This relationship can be explained by assuming that the silanol groups located beneath the BET-accessible surface area are not (or only weakly) affected by changes in the ionic strength, because the electrolyte counterions are too large to reach the internal silanol groups.

Previous experimental work has demonstrated that the charge density of porous synthetic silica is a function of the hydrated radius of the electrolyte counterion (de Keizer et al., 1998). Titrations in electrolytes such as $LiNO_3$ and KNO_3 yielded higher apparent surface charge

densities than titrations in electrolytes with significantly larger counterions such as Tetramethyl- or Tetrabutylammonium nitrate. In comparison, for AE, a non-porous pyrogenic amorphous silica, titrations in different electrolytes gave near-identical results. Thus, the acid-base behavior of porous silicas is not only a function of the physical properties of the solid but also those of the electrolyte.

Further evidence for the existence of two pools of silanol groups in $bSiO_2$ comes from the observed changes in charging behavior when fresh diatom frustules are aged in seawater. Five weeks of exposure to seawater markedly reduced the negative charge build-up of TP (Fig. 4.2), while increasing the sensitivity to the ionic strength of the electrolyte (Fig. 4.3). The BET surface area also increased after the 5-week exposure (Table 4.2), possibly due to dissolution of the outer silica layer, thereby exposing internal porosity previously inaccessible to N_2 molecules. Both the increase of the BET surface area and the decrease of the relative amount of internal silanol groups contributed to the appearance of a small but measurable ionic strength effect on $[H^+]_{XS}$ of the aged material (Fig. 4.3).

4.4.2 Surface Complexation Modeling

The surface complexation modeling builds on the interpretation of the acid-base titration results given earlier, by assuming that (1) a fraction of the ionizable functional groups of $bSiO_2$ resides below the outer surface area accessible to N_2 molecules, and (2) the dependencies of the proton exchange reactions of inner and outer sites on the concentration of the bulk electrolyte are fundamentally different. With these assumptions, and using reasonable model parameters, the two-site (surface and internal) model reproduces the acid-base behavior of the various $bSiO_2$ materials. A value of 6.8 for the intrinsic deprotonation constant pKa_{int} (eq. 2) produces good fits for all biogenic materials, and is in good agreement with previously reported values for $bSiO_2$ (Dixit and Van Cappellen, 2002). The higher pKa_{int} value for the synthetic silica AE (pKa_{int}=7.8) is also consistent with the observations of Dixit and Van Cappellen (2002), who used a value of 7.5 to reproduce titration curves for Aerosil® 200.

The $[H^+]_{XS}$ of the inner region was calculated using the constant capacitance model (CCM), which requires a capacitance value for the electrical double layer. Note that the choice of the CCM is arbitrary, as the structure and the physicochemical properties of the inner region (i.e. pore size/geometry, counterion concentration) that define the electrostatic conditions within the bulk solid are unknown. Nevertheless, good fits were obtained by setting the capacitance C to 1.5 Fm^{-2}, similar in magnitude to values reported in the literature for the silica-water interface (Dixit and Van Cappellen, 2002; Sahai and Sverjensky, 1997). It is important to stress, however, that the physical meaning of the bulk capacitance value cannot be ascertained. Sensitivity analyses show that capacitance values between 0.6 and 3 Fm^{-2} yield good model fits, although changing C requires the simultaneous adjustment of the inner site density. With C= 1.5 Fm^{-2}, the silanol density of the inner region calculated by the model ranges between zero for AE to $2.1x10^{21}$ sites g^{-1} for CY, in the order $AE<EQ\leq LM<TP_{AGED}<TP<CY$.

We hypothesize that the inner silanol groups are either on the surface of nanoscale size pores, or are part of a partially hydrated amorphous silica network where protons can be exchanged across water molecules inside a gel-like structure. The existence of such a gel-like structure has been previously proposed (de Keizer et al., 1998; Lyklema, 1968; Perram, 1973; Perram et al., 1973; Tadros and Lyklema, 1968) to explain the apparent inconsistency between high charge densities and relatively low electrophoretic mobilities observed for porous synthetic silicas (Lyklema, 1968). The latter observation implies that a significant fraction of the electrical charge measured through

acid-base titration is not located at the solid/solution interface, where it affects the electrophoretic mobility of the particles.

Tadros and Lyklema (1968) observed that the charge density of porous synthetic amorphous silica is a function of the ionic radius of the electrolyte's cation (i.e. $Li^+ < Na^+ < K^+ < Cs^+$), while the charge density measured in $(C_2H_5)_4NCl$ is independent of the concentration of the bulk electrolyte. de Keizer et al. (1998) reported a similar negative correlation between counterion radius and the charge density of porous synthetic silica. In line with this previous work, our titration results show a lower or even a complete lack of effect of the electrolyte concentration on the negative charge density of some of the $bSiO_2$ materials used. The lack of response to changes in the bulk ionic strength suggests that the access of electrolyte counterions to the inner region is restricted by the size of the micropores or the permeability of the gel-like layer. The results further suggest that the inner region of the $bSiO_2$ materials becomes saturated with Na^+ counterions already at the lowest electrolyte concentration used in the experiments (0.01M). Therefore, an increase in electrolyte concentration of the bulk solution affects only the negative charge carried by the outer region, which in some cases (TP, CY) is too small, relative to the inner charge density, to be detected.

The relative abundance of inner and outer sites determines the sensitivity of the total negative charge density to the electrolyte's concentration. The model-estimated inner and outer site densities for the different materials are compared in Table 4.2. The site densities of the inner region range between 0 for AE to 3.4×10^{-3} moles of sites g^{-1} for CY. The latter represents approximately 20% of all the Si atoms of the silica particle. If one assumes that all silanol groups are surface-bound, then based on a surface site density of 4.6 sites nm^{-2}, the specific surface area would range between 50 $m^2\ g^{-1}$ (AE) to 462 $m^2\ g^{-1}$ (CY). Specific surface areas in the order of 400 $m^2\ g^{-1}$ and larger are not unusual for porous synthetic silicas (Zhuravlev, 1993).

4.4.3 Spectroscopic Evidence

FTIR spectroscopy has been used previously to describe silica aging from fresh phytoplankton $bSiO_2$ to sedimentary opal (Schmidt et al., 2001). The Si-O stretching of silanol groups shows a band around 950 cm^{-1}, while at 800 cm^{-1} a vibration band corresponds to fully condensed Si atoms surrounded by four Si-O-Si linkages. The ratio of the two integrated peaks therefore provides an estimate of the abundance of silanol groups in the silica framework. The calculated ratios $A_{950/800}$ in Table 4.3 show that the relative abundance of silanol groups increases in the order of AE~DI<ER<EQ<TP_{AGED}<CY<LM<TP. In line with Schmidt et al. (2001), the silanol abundance generally decreases with the age of the $bSiO_2$ material.

The absence of a detectable absorption band at 950 cm^{-1} for AE is consistent with the absence of internal silanols for this synthetic silica. Previous FTIR studies of the surface of non-porous aerogels showed that the absorption band at 950 cm^{-1} only becomes visible at relatively high specific surface areas (>200m^2g^{-1}) (Gun'ko et al., 2005).

Gendron-Badou et al. (2003) propose that the ratio between the integrated intensities of the 800 and 1100 cm^{-1} ($A_{800/}A_{1100}$) absorption bands can serve as an indication of the degree of organization or ordering of the SiO_2 framework. These authors found that the $A_{800/}A_{1100}$ ratio of cultured diatoms (*Chaetoceros* genus) is about 0.003, while for fossil diatoms and sponge spicules the ratio is significantly higher (0.04). Surprisingly the $A_{800/}A_{1100}$ ratios calculated from our FTIR spectra do not vary much between aged and fresh $bSiO_2$ samples (Table 4.3). The young biosiliceous materials (TP, CY, LM, EQ) have $A_{800/}A_{1100}$ ratios (0.03) that are only slightly lower than those of the fossil diatoms (ER, DI) and the aged TP sample (0.04). This can be explained by the relatively low number of internal Si atoms that are hydroxylated (<20%, Table 4.2) in the fresh

$bSiO_2$ materials used here. Note that the A_{800}/A_{1100} ratio for AE (0.05) is practically the same value as that reported for quartz (Frohlich, 1989).

The A_{950}/A_{800} ratios estimated from the FTIR spectra support our hypothesis that fresh $bSiO_2$ exhibits a higher relative abundance of internal silanol groups than aged material. With one exception (EQ), the BET specific surface areas of the biogenic materials used in this study (Table 4.2) are less than that of AE. Thus, the FTIR absorption band at 950 cm^{-1} mainly represents silanol groups within the bulk of the material. It would thus appear that a major aging process of $bSiO_2$ involves the progressive disappearance of hydroxylated sites within the silica framework.

4.4.4 Electrical Charging and Dissolution Kinetics of Biogenic Silica

It is generally agreed that the pH dependence of silica dissolution kinetics reflects the speciation of the mineral-water interface (Dove and Elston, 1992; Fraysse et al., 2006b; Loucaides et al., 2008; Van Cappellen and Qiu, 1997b; Wirth and Gieskes, 1979). In particular, above pH_{zpc}, the acceleration of the dissolution rate with increasing pH is explained by the increase in concentration of deprotonated >Si-O^- sites at the solid's surface (Brady and Walther, 1990; Fleming, 1986; Grauer and Stumm, 1982; Wirth and Gieskes, 1979). The negatively charged sites promote dissolution kinetics, either by enhancing the nucleophilic properties of water (Dove, 1994) or polarizing, and thus weakening, surface siloxane bonds (Brady and Walther, 1990). For quartz and non-porous amorphous silicas, the dissolution rate is directly proportional to the surface density of deprotonated silanol groups (Brady and Walther, 1990; Fleming, 1986; Wirth and Gieskes, 1979).

In Fig. 4.6a and 4.6b, the dissolution rate constants of the various silicas used in the present study are plotted against the measured total excess proton concentrations and the model estimated surface excess proton concentrations (at pH 8 and in 0.7 M NaCl), respectively. The dissolution rate constants of AE, TP, LM, EQ, DI, and ER were derived from the dissolution rates and solubilities measured in seawater at 25°C by Loucaides et al. (2008), assuming a linear dissolution rate law (Van Cappellen et al. 2002a). For CY, the dissolution rate constant was obtained from the results of the dissolution experiments in artificial seawater (pH 7.8) and at 20°C of Roubeix et al. (2008).

The dissolution rate constants correlate poorly with the total excess proton concentration (Fig. 4.6a). In contrast, a strong correlation emerges when the dissolution rate constants are plotted against the excess surface proton concentrations (Fig. 4.6b). This suggests that only silicate groups located on the external surface are released to solution. As a corollary, the N_2-BET method should provide good estimates of the surface areas of biosiliceous materials that take part in the dissolution process.

It is important to note that the relationship between the dissolution rate constant and the excess surface proton concentration in Fig. 4.6b is not a linear one, as in the case of quartz (Brady and Walther, 1990) and non-porous amorphous silica (Fleming, 1986). The higher order dependency observed in our results can be explained by differences in solubility of the various biogenic silicas. More soluble, and hence thermodynamically less stable, silica phases dissolve intrinsically faster than less soluble ones (Wollast, 1974; Loucaides et al 2008). The former phases are generally also those exhibiting the highest outer surface excess $[H^+]_{XS}$. The non-linear relationship in Fig. 4.6b thus combines the co-varying effects of changes in $[H^+]_{XS}$ and silica solubility.

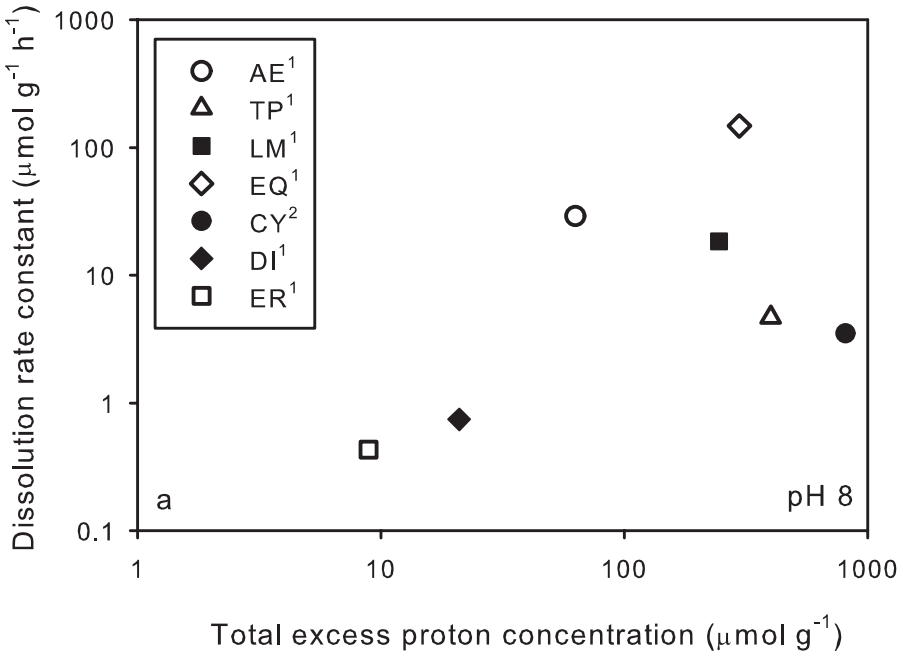
Dissolution rate constant (μmol g-1 h-1)
1000
100
10
1
0.1
1
10
100
1000
AE1
TP1
LM1
EQ1
CY2
DI1
ER1
a
pH 8
Total excess proton concentration (μmol g-1)

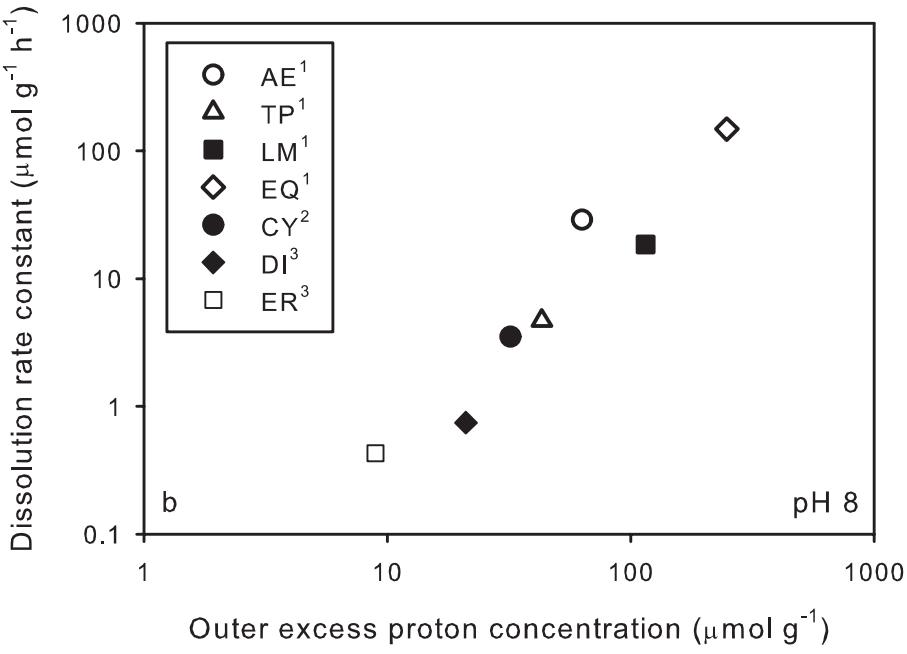
Dissolution rate constant (μmol g-1 h-1)
1000
100
10
1
0.1
1
10
100
1000
AE1
TP1
LM1
EQ1
CY2
DI3
ER3
b
pH 8
Outer excess proton concentration (μmol g-1)

← *Figure 4.6* Dissolution rate constants versus model-derived estimates of total (a) and (external) surface (b) excess proton concentrations at pH 8 and in 0.7 M NaCl. The rate constants were determined in seawater and at 25°C (Loucaides et al. 2008), except for the euryhaline diatom frustules (CY), which was determined at 20°C in diluted seawater (Roubeix et al. 2008). For the diatomite (DI) and Southern Ocean biosiliceous ooze (ER), the proportion of internal silanols is assumed to be negligible, that is, the total and surface excess proton concentrations are assumed to be identical (see text for justification).

4.5 Conclusions

The large variability in electrical charging of biogenic silicas ($bSiO_2$) is ascribed to the existence of two distinct pools of ionizable sites, those located on the external surface and those inside the $bSiO_2$ particles. The latter may be either on the surfaces of small micropores or within a gel-like hydrated layer. The internal sites are accessible to protons, but not to the relatively large N_2 molecules that are commonly used to measure the specific surface areas of $bSiO_2$. Furthermore, the protonation and deprotonation reactions of the internal silanol groups are much less sensitive to changes in ionic strength than those involving silanols in direct contact with the outside solution.

Particularly for fresh $bSiO_2$, such as the frustules of cultured diatoms or phytoliths extracted from land plants, the number of internal silanol groups may be of the same order of magnitude or larger than that of groups located on the outside surface. Older $bSiO_2$ samples have lower proportions of internal sites, due to their progressive elimination with time. Diatom frustules artificially aged in seawater also exhibit a decrease in the relative abundance of internal silanol groups, compared to fresh frustules. The accompanying increase in siloxane bonding within the bulk solid should increase the thermodynamic stability of $bSiO_2$, and may be partly responsible for the observed decrease in silica solubility of diatom debris during diagenesis.

The dissolution rate constants of the various $bSiO_2$ materials correlate with the density of surface silanol groups, rather than with the total silanol density. This is expected in as far as dissolution involves the removal to solution of silicate units located on the outside surface area only. As a corollary, specific surface area measurements using the standard N_2 BET method should provide adequate estimations of the reactive surface area during dissolution of $bSiO_2$.

CHAPTER 5

Dissolution of biogenic silica from land to ocean: Role of salinity and pH

Socratis Loucaides, Philippe Van Cappellen, and Thilo Behrends

Published in Limnology and Oceanography, 53(4), 2008, 1614-1621

Abstract

The dissolution rates of diatom frustules, phytoliths, two diatomaceous lake sediments, a siliceous ooze from the Southern Ocean, a diatomite deposit, and a synthetic amorphous silica were measured in flow-through reactors supplied with either seawater or freshwater. Although the rates varied by more than one order of magnitude among the different siliceous materials, for any given solid the rate was systematically higher in seawater than freshwater, on average by a factor of five. Flow-through reactor experiments with the diatom frustules and synthetic silica using mixtures of freshwater and seawater indicated that most of the rate increase occurred for seawater fractions between 0 and 50%. The observed rate-enhancement is attributed to the higher pH of seawater, and the catalytic effect of seawater cations on the hydrolysis of siloxane bonds at the silica surface. Because of their abundance in seawater, Na^+ and Mg^{2+} are mainly responsible for the salinity-induced rate increase. The large difference in dissolution kinetics between freshwater and seawater helps explain the very efficient recycling of biogenic silica in marine environments compared to freshwater lakes. Enhanced dissolution at the land-ocean transition of biogenic silica produced by terrestrial plants and freshwater diatoms may represent a significant, but largely overlooked, source of nutrient silicon for estuarine and nearshore marine ecosystems.

5.1 Introduction

The production and dissolution of biogenic silica ($bSiO_2$) in the oceans has been studied extensively, given the importance of diatom primary productivity for the export of organic carbon to the deep sea (Smetacek, 2000). However, fixation of silica by land plants, mainly under the form of phytoliths, has been proposed to be of similar magnitude as that by marine diatoms (Conley, 2002). Because of the production of $bSiO_2$ by terrestrial plants, but also by riverine and lacustrine diatoms, much of the reactive Si reaching the oceans has undergone prior biological cycling on the continents. A major fraction of the dissolved Si (dSi) load of the world's rivers may in fact originate from the dissolution of plant litter, soil phytoliths, and freshwater diatom frustules, rather than directly from the chemical weathering of silicate rocks (Derry et al., 2005). In addition, a significant portion of the riverine export of reactive Si may be under the form of $bSiO_2$ produced on the continents (Conley 1997). Dissolution of this $bSiO_2$ may constitute an important, but so far largely overlooked, source of nutrient Si for nearshore ecosystems. (Note: reactive Si is defined here as Si that is, or can become, bioavailable on time scales of less than a few years.)

The riverine supply of reactive Si, combined with the availability of light and increased water residence times, creates favorable conditions for biosiliceous productivity in estuaries and coastal embayments (Lemaire et al., 2002). It has long been suspected that the large increase in salinity at the land-ocean interface promotes diatom production by enhancing the dissolution of $bSiO_2$ and, thus, the regeneration of bioavailable dSi (Anderson, 1986). Nonetheless, to the authors' knowledge, there have been no systematic studies of the role of salinity in the dissolution kinetics of $bSiO_2$ under earth surface conditions. Here, we present dissolution rates of a variety of biosiliceous materials measured under ambient conditions in freshwater and seawater, as well as mixtures of both end-member solutions. The goal is to assess to what degree differences in aqueous electrolyte composition may contribute to differences in the recycling efficiency of $bSiO_2$ in continental, estuarine, and marine environments.

5.2 Materials and methods

5.2.1 Biosiliceous materials

Dissolution experiments were carried out with a range of continental and marine biosiliceous materials (Table 5.1). They include frustules of cultured marine diatoms, phytoliths, siliceous lake sediments, a siliceous ooze from the Southern Ocean, and a diatomite ore deposit. The non-siliceous fractions of the natural samples were removed as much as possible with the treatments described below. Afterwards the samples were rinsed several times with deionised water and freeze-dried, prior to being used in the dissolution experiments.

The fresh diatoms (*Thalassiosira punctigera*) were cultured at the Royal Netherlands Institute for Sea Research (NIOZ) in central North Atlantic seawater containing low nutrient and trace metal levels. After harvesting the cells, organic matter was removed by low-temperature ashing (Van Beusekom, 1989). Descriptions of the culturing conditions and ashing protocol are given in Koning et al. (2007). Phytoliths were extracted from grass horsetail (*Equisetum arvense*), a known silicon accumulating plant, by means of a chemical oxidation method combining hydrogen peroxide and nitric acid (Juillet-Leclerc 1984). Plant tissue was boiled in 30% H_2O_2 until the reaction ceased, and then digested in concentrated HNO_3 at 60° C for 1-2 hours. Information on the morphology, surface chemical properties, and dissolution kinetics of horsetail phytoliths can be found in Fraysse et al. (2006*a, b*).

Core-top sediments were collected from two shallow lakes, one located in France (Pavin) the other in Iceland (Myvatn). Both lakes experience seasonal diatom blooms, which cause the accumulation of biosiliceous sediments (Einarsson, 2004; Viollier et al., 1997). The marine biosiliceous ooze is of Pliocene age; it was obtained from a core from the Weddell Sea, within a layer consisting nearly exclusively of fragments of frustules from the diatom species *Ethmodiscus Rex*. Descriptions of the core and the *E. rex* layer sampled are given in Abelmann et al. (1988). The diatomite was obtained as untreated ore material from a commercial mine in Lompoc, California, and dates from the Miocene. Details on the depositional setting and composition of the diatomite are summarized in Moyle and Dolley (2002). The various sediment samples were homogenized and air-dried prior to cleaning. Organic matter was removed by low-temperature ashing (Van Beusekom, 1989), by placing the samples for 4 hours in a Plasmaprep 300 plasma oven (~40°C). Subsequently, they were washed in 1 mol L^{-1} HCl overnight, in order to remove traces of $CaCO_3$.

Table 5.1 Siliceous materials used in the dissolution experiments.

ID	Material	Origin/description	Composition*	Further information
TP	Fresh diatom frustules	Monoculture of marine diatom *Thalassiosira punctigera* grown in open ocean surface water	Very low impurity levels Al/Si=0.001	Dissolution kinetics (Van Cappellen et al. 2002b); ultrastructure (Vrieling et al. 2000)
EQ	Fresh phytoliths	Oxidative extraction of whole plant horsetails (*Equisetum arvense*)	Very low impurity levels Al/Si<0.001	Morphology, surface chemistry and dissolution kinetics (Fraysse et al. 2006a; Fraysse et al. 2006b)
LP	Biosiliceous lake sediment	Lake Pavin upper 2 centimeters of sediment core collected at 61 m water depth	Al/Si = 0.012 Fe/Si = 0.003 K/Si = 0.002	Geochemical studies/ environmental setting (Viollier et al. 1997)
LM	Biosiliceous lake sediment	Lake Myvatn upper 2 centimeters of sediment core collected at 31 m water depth	Al/Si = 0.008 Fe/Si = 0.009 K/Si = 0.001	Environmental setting/ecology (Einarsson 2004)
ER	*E. Rex* Biosiliceous ooze sample	Weddell Sea: sample from 1 m thick diatomaceous layer in core collected at 3550 m water depth	Al/Si=0.003	Core location, dating, formation, environmental setting (Abelmann et al. 1988); dissolution kinetics (Koning et al. 2007 and references therein)
DI	Diatomite ore	Miocene diatomaceous earth deposit from a mine in Lompoc, California (USA)	Al/Si = 0.029 Fe/Si = 0.007 K/Si = 0.005	Paleoenvironment and species composition (Moyle et al. 2002)
AE	Aerosil® OX50 Synthetic amorphous silica	Fumed silica	Very pure; well characterized physico-chemical properties	www.aerosil.com

* Atomic ratios are based on ICP-MS analyses after total destruction of the samples.

A fumed silica (Aerosil® OX50, Degussa GmbH) of high chemical purity was used as a synthetic reference material. Its specific surface area (50 $m^2\ g^{-1}$) falls within the typical range of diatom frustules and plant phytoliths (Dixit et al., 2001; Fraysse et al., 2006b). The material was used as received in the experiments.

5.2.2 Flow-through reactors

The application of flow-through reactors to measure dissolution rates of marine and terrestrial biosiliceous materials is described in detail in a number of publications (Van Cappellen 2002*a* and references therein). Briefly, a known mass of siliceous solid is suspended in a reactor cell through which an undersaturated solution flows at a constant rate controlled by a peristaltic pump. After the dSi concentration in the outflow reaches a constant value, the steady state dissolution rate R is calculated according to:

$$R = \frac{([dSi]_{out} - [dSi]_{in})q}{M} \quad (1)$$

where $[dSi]_{out}$ and $[dSi]_{in}$ are the dSi concentrations measured in the out- and inflow solutions, respectively, q is the volumetric flow rate through the reactor, and M is the mass of siliceous solid material in the reactor. Note that, due to dissolution, M decreases with time, and its value in Eq. 1 was therefore corrected after each sampling to account for the silica mass loss due to dissolution. The total fraction of solid silica dissolved by the end of the experiments varied from 1% for the least reactive materials (DI and ER, Table 5.1) to 25% for the phytolith sample (EQ).

The flow-through reactors used in this study consisted of a cylindrical Plexiglas® cell with a fixed bottom and a removable top. A floating Teflon-coated magnetic stir bar kept the suspension inside the reactor well mixed, and a 0.45 μm pore size membrane filter at the outflow prevented the solid material from leaving the reactor. The net volume of each reactor (stir bar volume subtracted) was 25 mL. The flow rate in all experiments was adjusted to 1 mL h^{-1} using a peristaltic pump. The reactors were kept at a constant temperature of 25°C in a water bath placed on top of a 15 position multi-stirring plate.

The initial solid-to-solution ratio was 4 g L^{-1} in all flow-through experiments. The outflow of the reactors was sampled every reactor volume (i.e., each 25 h) for periods of 7-10 days. Samples were collected in plastic 15 mL Greiner® centrifuge tubes and the dissolved silica content was analyzed colorimetrically on a nutrient Bran and Luebbe auto-analyser (relative standard deviation 0.5%). The pH values of inflow and outflow solutions were measured using a Metrohm Unitrode combined glass pH electrode calibrated daily with commercial buffers.

The dissolution rates reported are averages of the rates calculated with Eq. 1, using the measured outflow concentrations $[dSi]_{out}$ and the corrected solid masses M. Typically, the outflow dSi concentrations stabilized after 3-4 reactor volumes (i.e., after 75-100 h), and the average dissolution rates were based on the $[dSi]_{out}$ values measured in the subsequent 5-7 reactor volumes of outflow.

5.2.3 Flow-through dissolution experiments

In a first series of flow-through reactor experiments (series A, Table 5.2), dissolution rates were measured using either filtered (0.45 μm pore size) seawater from the oligotrophic central part of the North Atlantic (dSi ~ 2 μmol L^{-1}, pH 8.1), or a very dilute (ionic strength ~ $2x10^{-4}$ mol L^{-1}), slightly acidic (pH 6.3) Ca-Na-HCO_3 commercial mineral water (SPA Bleu®). In addition to the end-member seawater and freshwater solutions, dissolution rates of fresh diatom frustules (TP) and synthetic amorphous silica (AE) were also measured in freshwater-seawater mixtures (series B, Table 5.2). Five intermediate salinities were created corresponding to solutions of 1, 10, 25, 50, and 75% seawater. Of the natural biosiliceous materials, only TP was available in large enough quantities to carry out the full set of mixture experiments.

To separate the effects of dissolved salts and pH, further flow-through experiments were carried out with freshwater inflow solutions whose pH was adjusted to that of seawater (8.1) by the addition of 0.01 mol L^{-1} NaOH (series C, Table 5.2). The addition of base 0.01 (2.2 mL of 0.01 mol L^{-1} NaOH in 500 mL freshwater) increased the ionic strength of the solution by less than $5x10^{-5}$ mol L^{-1}. Three of the natural materials were used in these experiments (TP, LM, and EQ). Finally, the effects of the major seawater cations (Na^+, K^+, Mg^{+2}, and Ca^{+2}) on the dissolution kinetics of synthetic amorphous silica (AE) were investigated by adding chloride salts (reagent grade NaCl, KCl, $MgCl_2$, or $CaCl_2$) separately to the end-member freshwater (series D, Table 5.1). Two sets of inflow solutions were prepared: in the first one, the amount of salt was adjusted to reach the average seawater concentration of the corresponding cation, in the second one, salt addition was adjusted to obtain solutions of constant ionic strength, equal to that of seawater (I = 0.7 mol L^{-1}).

Table 5.2 Summary of experimental conditions and results of flow-through dissolution experiments. Each listing corresponds to a separate reactor experiment. *See* Table 5.1 for the identification of the solids. The pH values are those of the inflow solution. The dissolution rates R were calculated using Eq. 1; standard deviations (s.d.) are given in parentheses. All experiments were performed at 25°C. FW = freshwater; SW = seawater.

Series	Solid	Input solution	pH	[dSi]in ($\mu mol\ L^{-1}$)	[dSi]out ($\mu mol\ L^{-1}$)	R (s.d.) ($\mu mol\ g^{-1}\ h^{-1}$)
A	EQ	FW	6.3	120	440	3.2 (0.9)
	EQ	SW	8.1	2.4	1699	17 (0.4)
	LP	FW	6.3	120	260	1.4 (0.2)
	LP	SW	8.1	2.4	867	8.7 (0.4)
	LM	FW	6.3	120	361	2.4 (0.2)
	LM	SW	8.1	2.4	949	9.5 (0.9)
	ER	FW	6.3	120	130	0.1 (0.03)
	ER	SW	8.1	2.4	42	0.4 (0.06)
	DI	FW	6.3	120	143	0.2 (0.02)
	DI	SW	8.1	2.4	68	0.7 (0.04)
B	AE	FW	6.3	120	358	2.4 (0.4)
	AE	1%SW	6.5	117	439	3.2 (0.7)
	AE	10%SW	7.4	109	700	5.9 (1.3)
	AE	25%SW	7.6	91	810	7.2 (0.7)
	AE	50%SW	7.7	69	1081	10.1 (1.3)
	AE	75%SW	7.9	31	1146	11.2 (1.4)
	AE	SW	8.1	2.4	1169	11.7 (1.0)
	TP	FW	6.3	120	209	0.9 (0.1)
	TP	1%SW	6.5	117	252	1.3 (0.2)
	TP	10%SW	7.4	109	364	2.5 (0.4)
	TP	25%SW	7.6	91	451	3.6 (0.2)
	TP	50%SW	7.7	69	484	4.1 (0.6)
	TP	75%SW	7.9	31	393	3.6 (0.3)
	TP	SW	8.1	2.4	365	3.7 (0.3)
C	AE	FW	8.1	120	542	4.2 (0.2)
	TP	FW	8.1	120	298	1.8 (0.2)
	EQ	FW	8.1	120	740	6.2 (0.5)
	LM	FW	8.1	120	630	5.1 (0.6)
D	AE	0.05 mol L^{-1} $MgCl_2$	6.3	120	521	4.0 (0.3)
	AE	0.01 mol L^{-1} KCl	6.3	120	444	3.2 (0.2)
	AE	0.41 mol L^{-1} NaCl	6.3	120	569	4.5 (0.3)
	AE	0.01 mol L^{-1} $CaCl_2$	6.3	120	458	3.4 (0.5)
	AE	$MgCl_2$ I=0.7 mol L^{-1}	6.3	120	818	7.0 (0.8)
	AE	KCl I=0.7 mol L^{-1}	6.3	120	708	5.9 (0.8)
	AE	NaCl I=0.7 mol L^{-1}	6.3	120	719	6.0 (0.7)
	AE	$CaCl_2$ I=0.7 mol L^{-1}	6.3	120	565	4.4 (0.5)

5.2.4 Solubility measurements

The solubilities of the various siliceous materials were measured in 15 mL batch reactors placed in a 25°C water bath. The solid-to-solution ratios were relatively high, 10 g L^{-1}, in order to reduce the time required to reach solubility equilibrium. The solids were suspended in 0.1 mol L^{-1} NaCl solutions made up of deionized water and reagent grade NaCl to which Tris-base buffer was added in order to maintain pH at 8.0±0.2. The dissolved silica concentration was monitored periodically; the value at which it stabilized was considered the apparent silica solubility of the corresponding material. An additional series of batch experiments with the fresh diatom frustules (TP) was carried out in freshwater-seawater mixtures identical to those of series B (Table 5.2). These experiments were designed to determine whether the apparent solubility of biogenic silica depends on the solution composition.

5.3 Results

Dissolution rates reached steady state after 3-4 reactor volumes of flow (Fig. 5.1). Standard deviations on the average steady state rates were on the order of 10-15%. These standard deviations are reported in Table 5.2 and represented by error bars in the figures where appropriate. The

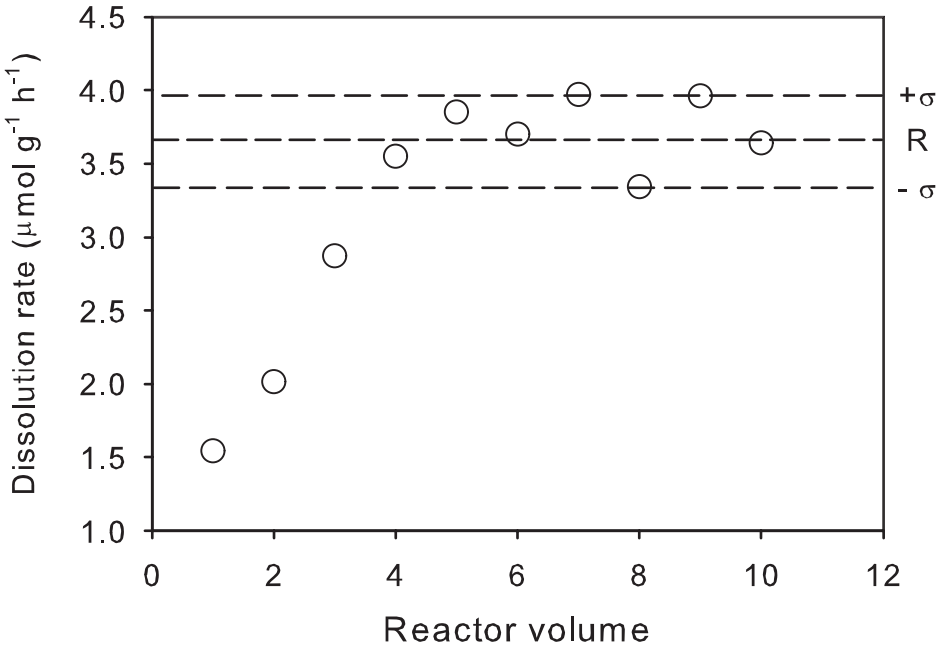

Figure 5.1 Dissolution rate of fresh diatom frustules (TP) measured in a flow-through reactor supplied with seawater. The points correspond to rates calculated with Eq. 1, using the measured outflow concentrations of dissolved silica ($[dSi]_{out}$). The rates are plotted against the volume of seawater that has flown through the reactor, expressed in units of reactor volumes. Steady state outflow $[dSi]_{out}$ concentrations are reached after 3 reactor volumes of flow. The dissolution rates R reported in Table 5.2 are the average rate values obtained, after steady state conditions were reached. Standard deviations (σ) of the rates are also reported in Table 5.2. They mainly reflect the experimental variations in the measured $[dSi]_{out}$ values.

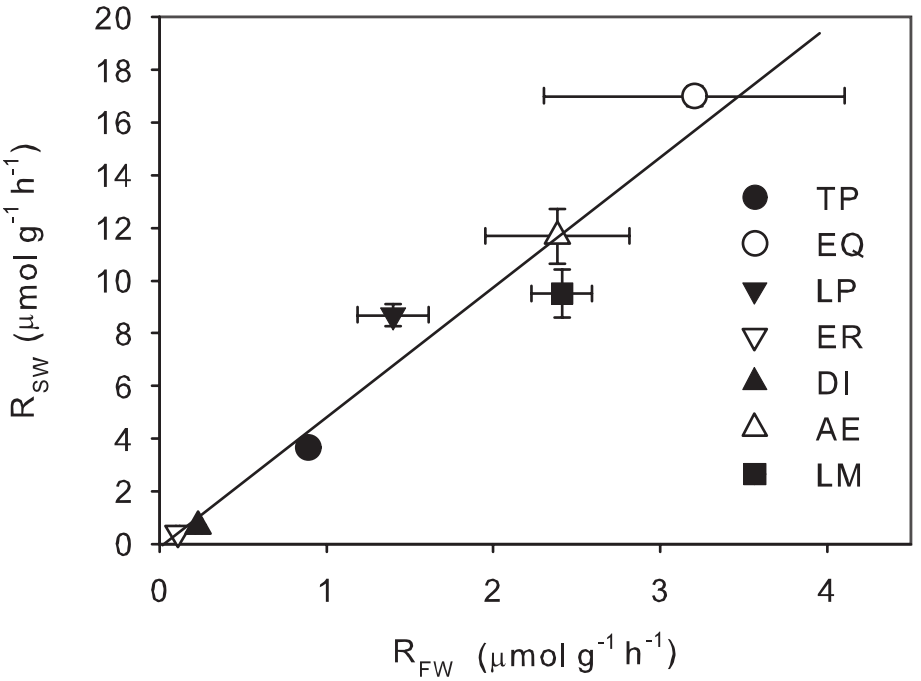

Figure 5.2 Dissolution rates in seawater versus dissolution rates in freshwater at 25°C of all siliceous materials (Table 5.1). The strong linear relationship (r^2=0.95) indicates an average 5-fold rate increase in seawater versus freshwater. The error bars represent standard deviations of the rate determinations (*see* Fig. 5.1).

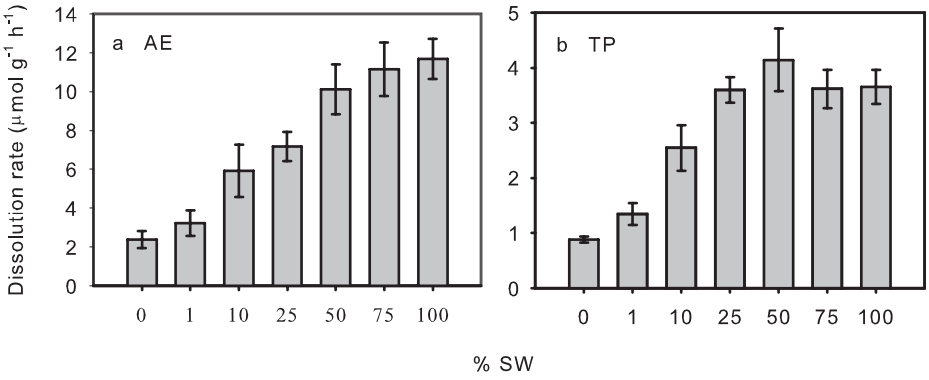

Figure 5.3 a) Dissolution rates R of Aerosil® OX50 (AE) and b) fresh diatom frustules (TP) at 25°C in freshwater-seawater mixtures. The x-axis indicates the percentage of seawater (SW) in the mixtures. The error bars represent standard deviations of the rate determinations (*see* Fig. 5.1).

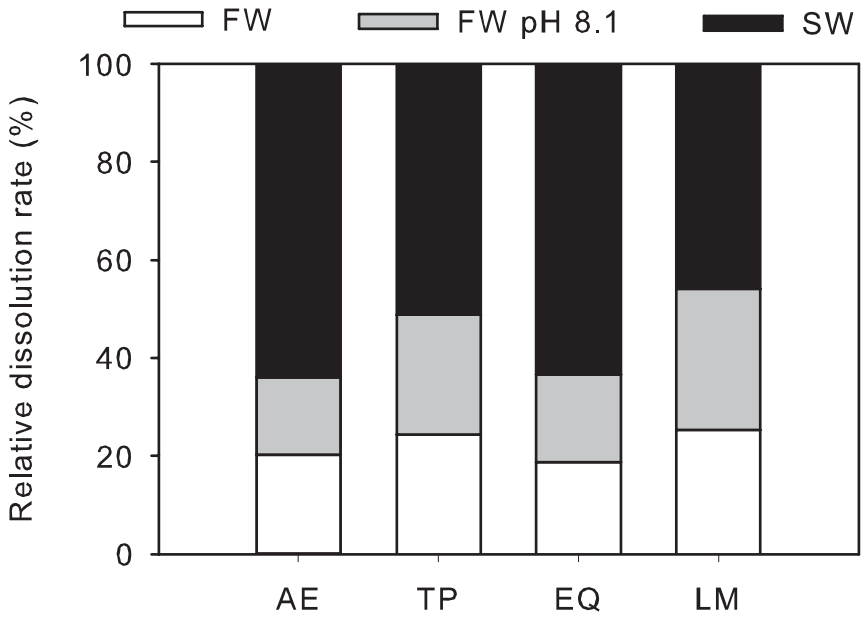

Figure 5.4 Dissolution rates of the synthetic silica (AE), fresh diatom frustules (TP), phytoliths (EQ), and Lake Myvatn sediments (LM) measured in freshwater and in freshwater with pH adjusted to that of seawater (pH 8.1), relative to the dissolution rates in seawater. The gray and black bars indicate the relative contributions to the rate enhancement in seawater of pH and dissolved salts, respectively. All rate measurements were done at 25°C.

measured dissolution rates varied over more than two orders of magnitude (Table 5.2). As shown by the results for series A and B, a significant part of this variability could be ascribed to the nature of the inflow solution. For any given siliceous material, the rate was systematically higher in seawater than in freshwater (Fig. 5.2): rates increased on average by a factor of 5 between freshwater and seawater.

Not unexpectedly, the slowest rates were observed for the oldest materials (ER and DI). These materials also experienced somewhat lower increases in rate between freshwater and seawater (3.8 times higher for ER and 2.9 for DI). The highest rates were obtained for the fresh phytoliths (EQ) and synthetic amorphous silica (AE). Intermediate rates were observed for the core-top lake sediments (LP and LM) and fresh diatom frustules (TP).

The rates measured for TP and AE in freshwater-seawater mixtures (series B, Table 5.2) progressively increased with increasing seawater addition, leveling off beyond a 1:1 mixing ratio (Fig. 5.3). The largest relative increases in dissolution rates were observed between pure freshwater and the 10% seawater mixture. The rates measured in pH 8.1 freshwater were higher than those in pH 6.3 freshwater (series C, Table 5.2). For the four materials used (EQ, TP, LM, and AE), on the order of 44 ± 9% of the rate increase between freshwater and seawater could be attributed to the change in pH from 6.3 to 8.1, with the remaining increase representing the effect of the dissolved seawater salts on the dissolution kinetics (Fig. 5.4).

The salt-amended freshwater experiments (series D, Table 5.2) clearly showed the rate enhancing effects of dissolved cations (Fig. 5.5). Together the individual effects of the two major seawater cations, Na^{+} and Mg^{+2}, could largely account for the salt induced increase in dissolution rate of AE between freshwater and seawater (i.e., after accounting for the pH difference). At

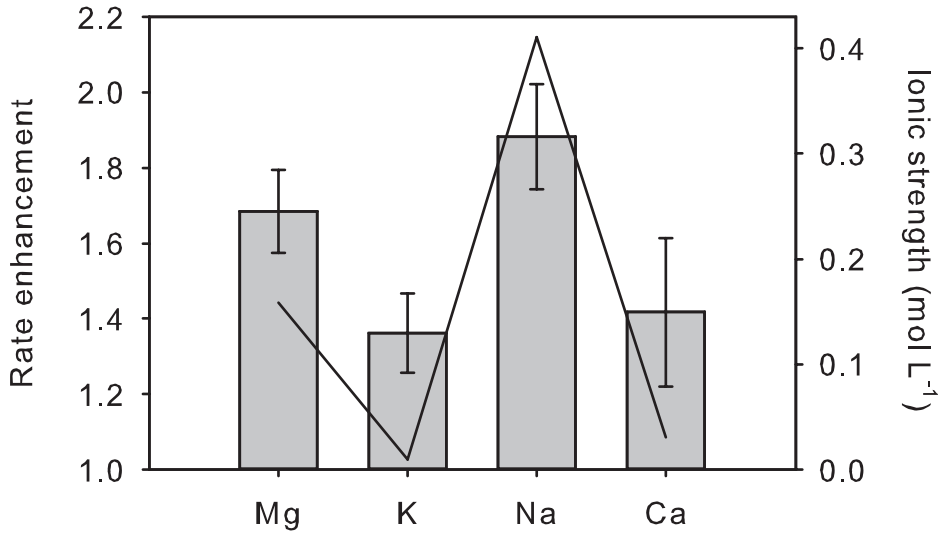

Figure 5.5 Dissolution rate enhancements by individual seawater cations at 25°C and pH 6.3. The cations were added as chloride salts to the freshwater to match their respective concentrations in seawater. The bars represent the rate enhancement in the cation-amended solution, relative to the rate in freshwater, and the line indicates the ionic strengths of the cation-amended solutions. The error bars represent standard deviations of the rate determinations (*see* Fig. 5.1).

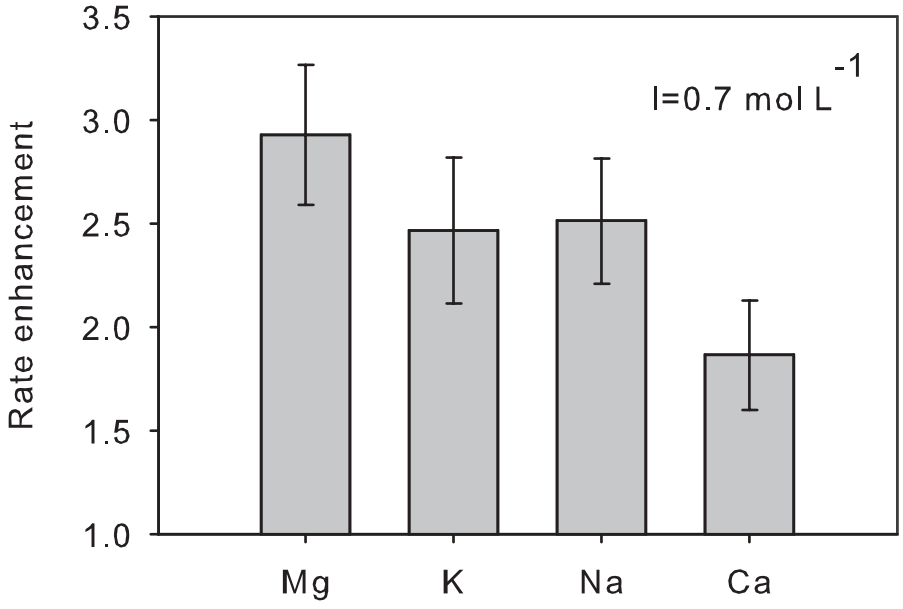

Figure 5.6 Dissolution rate enhancement by individual seawater cations at 25°C and pH 6.3. The cations were added as chloride salts to freshwater to a constant ionic strength of 0.7 mol L^{-1}. The error bars represent standard deviations of the rate determinations (*see* Fig. 5.1).

Table 5.3 Apparent silica solubilities of the various siliceous materials in 0.1 mol L^{-1} NaCl, at pH 8.0 and 25°C (*see* Table 5.1 for identification of the solids). The value reported for the *E. rex* ooze is a minimum estimate, as the concentration of dissolved silica was still slowly increasing after 107 weeks of incubation.

Solid	$[dSi]_{eq}$ (µmol L^{-1})
TP	1750
EQ	1920
LP	1850
LM	1950
ER	600
DI	1150
AE	1960

constant seawater ionic strength, the rate enhancements of Mg^{+2}, Na^{+} and K^{+} were comparable within errors, while Ca^{+2} had a distinct lesser effect (Fig. 5.6).

The dSi build-up in the (0.1 mol L^{-1} NaCl) batch solubility experiments with fresh biosiliceous materials (EQ and TP), core-top lake sediments (LP and LM) and synthetic amorphous silica (AE) stabilized after 1-4 weeks of equilibration time. For the diatomite (DI), apparent solubility equilibrium was reached after 24 weeks, while for the *E. rex* ooze (ER) continued increase in dSi was observed for a period exceeding two years. The solubility value reported for ER in Table 5.3 corresponds to the dSi concentration measured after 107 weeks. For both end-member solutions (freshwater and seawater), the observed dissolution rates of the different materials correlated positively with the apparent silica solubilities (Fig. 5.7). The batch experiments with TP in freshwater-seawater mixtures showed no significant variation of the solubility with solution composition (<10%, results not shown).

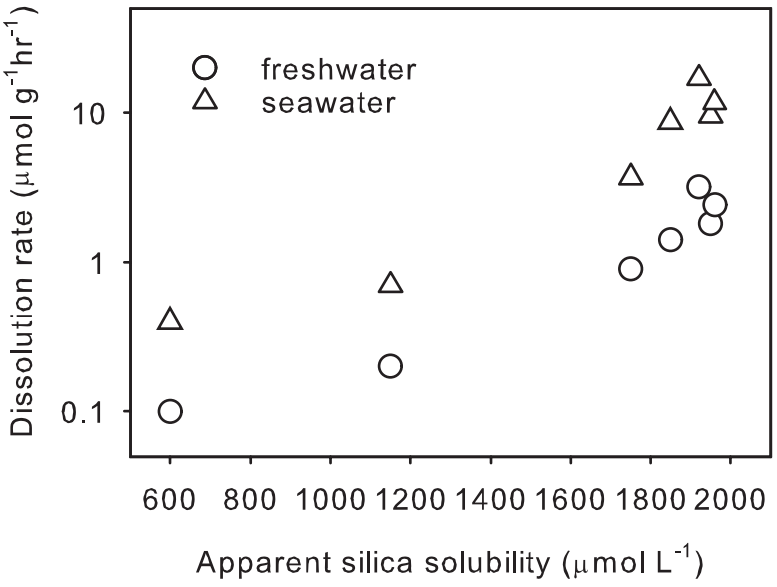

Figure 5.7 Dissolution rates of all the biogenic and synthetic siliceous materials measured at 25°C in freshwater and seawater, plotted against the apparent silica solubility measured in 0.1 mol L^{-1} NaCl, at pH 8 and 25°C.

5.4 Discussion

Both increased salt concentration and increased pH contribute to the rate enhancement of $bSiO_2$ in seawater relative to freshwater (Fig. 5.4). The observed solution effects on the dissolution kinetics can be understood in terms of the chemical structure and reactivity of the silica-water interface (Dove, 1999; Van Cappellen et al., 2002a).

There is general agreement that dissolution of SiO_2 at near-neutral pH is due to nucleophilic attack of water molecules that cause the breaking of siloxane bonds, >Si-O-Si<, at the particle surface (Dove and Crerar, 1990). As a water molecule approaches a surface silicon atom, the transfer of electron density weakens the adjacent siloxane Si-O bond, which eventually breaks. The now open linkages bind with the dissociating water molecule to form >Si-OH (silanol) groups. The process is then repeated until all siloxane bonds surrounding the surface silicon are broken, and the latter leaves the surface under the form of a silicic acid molecule, $Si(OH)_4$.

Increasing pH leads to the deprotonation of surface silanol groups, thereby further facilitating the breaking of the bridging siloxane bonds (Dove and Elston, 1992). Base-promoted dissolution occurs when the solution pH exceeds the point of zero surface charge (pH_{zpc}) of the solid, which for $bSiO_2$ falls in the range 1.2-4 (Dixit and Van Cappellen, 2002; Fraysse et al., 2006b). The catalyzing effect of increased pH, for pH > pH_{zpc}, has been demonstrated previously for marine diatomaceous silica (Van Cappellen and Qiu, 1997b) and plant phytoliths (Fraysse et al., 2006a).

Enhanced dissolution rates of quartz in salt solutions is well-documented (Dove 1999 and references therein). Dove (1999) proposes that the cations of alkali metals and alkaline-earth elements strengthen the nucleophilic properties of water molecules at the quartz surface. Hydrated cations adsorbed to the negatively charged SiO_2 surface improve the physical access of water to siloxane bonds by redirecting hydration waters into more favorable positions, thereby increasing the rate of hydrolysis of the bonds. It should be noted, however, that the exact molecular mechanism whereby aqueous cations catalyze silica dissolution is not yet fully elucidated.

Dove and Crerar (1990) showed that the dependence of the dissolution rate of quartz on the concentrations of individual alkali and alkaline earth cations follows Langmuir-type isotherms, where the rate initially increases sharply upon addition of the cation and then asymptotically approaches a maximum value with continued increase in cation concentration. This behavior is in line with the freshwater-seawater mixture experiments, where the dissolution rates level off for the highest admixtures of seawater (Fig. 5.3). The results shown in Fig. 5.5 also indicate that the rate-enhancing effects of Na^+, K^+, Mg^{2+}, and Ca^{2+} depend non-linearly on the cation concentrations. While Na^+ and Mg^{2+} are the main rate-enhancing cations in seawater by virtue of their abundance, Ca^{2+} and K^+ have nonetheless significant catalytic effects despite their much lower concentrations.

Solutions of $MgCl_2$, NaCl, and KCl appear more effective in enhancing the rate of synthetic amorphous silica than $CaCl_2$ (Fig. 5.6). In contrast, for quartz, Dove and Nix (1997) found that the dissolution rate enhancement in single cation solutions increases in the order $Mg^{2+}<Ca^{2+}\approx Li^+\approx Na^+\approx K^+<Ba^{2+}$ at 200°C and near-neutral pH, while House (1994) reports higher quartz dissolution rates in $CaCl_2$ than in NaCl solution at 25°C and pH 10. Thus, further studies in single and multiple salt solutions are needed to systematically delineate the effects of ionic constituents on the dissolution of $bSiO_2$ under earth surface conditions. Preliminary results, for instance, indicate that the rate enhancement of amorphous silica at 25°C and near-neutral pH may be less in Na_2SO_4 than in NaCl solution (results not shown).

All the siliceous materials used in this study exhibit significant rate-enhancement in seawater relative to freshwater, although the absolute dissolution rates vary over more than one order of magnitude (Fig. 5.7). The rates correlate positively with the apparent silica solubilities, in agreement with the Linear Free Energy Relationship (LFER) for silica dissolution proposed by Wollast (1974), which includes crystalline as well as amorphous forms of SiO_2.

The pure synthetic amorphous silica (AE) exhibits the highest solubility of all the samples used (1960 μmol L^{-1}). The solubilities of the phytoliths, fresh diatom frustules, and core-top lake sediments (1750-1950 μmol L^{-1}), however, are very close to that of AE, and similar to 25°C solubility values for fresh diatoms reported in the literature (Dixit et al. 2001 and references therein). The significantly lower solubilities of the diatomite (DI) and *E. rex* ooze (ER) fall in between the apparent silica solubilities measured on Southern Ocean core-top siliceous oozes (Van Cappellen and Qiu, 1997a) and the lowest values reported for fossil diatoms (~ 200 μmol L^{-1}, Hurd and Treyer 1974). The concomitant drop in solubility and reactivity of fossil biogenic silicas relative to fresh $bSiO_2$ reflects alterations of the bulk structure and surface chemistry. For diatom frustules, these changes may start during sedimentation through the water column (Rickert et al., 2002) and continue after burial in sediments (Van Cappellen et al., 2002a; Van Cappellen et al., 2002b). Processes that may decrease the solubility and reactivity of $bSiO_2$ include the incorporation of impurities, such as aluminum (Van Cappellen et al., 2002b), the lowering of the specific surface area (Van Cappellen et al., 2002b), and the progressive condensation of the silica framework (Gendron-Badou et al., 2003).

5.5 Implications

The regeneration of dSi from $bSiO_2$ depends on a variety of environmental conditions, processes and material properties (for a review, *see* Van Cappellen et al. 2002*a*). An important first step is the removal of protective organic coatings covering the silica surfaces, typically through bacterial activity (Bidle and Azam, 1999). Once exposed, the silica surfaces dissolve because most natural waters are undersaturated with respect to $bSiO_2$. In addition to the degree of undersaturation, the dissolution rate of a given biosiliceous material depends on the temperature, pH and, as shown here, the ionic composition of the aqueous medium.

The large, five-fold, enhancement of the dissolution rate of $bSiO_2$ observed in seawater relative to freshwater implies that changes in salinity and pH should significantly modify the biogeochemical cycling of nutrient silicon across the land to ocean transition. In particular, it helps explain differences in recycling efficiency of silica in marine and freshwater ecosystems. Recycling of $bSiO_2$ in the oceans is extremely efficient, with globally only about 5-7% of the diatomaceous $bSiO_2$ exported from the euphotic zone ultimately being buried in sediments (Tréguer et al. 1995). In comparison, recent mass balance estimates for Lake Baikal, one of the world's largest (31,500 km^2) and deepest (1637 m maximum water depth) freshwater lakes, indicate that more than 50% of the $bSiO_2$ export production is buried in the sediments (Muller et al., 2005). While a variety of factors may contribute to the high preservation potential of $bSiO_2$ in Lake Baikal, the low salinity (<0.1 PSU) and near-neutral pH (7.1-7.2) (Falkner et al., 1997) are likely to play an important role.

A significant fraction of reactive Si is exported from the continents as phytoliths or diatom frustules (Conley, 1997). Survival of $bSiO_2$ during river transport is consistent with its relatively slow dissolution kinetics in continental freshwaters. For example, the dissolution rate of *T.*

punctigera measured in the freshwater end-member corresponds to a half-life of the frustules of 1.3 years. Siliceous productivity in estuaries and marginal environments further increases the proportion of reactive Si that reaches the oceans under the form $bSiO_2$. According to a recent reassessment of the biogeochemical Si cycle, $bSiO_2$ could represent up to 40% of the reactive Si input to the distal coastal ocean (Laruelle et al., 2008).

The large influx of $bSiO_2$, together with the salinity-dependent dissolution kinetics, creates favorable conditions for intense regeneration of nutrient silicon at the confluence of continental and marine waters. A recent comparison of Si cycling in intertidal marshes suggests that salinity may be a determining factor responsible for faster $bSiO_2$ recycling in salt marshes of the Scheldt estuary, compared to upstream, freshwater marshes (Struyf et al., 2006). Other workers have also proposed that salinity increase may in part be responsible for the high regeneration of dSi in the mid-salinity regions of estuaries (Anderson, 1986).

While the results of this study clearly show that the alkaline and saline nature of seawater greatly enhances the oceanic recycling of $bSiO_2$, they also emphasize the need to better understand the fate of $bSiO_2$ produced on the continents. The latter is crucial in view of the large changes in nutrient fluxes induced by human activity. In particular, sediment retention by damming and river diversion has a major impact on the riverine export of $bSiO_2$, which may further exacerbate the proliferation of non-siliceous phytoplankton in coastal marine environments (Humborg et al., 2000).

CHAPTER 6

Seawater-mediated interactions between diatomaceous silica and terrigenous sediments: Results from long-term incubation experiments

Socratis Loucaides, Panagiotis Michalopoulos, Massimo Presti, Erica Koning, Thilo Behrends and Philippe Van Cappellen

Submitted to Chemical Geology
December, 2008

Abstract

Reactors containing frustules of the cultured diatom *Thalassiosira punctigera* suspended in seawater were incubated with or without added sediment from the Mississippi River Delta or the Congo River Fan. The diatom frustules were separated from the terrigenous sediments by a dialysis membrane, thereby only allowing the exchange of dissolved species. One series of incubations was carried out in the laboratory, at room temperature (21°C) and for a period of 10 months. Another series of reactors was deployed along a mooring in the Mozambique Channel at three water depths (500, 1250, and 2000 m), for a period of 22 months. Chemical analyses after total destruction of frustules collected at the end of the incubations showed elemental transfer from seawater (Mg, K) and the sediments (Al, Fe, Mn, P, Ca) to the frustules. In the presence of the terrigeneous sediments, the dissolved silicate concentrations at the end of the incubations were systematically lower that those measured in the incubations without the sediments. In addition, electron microscopy revealed the formation of new mineral precipitates. These included amorphous deposits containing Si, Fe, Al, Mg, K and P, as well as euhedral clay crystallites. Differences were observed between the incubations performed in the laboratory and those deployed at sea, likely as a result of differences in redox conditions, temperature and reaction time. Overall, the interactions between biogenic silica, seawater and lithogenic minerals reduce the regeneration of nutrient silicon fixed by siliceous organisms. These interactions take place on relatively short time scales (months to years), and affect not only the marine cycle of silicon, but also those of other major and minor elements, such as Al, Fe, Mn, K, and Mg.

6.1 Introduction

Silicon (Si) is the second most abundant element in the Earth's crust after oxygen. Weathering of silicate rocks at the earth's surface is the ultimate source of dissolved silicate (dSi), which is an essential nutrient for numerous organisms, both in the oceans and on land (Conley, 2002; Ittekkot et al., 2006). The biological fixation of dSi under the form of structural elements composed of

amorphous biogenic silica ($bSiO_2$) initiates the biological cycle of Si and links the Si and carbon (C) cycles.

The oceanic Si cycle has received significant attention during the last decades, because of the role of diatom production as a major organic carbon exporter to the deep ocean via the so-called biological pump (Dugdale et al., 1995). Unlike non-siliceous phytoplankton, diatoms are limited by the availability of dSi in oceanic surface waters, which they use to build their silica frustules. Because the ocean is highly undersaturated with respect to $bSiO_2$, the dissolution of frustules of dead diatoms is relatively fast. Therefore, on time scales significantly shorter than the oceanic residence time of reactive Si (~15 000 years), the recycling of diatom frustules by dissolution is a key process determining the availability of dSi in the ocean (DeMaster, 2002; Tréguer et al., 1995).

The main sink for reactive Si in the oceans is burial in marine sediments, about half of which occurs in nearshore and continental shelf sediments (DeMaster, 2002; Laruelle et al., 2008). These sediments are also the main recipients of particulate matter originating from the continents, especially terrigenous clays. It has long been suspected that early diagenetic interactions in continental margin sediments exert a major control on the biogeochemical cycle of Si and, ultimately, on the siliceous productivity of the oceans (Mackenzie and Garrels, 1966).

Michalopoulos et al. (2000) provided the first direct evidence for the complete conversion of diatom frustules into authigenic clays in sediments of the Amazon River delta. These authors showed that the conversion process is surprisingly fast, occurring within 20-23 months. As a consequence, previous estimates of burial of reactive Si in river deltas may have been biased by the commonly used leaching techniques for $bSiO_2$, which fail to measure the diagenetically altered material. Recent estimates based on improved leaching techniques suggest that river deltas may be a far more important marine sink of reactive Si than previously thought (Michalopoulos and Aller, 2004; Presti and Michalopoulos, 2008). Rapid formation of authigenic clays during early diagenesis represents a sink not only for reactive Si, but also for a number of other elements (Mackenzie and Garrels, 1966; Michalopoulos and Aller, 1995). The currently available data indicates a close link between the precipitation of authigenic clays and the presence of $bSiO_2$ in which the latter provides not only an essential reactant (silicate), but also acts as a substrate for new mineral formation (Michalopoulos and Aller, 2004; Presti and Michalopoulos, 2008).

Early diagenetic reactions involving $bSiO_2$ have also been invoked to explain variations in asymptotic pore water dSi concentrations and benthic dSi fluxes in the deep and coastal ocean (Dixit and Van Cappellen, 2003; King et al., 2000; McManus et al., 1995; Michalopoulos and Aller, 2004; Presti and Michalopoulos, 2008; Ragueneau et al., 2001). Even though direct evidence for such processes in abyssal sediments is not yet available, the evidence suggests that interactions between $bSiO_2$ and lithogenic silicate minerals may be an ocean-wide phenomenon, whose role in the marine biogeochemical cycling of Si remains to be fully assessed.

In this paper, results are presented of long-term (10-22 months) batch reactor experiments, carried out in the laboratory or deployed along moorings, where cultured diatom frustules were incubated in the presence or absence of clay-rich delta sediments from the Mississippi and Congo Rivers. Relatively low sediment-to-silica ratios were used to capture the early stages of the interactions between $bSiO_2$ and the terrigenous clays. Emphasis was on identifying which chemical elements are involved in the interactions and what reaction products are formed. Concurrently, the net effect of the $bSiO_2$-seawater-clay interactions on the apparent silica solubility was measured. To distinguish newly formed mineral precipitates from terrigenous clays, the frustules were separated from the sediments by dialysis membranes. In addition, control experiments were run in which the

frustules were incubated without the sediments, in order to account for chemical alterations of the frustules due to uptake of seawater ions alone.

6.2 Materials and methods

6.2.1 Diatom frustules

Cultures of *Thalassiosira punctigera*, a common marine diatom species (Hasle 1983), were grown at the Royal Netherlands Institute of Sea Research (NIOZ) in autoclaved central North Atlantic seawater containing low nutrient and trace metal levels. After harvesting the cells, organic matter was removed by low-temperature ashing. Details on the culturing conditions and ashing protocol can be found in Koning et al. (2007). The microstructure (Vrieling et al., 2000), dissolution kinetics and solubility (Loucaides et al., 2008; Van Cappellen et al., 2002b) of frustules of *T. punctigera* have been well-studied. The specific surface area of the frustules is relatively low (~16 m^2g^{-1}, Loucaides et al. 2008). Hence, *T. punctigera* is representative of the highly silicified diatom species that withstand complete dissolution in the water column and accumulate at the seafloor.

6.2.2 Terrigeneous sediments

Mississippi Delta sediment was collected in 2003 with a Kasten corer at a site approximately 10 km offshore from the southwestern river mouth, at about 8 m water depth. Details on the cruise and study area can be found in Presti and Michalopoulos, (2008); the sediment composition and distribution along the Mississippi Delta are discussed in Sionneau et al. (2008). Sediment from the Congo River Fan was collected in 2003 with a multi-corer about 50 nautical miles northwest from the river's mouth at a water depth of about 230 m. For details on the cruise and study area, see Khripounoff and Fabri, (2004); information on the mineralogical and chemical composition of the Congo Fan sediments can be found in Van der Gaast and Jansen, (1984).

Initially, homogenized (not ground) sediment samples were wet sieved to remove particles larger than 63μm. In order to separate the < 5μm fraction from the silt fraction, the clay-silt fraction was repeatedly resuspended in deionised water and centrifuged. After each resuspention and centrifugation cycle, the supernatant containing the < 5μm fraction was decanted and stored. The process was repeated until supernatants were clear (8-10 cycles). Suspensions containing the fine fraction were combined and centrifuged in order to concentrate the clay. The latter was used in the experiments. Total elemental compositions of the clay fractions of the two sediments were measured by X-Ray Fluorescence (XRF) and are presented in Table 6.1.

Table 6.1 Major element composition of the sediments used in the incubation experiments determined by X-Ray Fluorescence (XRF).

Sediment	SiO_2 (%)	Al_2O_3 (%)	Fe_2O_3 (%)	K_2O (%)	MgO (%)	CaO (%)	TiO_2 (%)	Na_2O (%)	P_2O_5 (%)	MnO (%)
Mississippi Delta	57.1	16.7	7.1	2.6	2.0	1.1	0.8	0.4	0.3	0.3
Congo River Fan	51.3	29.6	10.3	1.6	1.8	1.8	1.3	0.6	0.4	0.03

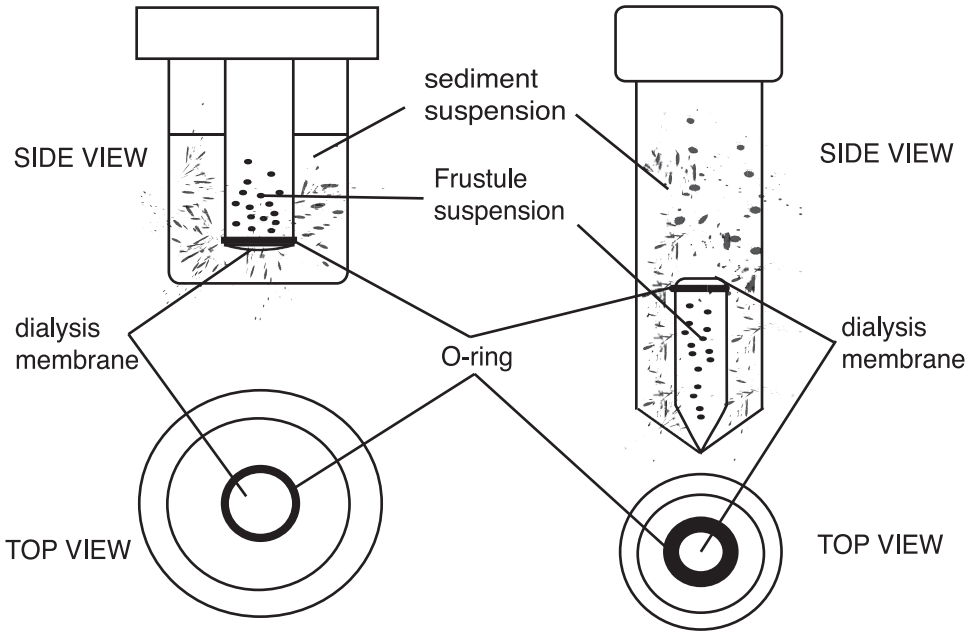

Figure 6.1 Incubation reactors used in the laboratory (Left) and field (Right) experiments (see text for detailed description).

6.2.3 Incubations

6.2.3.1 Laboratory experiments

Laboratory incubations lasted 10 months. About 50 mg of cleaned diatom frustules were suspended in a Teflon tube, whose lower opening was sealed with a dialysis membrane (Fig. 6.1). The tube was submerged in 50 mL of Mississippi Delta sediment suspension (10 g L^{-1}) in a screw-top 90 mL Teflon container. The dialysis membrane prevented direct contact between diatoms and sediments, but allowed the diffusion of dissolved constituents between the diatom and sediment compartments. Note that the headspace of the reactors was filled with air.

The diatoms and sediments were suspended in filtered North Atlantic seawater ([dSi] ~ 2μM, pH 8.1), and in 50-50 and 10-90 mixtures of filtered North Atlantic seawater and deionized water. The reactors were placed on a rotating table in a 21° C thermostated room for the duration of the experiments. Table 6.2 gives an overview of the experiments performed. The dissolved silicate (dSi) build-up in the reactors was monitored by periodically sampling 200 μL of suspension and, after filtration through 0.2 μm pore size filters, analyzing them for dSi colorimetrically on a nutrient Bran & Luebbe continuous flow analyzer (relative standard deviation 0.5%). At the end of the experiment, the suspended diatom frustules were centrifuged, rinsed 3 times with deionised water, and subsequently frozen and freeze-dried.

The elemental compositions of the incubated diatom frustules were determined by total destruction using a combination of concentrated HF, $HClO_4$, and HNO_3 (Reitz et al., 2004), followed by ICP-MS analysis. Dried frustules were also analyzed by transmission electron microscopy (TEM). Freeze dried frustules were dispersed in deionized water and drops of the suspension were

Table 6.2 Experiments performed in the laboratory (10 months) and deployed at sea (22 months).

ID	Solid material	Solution	Temperature	Pressure
Laboratory incubations				
L10D	Diatom frustules	10% Seawater	21°C	1 bar
L10DS	Diatom frustules + Mississippi Delta sediment	10% Seawater	21°C	1 bar
L50D	Diatom frustules	50% Seawater	21°C	1 bar
L50DS	Diatom frustules + Mississippi Delta sediment	50% Seawater	21°C	1 bar
L100D	Diatom frustules	Seawater	21°C	1 bar
L100DS	Diatom frustules + Mississippi Delta sediment	Seawater	21°C	1 bar
L100S	Mississippi Delta sediment	Seawater	21°C	1bar
Field incubations				
F500D	Diatom frustules	Seawater	10°C	50 bar
F500DS	Diatom frustules + Mississippi Delta sediment	Seawater	10°C	50 bar
F500S	Mississippi Delta sediment	Seawater	10°C	50 bar
F1250D	Diatom frustules	Seawater	4°C	125 bar
F1250DS	Diatom frustules + Congo River Fan sediments	Seawater	4°C	125 bar
F1250S	Congo River Fan sediment	Seawater	4°C	125 bar
F2000D	Diatom frustules	Seawater	2°C	200 bar
F2000DS*	Diatom frustules + Mississippi Delta sediment	Seawater	2°C	200 bar
F2000S	Mississippi Delta sediment	Seawater	2°C	200 bar

* The dialysis membrane was broken upon retrieval, therefore no ICP-MS or TEM analyses were performed on this sample.

transferred onto copper TEM grids with carbon support membranes. The grids were placed in a drying oven at 60°C until dry. The specimens were examined with a FEI Tecnai G^2 transmission electron microscope equipped with an EDAX Super Ultra Thin Window (SUTW) EDX detector for semi-quantitative elemental analysis.

6.2.3.2 Moorings

A modified version of the dual compartment reactors (Fig. 6.1) was deployed during the LOCO (Long-Term Ocean Climate Observations) cruise D301/302 in the Mozambique Channel (March-April, 2006). About 50 mg of cleaned diatom frustules were suspended in a Teflon tube, whose opening was sealed with a dialysis membrane. The tube was submerged in a 10 g L^{-1} Mississippi Delta or Congo Fan sediment suspension (Table 6.2) in a 50 mL Falcon centrifuge tube. The centrifuge tubes were completely filled with filtered seawater to avoid deformation and leakage due to pressure. The seawater was collected from a depth of about 1200 m at the location of the mooring. Three reactors were placed in each of three stainless steel cages attached on a mooring line 500, 1250, and 2000 m below the sea surface (Table 6.2). The temperature at each depth was measured with a CTD at the time of deployment (Table 6.2).

The reactors were recovered after a period of 22 months during the LOCO cruise M75/1B in January, 2008. Upon recovery, the sediment suspension was filtered through a 0.2 µm pore size nylon filter, and the filtrate was refrigerated before analysis for dSi. The frustules were also recovered by centrifugation, rinsed, and subsequently frozen and freeze dried. The siliceous materials were analyzed chemically and microscopically as described before for the laboratory incubations.

6.3 Results

6.3.1 Dissolved silicate concentrations

Dissolved silicate (dSi) levels in the laboratory incubations stabilized after about 3 to 4 months. The dSi concentrations recorded at the end of the laboratory experiments (i.e., after 10 months) are presented in Fig. 6.2. The concentrations were independent of the fraction of seawater (10, 50 or 100% seawater). For the diatom frustules incubated without terrigenous sediment, the apparent silica solubilities ranged from 1130 to 1170 μM. In the reactors containing both diatoms and sediment, however, the concentrations were 30±3% lower. Mississippi Delta sediment suspended alone in seawater (experiment L100C) yielded a dSi concentration of 220 μM after the 10-month incubation.

The dSi concentrations measured immediately after recovering the reactors from the mooring line are shown in Fig. 6.3. The concentrations in the reactors containing only diatom frustules were 930, 810, and 770 μM, at 500, 1250, and 2000 m water depth, respectively. Reactors containing both frustules and terrigenous sediment exhibited dSi concentrations 35-46% lower than the frustules-only reactors deployed at the same depths. Concentrations of dSi measured in reactors

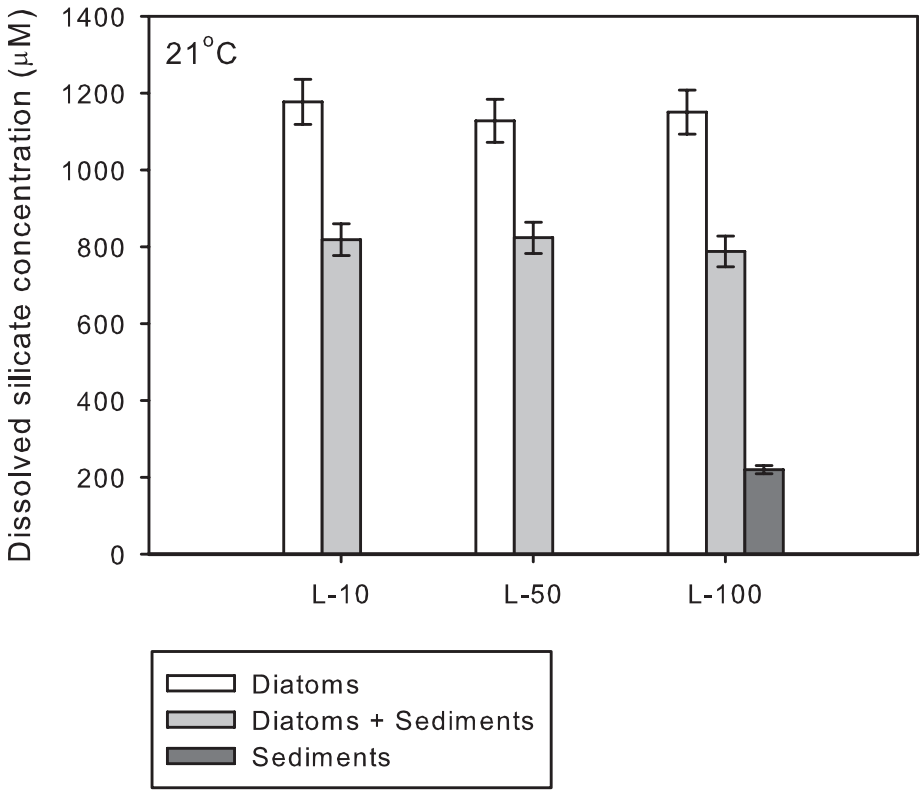

Figure 6.2 Dissolved silicate concentrations at the end of the laboratory experiments (10 months). L-10, L-50, and L-100 represent the 10% seawater, 50% seawater, and 100% seawater incubations (See Table 6.2 for details). Error bars correspond to the relative standard deviation of the colorimetric technique used for dSi analysis.

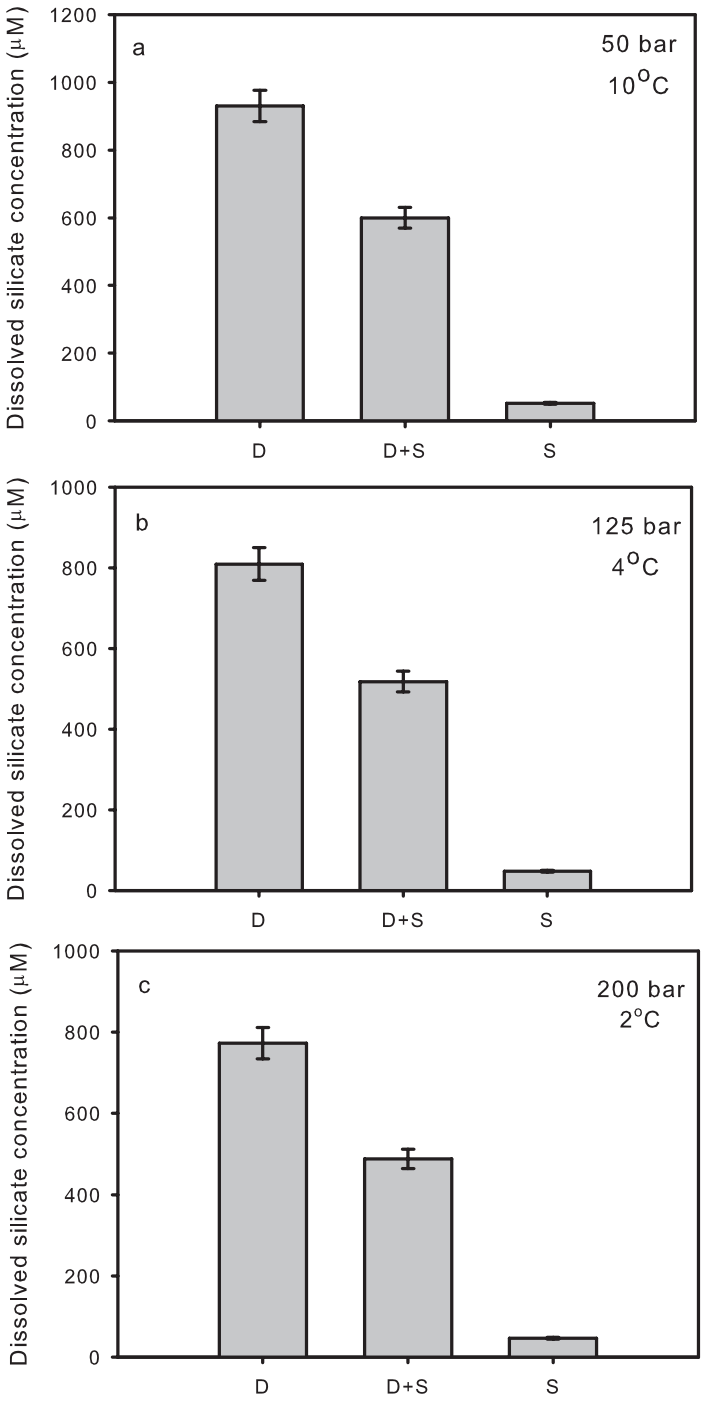

Figure 6.3 Dissolved silicate (dSi) concentrations at the end of the field experiments (22 months). Incubations deployed at 500m (a), 1250m (b), and 2000m (c) water depth. D = Diatom frustules only, D+S = Diatom frustules with sediment, and S = Sediment only (See Table 6.2 for details). Error bars represent the relative standard deviation of the colorimetric technique used to measure dSi.

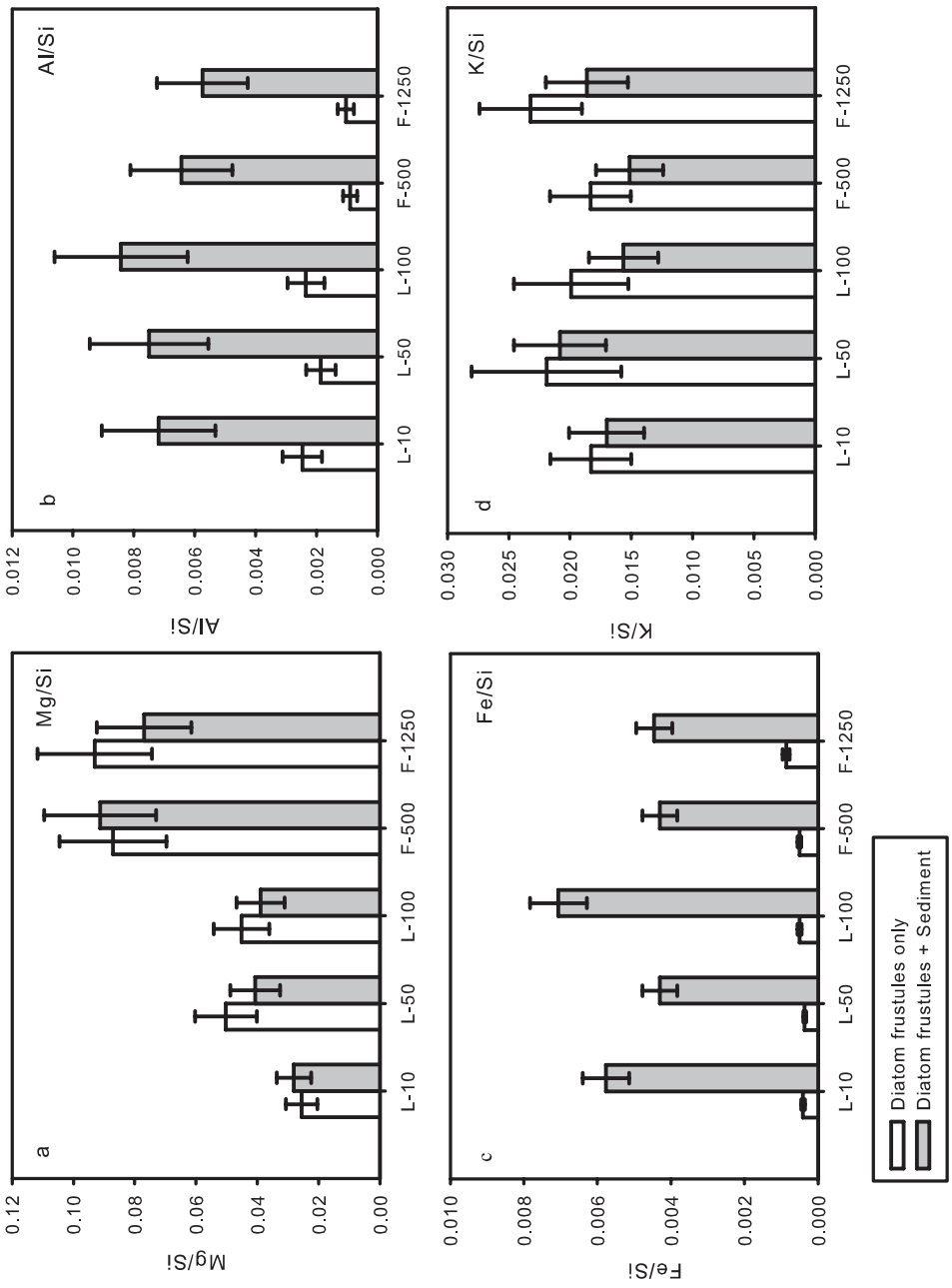

Figure 6.4 Mg/Si (a), Al/Si (b), Fe/Si (c), and K/Si (d) atomic ratios of the frustules incubated in the laboratory (L-10, L-50, L-100) and deployed at sea (F-500, F-1250), measured after total destruction by ICP-MS analysis. Error bars correspond to the reproducibility of the analytical technique.

containing only the terrigenous sediments were 52, 48, and 46 μM, at 500 (experiment F500S), 1250 (experiment F1250S), and 2000 m water depth (experiment F2000S), respectively.

The dSi concentrations measured in the incubations without terrigenous sediment were used to calculate how much of the initial $bSiO_2$ had dissolved by the end of the incubations. In the laboratory experiments, 7±0.2 % of $bSiO_2$ dissolved; in the incubations deployed at sea, 5.6, 4.9, and 4.6% dissolved at 500, 1250, and 2000 m water depth, respectively.

6.3.2 Bulk elemental compositions of frustules

The freshly grown frustules of *T. punctigera* consisted of nearly pure silica; concentrations of elements other than Si and O were close to or below detection (data not shown). In contrast, frustules recovered from the incubations performed in the laboratory or deployed at sea exhibited measurable impurity levels, as illustrated in Fig. 6.4 for a number of selected elements.

The atomic Mg/Si ratios of frustules incubated in the laboratory (0.02-0.05) were lower than those of frustules incubated at sea (0.07-0.09) (Fig. 6.4a). There was, however, no systematic difference in Mg/Si ratios between the diatom frustules incubated with terrigenous sediment and those incubated without. The lowest Mg/Si ratios were measured for the incubations in 10% seawater solutions. As for the Mg/Si ratios, the K/Si ratios showed no systematic differences between frustules incubated with or without terrigenous sediment (Fig. 6.4d). The values of the K/Si ratios were similar for incubations in the laboratory and those deployed in the Mozambique Channel (0.015-0.03). These results suggest that seawater was the main source of Mg and K uptake by the frustules.

A different picture emerged for Al and Fe. The Al/Si ratios of diatom frustules incubated in seawater without sediment were on the order of 0.002 for the laboratory experiments and 0.001 for the mooring deployment (Fig. 6.4b). Frustules incubated with terrigenous sediment exhibited ~5-fold higher Al/Si ratios (0.009-0.012 for the laboratory incubations, and ~0.006 for the mooring incubations). Similarly, Fe/Si ratios measured on frustules incubated with sediment (0.004-0.007) were about one order of magnitude higher than for those incubated without sediment (0.0003-0.0007) (Fig. 6.4c). The frustules incubated with sediment in the laboratory appeared to have slightly higher Al/Si and Fe/Si ratios than their counterparts incubated at sea. Overall, the results implied that the clay-rich terrigenous sediments were the source of Al and Fe.

6.3.3 Transmission electron microscopy

The frustules showed no obvious dissolution features at the end of the incubations, in line with the inferred low extent of dissolution (section 4.1). The well-preserved fine architecture of the frustules can be seen in Fig. 6.5a. In the incubations without terrigenous sediment, no visual evidence for newly formed mineral precipitates was found. EDX analyses showed invariably low, but detectable, trace levels of K, Na and Mg (Mg/Si, Na/Si, K/Si < 0.03) in exposed surfaces of the frustules. In the incubations with sediments, however, visual evidence and EDX compositional data clearly revealed the formation of new mineral phases inside the reactor compartments containing the diatom frustules (Fig. 6.5-6.7 and 6.9-6.11). These precipitates were in most cases closely associated with the frustules.

Examples of precipitates produced during the laboratory incubations with terrigenous sediment are shown in Fig. 6.5b and c. The precipitates were enriched in Al and contained some Ca, Mg and K. In the same laboratory experiments, euhedral crystallites composed mainly of Si, Al, and O were also observed (Fig. 6.6). The crystallite in Fig. 6.6a was not associated with a frustule, making

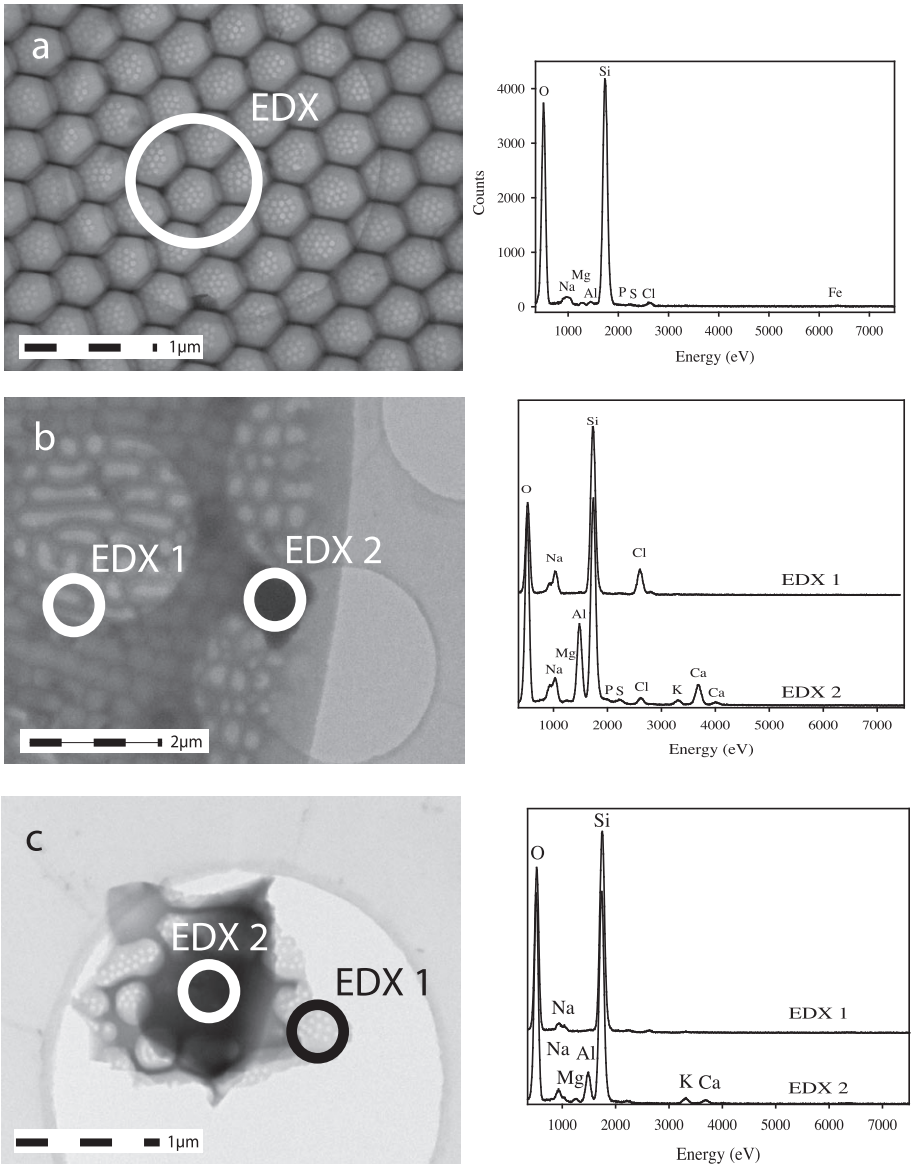

Figure 6.5 TEM images (Left) and EDX spectra (Right). a) Experiment L100DS: diatom frustule incubated in 100% seawater with Mississippi Delta sediment in the laboratory. b) Experiment L10DS: diatom frustule incubated in 10% seawater with Mississippi Delta sediment. The elemental composition of the dark area (EDX2) is compared to that of a clean (precipitate-free) area of the frustule (EDX2). c) Experiment L50DS: Fragment of diatom frustule incubated in 50% seawater with Mississippi Delta sediment. The elemental composition of the dark feature in the center (EDX2) is compared to that of the exposed frustule (EDX1).

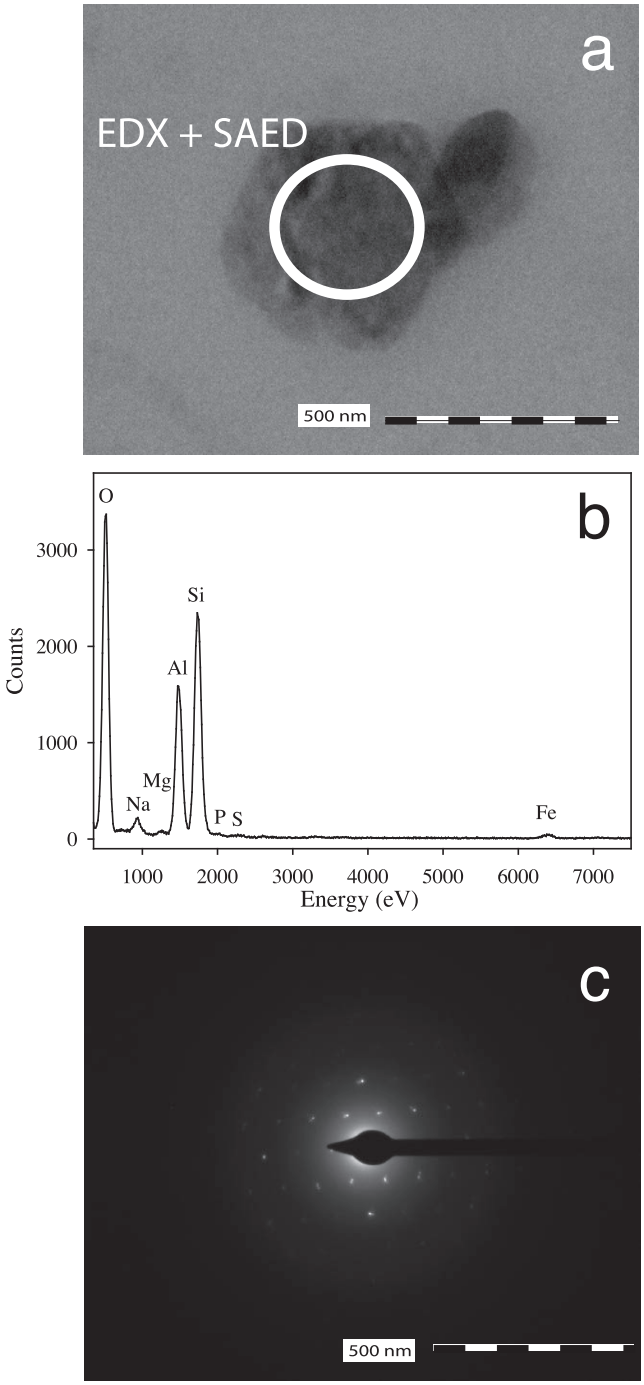

Figure 6.6 Experiment L50DS: a) Euhedral crystallite resting on the TEM grid. b) EDX spectrum indicates a mainly alumino-silicate composition. c) SAED diffraction pattern (see text for d values).

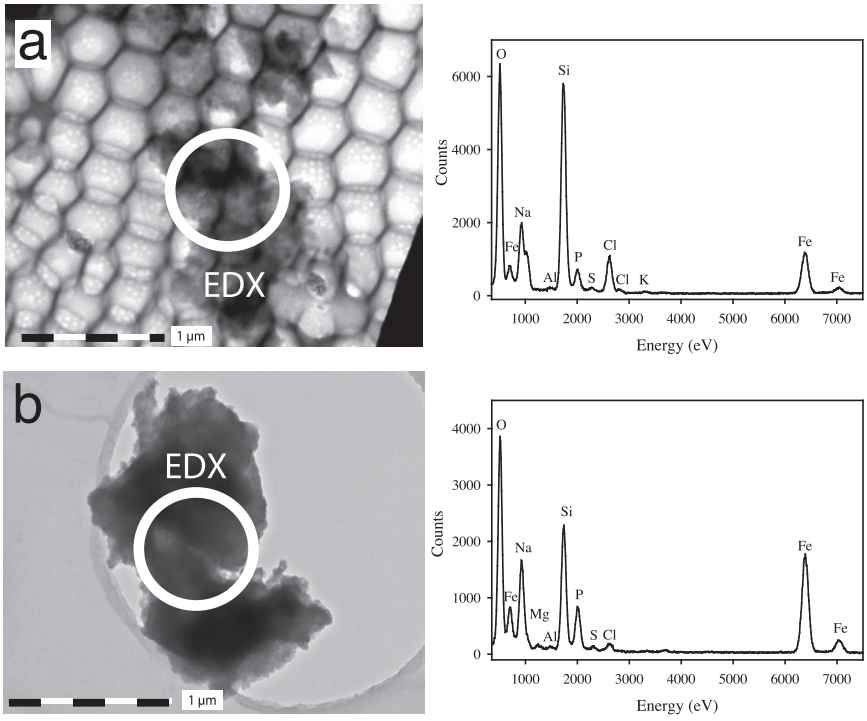

Figure 6.7 Experiment L100DS: Amorphous precipitates found on the surface of the diatom frustules incubated in 100% seawater with Mississippi Delta sediment (a) and on the TEM grid of the same incubation (b). The panels on the right are the corresponding EDX spectra. The white circles on the images represent the areas covered by the electron beam.

it possible to use the EDX spectrum (Fig. 6.6b) to semi-quantitatively estimate the elemental composition: Al/Si, Mg/Si and Fe/Si ratios were 0.7, 0.03 and 0.02, respectively. Selected Area Electron Diffraction (SAED) revealed a pseudohexagonal pattern characteristic of clay minerals with the (001) plane normal to the electron beam (Fig. 6.6c). Indexing of the diffraction pattern yielded d values of 4.20, 2.60, and 1.40Å.

Also characteristic of all the laboratory incubations with Mississippi Delta sediment were the amorphous precipitates illustrated in Fig. 6.7. These precipitates were mostly deposited onto the surfaces of the diatom frustules (Fig. 6.7a), although some detached precipitates were also found (Fig. 6.7b). The EDX analyses revealed the systematic presence of Fe and P in amorphous precipitates, with a remarkably uniform atomic P/Fe ratio of around 0.4 (Fig. 6.8).

The precipitates observed in the incubations with terrigeneous sediment deployed along the mooring line were distinct from those observed in the laboratory incubations. Most characteristic were amorphous-looking infillings of the nanoscale pores inside the frustules' areolae (Fig. 6.9). The infillings were observed for frustules incubated with sediment at the three water depths. Frustules incubated without sediment did not exhibit this feature. EDX analysis showed that the precipitates were mainly composed of Si and Mg (Fig. 6.9a and 6.9b). The relative abundances of Si and Mg could not be accurately determined, due to interference of the Si from the frustules themselves.

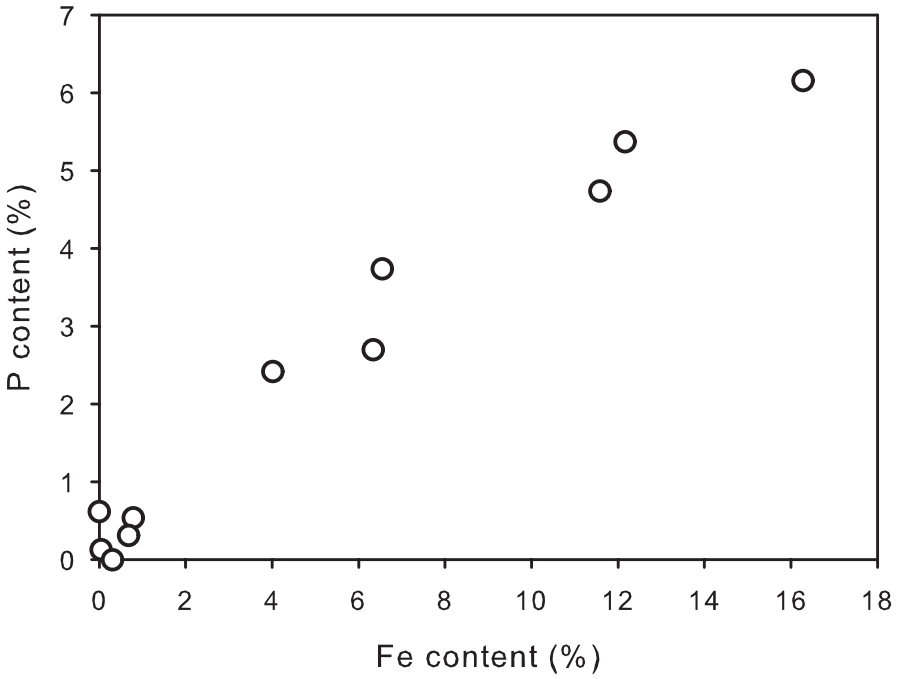

Figure 6.8 P and Fe contents of the ubiquitous amorphous Fe-P precipitates found in the laboratory incubations with diatom frustules and Mississippi Delta sediment. Each point represents a distinct precipitate. The P and Fe concentrations are semi-quantitative estimates obtained from the EDX spectra. Linear fitting gives an atomic P/Fe ratio of ~0.4.

Two other types of precipitates were systematically found in the incubations with sediment deployed at sea (Fig. 6.10 and 6.11). The first one consisted of amorphous accumulations on the surface of frustules, which contained Mg, Fe, Mn, Al, and P (Fig. 6.10). EDX line profiles revealed strong correlations between the Fe, Mg, and Mn distributions (Fig. 6.10c): average atomic Fe/Mg and Mn/Mg ratios were around 0.6 and 0.1, respectively. In contrast, the relative concentrations of the other elements (Al, S, and P) in the precipitates were variable. The second type of precipitates is illustrated in Fig. 6.11. These amorphous precipitates were rich in Al, and contained significant levels of Mg, Na, K, and Fe.

In addition of newly formed mineral deposits, EDX analyses also revealed the incorporation of Fe (and Mg) into structural elements of the frustules. This is illustrated in Fig. 6.12, where the covariance of Mg and Fe with Si suggests a uniform distribution of the chemical elements in the silica framework. For the area of the frustule shown in Fig. 6.12, the Fe/Si and Mg/Si ratios were about 0.3 and 0.03, respectively.

6.4 Discussion

Biogenic silica is unstable under conditions encountered in the oceans. First-order dissolution rate constants measured for freshly exposed diatom frustules can be as high as 16 y^{-1} (Van Cappellen et al., 2002b), implying half-lives of $bSiO_2$ of only a few weeks. Thus, in principle, only a negligibly

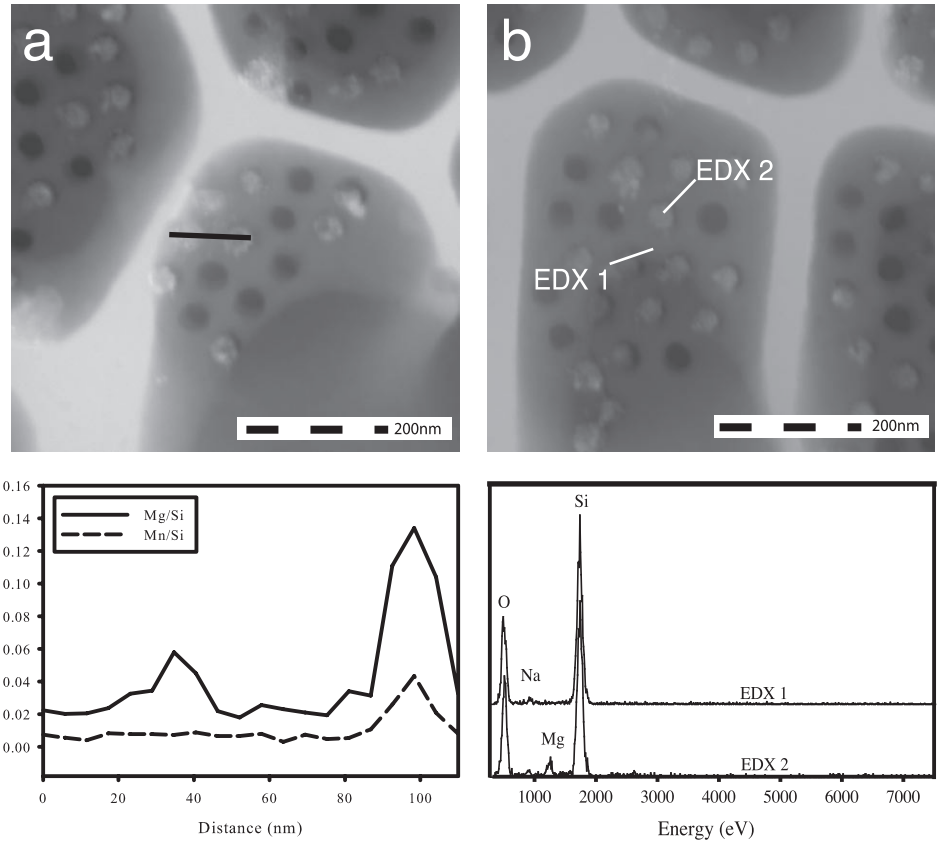

Figure 6.9 a) Experiment F500DS: STEM image showing the infilling of small pores of frustules incubated with Mississippi Delta sediment at sea, at 500m depth. A number of pores are filled with Mg and Mn-rich precipitates. This is the case for the pore at the right end of the EDX line profile (black line). The line profile below the STEM image is based on 20 EDX point analyses along the black line. b) Experiments F1250DS: STEM image of a frustule incubated with Congo Fan sediment at 1250m depth. The panel below compares the EDX spectra of a point on the frustule surface (EDX 1) and that of a pore filling (EDX 2).

small fraction of $bSiO_2$ produced by marine organisms should make it into the sedimentary record. This is not the case, as evidenced by the preservation of biosiliceous remains in many marine deposits, including high-latitude siliceous oozes.

One reason a non-negligible fraction of $bSiO_2$ escapes dissolution and is buried in marine sediments is that the solubility of diatom frustules starts to decrease once the silica surfaces are exposed to seawater, thereby reducing the thermodynamic driving force for $bSiO_2$ dissolution. The apparent silica solubilities measured at the end of the 10 and 22 month long incubations without terrigenous sediment are in fact substantially lower than the solubility of the same diatom frustules measured by Loucaides et al. (2008) in much shorter incubations (two weeks), at a higher solid to solution ratio (10g L^{-1}) than used here (1750 µM at 25°C and 0.1M NaCl; Fig. 6.13).

Rickert et al. (2002) and Schmidt et al. (2004) observed that the solubility of diatomaceous silica declined with depth in the water column, which the ascribed to a progressive change in the

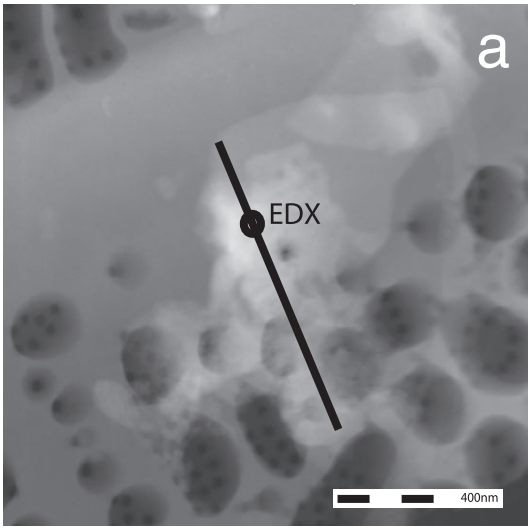

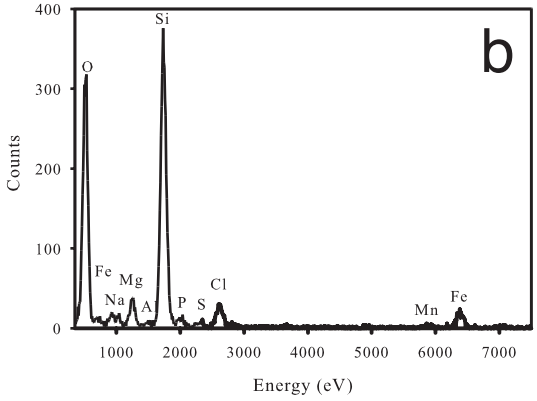

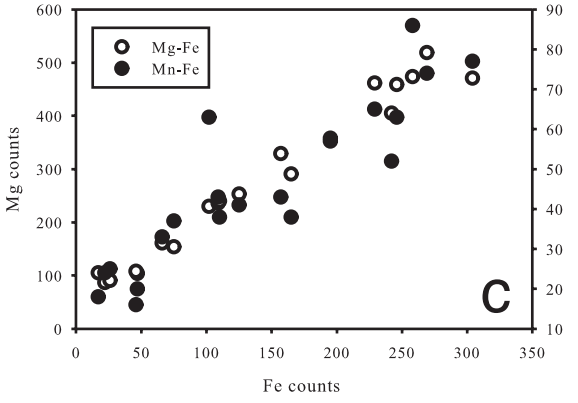

Figure 6.10. Experiment F1250DS: a) STEM image of an amorphous deposit on a diatom frustule incubated at sea at 1250m. b) EDX spectra of a point analysis whose location is indicated on the image by the small circle. c) Correlations between the Fe, Mg, and Mn EDX counts along the dark line (Panel a) based on 20 discrete EDX point measurements.

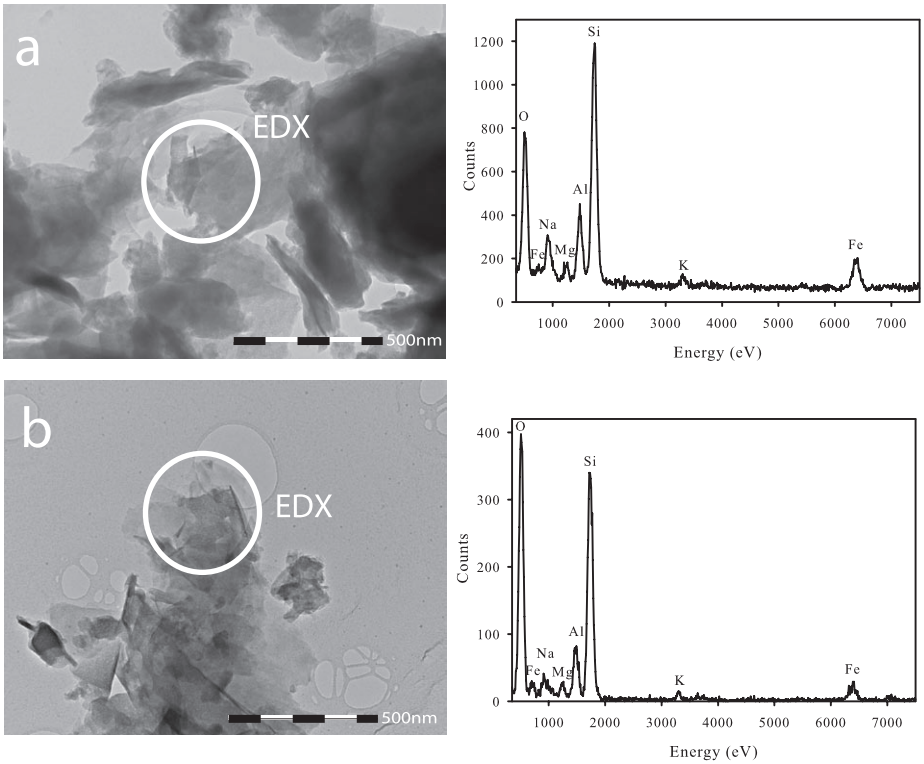

Figure. 6.11. Amorphous precipitates found in the incubations deployed at sea, at a) 500m (F500DS) and b) 1250m (F1250DS), and corresponding EDX spectra. The white circles on the images represent the area covered by the electron beam.

physicochemical properties of the diatom frustules during settling. As suggested by the results of the incubations presented here, the decrease in solubility may in part be due to the uptake of seawater ions by the diatom frustules (Fig. 6.4). In particular, our EDX measurements show that Mg ions may penetrate the surface layers of silica (Fig. 6.12). Given the minimal amounts of silica that dissolved during the incubations (≤ 7%), it appears plausible that the lower apparent silica solubilities at the end of the frustule-seawater incubations are caused by chemical interactions of the $bSiO_2$ with seawater. A lowering of the solubility of synthetic amorphous silica in electrolyte solutions has been reported in earlier studies (Chen and Marshall, 1982; Weres et al., 1981). The authors noted that the presence of Mg^{2+} ions, in particular, decreases the solubility of amorphous silica.

Uptake of additional ions in the presence of the terrigenous sediments (Fig. 6.4) coincides with a further drop in apparent silica solubilities (Fig. 6.2 and 6.3). These results are in line with the findings of Dixit et al. (2001). These authors found that the build-up of dissolved silicate, in batch experiments where $bSiO_2$ and either kaolinite or ground basalt were suspended together in 0.7 M NaCl solution, decreased systematically as the mass ratio of the lithogenic constituent to $bSiO_2$ increased. This inverse relationship is reminiscent of that observed between the asymptotic pore water dSi concentration and the abundance of lithogenic mineral compounds, relative to that of $bSiO_2$, in deep-sea sediments of the Southern Ocean (Van Cappellen and Qiu, 1997b). In contrast

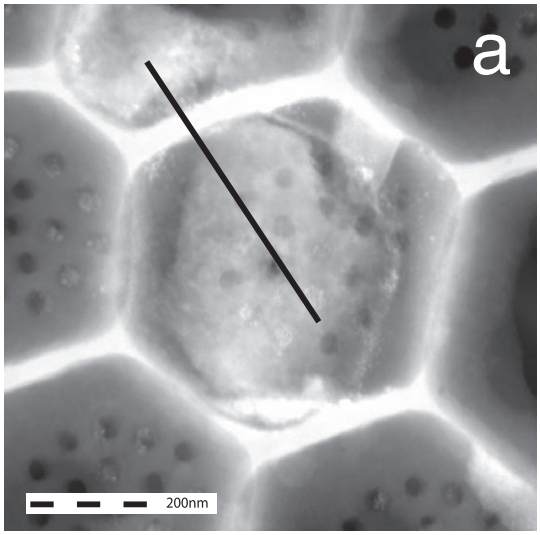

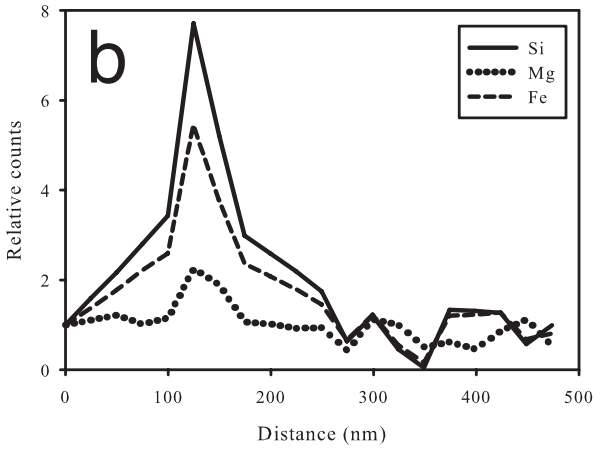

Figure 6.12. Experiment F1250DS. a) Scanning Transmission Electron Microscopy (STEM) image of an areola of a diatom frustule incubated at sea with Congo River Fan sediment at a water depth of 1250m. Bright areas correspond to thicker parts of the frustule. b) Line EDX profiles based on 20 discrete analysis points along the black line (from top left to bottom right).

to the present study, however, no attempt was made by Dixit et al. (2001) to identify the reaction products of the interactions between the $bSiO_2$ and the lithogenic compounds.

Previous studies dealing with variations of pore water dSi concentrations and $bSiO_2$ preservation in marine sediments have stressed the role of Al uptake by biosiliceous debris (Dixit et al., 2001; Van Bennekom et al., 1989; Van Bennekom et al., 1991; Van Cappellen and Qiu, 1997b). Diatom frustules retrieved from Congo Fan sediments have clearly shown that $bSiO_2$ can take up significant amounts of Al during early diagenesis (Van Bennekom et al., 1989). Results from experimental studies further demonstrate that sorption of aluminum reduces both the solubility and dissolution kinetics of $bSiO_2$ (Iler, 1979; Van Bennekom et al., 1989; Van Bennekom et al., 1991).

The results of the present study confirm that Al is transferred from the terrigenous clay-rich sediments to the diatom frustules (Fig. 6.4). Because of the presence of a dialysis membrane in the reactors, the transfer must be mediated by soluble Al diffusing from the sediment suspension to the

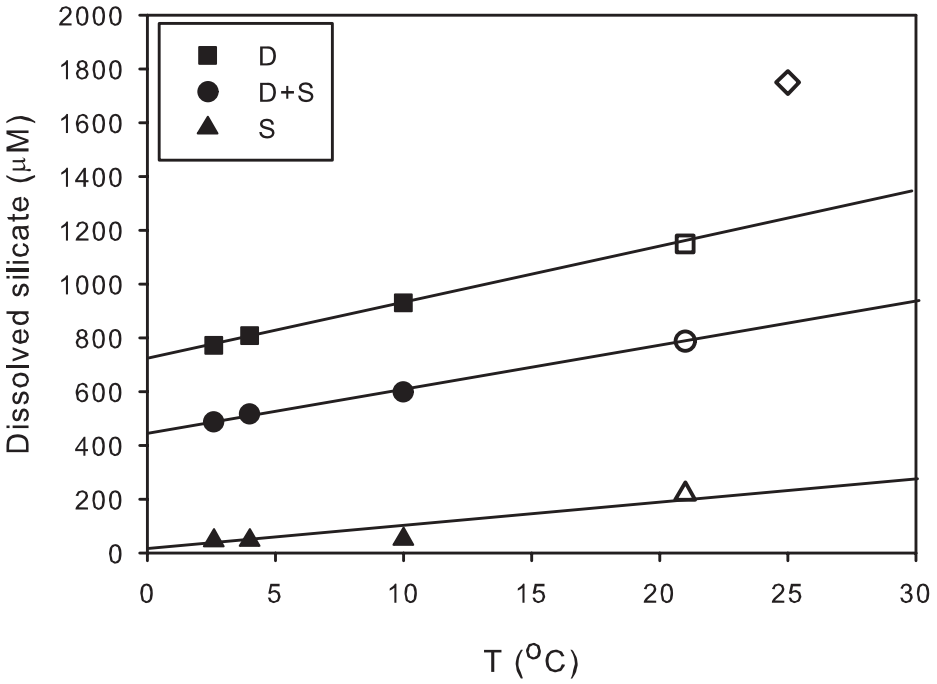

Figure 6.13. Apparent silica solubilities as a function of temperature measured at the end of the incubations deployed at sea (filled symbols) and carried out in the laboratory (open symbols). The open diamond represents the solubility concentration of *T. punctigera* determined in 0.1M NaCl solution and a solid/solution ratio of 10 g L^{-1}. D = Diatom frustules only, D+S = Diatom frustules with sediment, and S = Sediment only (See Table 6.2 for details).

frustules. The bulk Al/Si ratios of the diatom frustules incubated with sediment (0.005-0.008) are similar to those reported for diatom remains recovered from siliceous sediments of the Southern Ocean (Dixit et al., 2001), and fresh frustules equilibrated with aluminum enriched seawater (Koning et al., 2007).

A significant fraction of Al associated with diatom frustules at the end of the incubations with the terrigenous sediments is present as newly formed precipitates (Fig. 6.5b, 6.5c and 6.6a). The aluminosilicate crystallites formed during the laboratory incubations exhibit elemental compositions and electron diffraction patterns (Fig. 6.6c) that are similar to those reported by Michalopoulos et al. (2000) in sediments of the Amazon River delta. In addition to Si, Al is mainly associated with Ca, Mg, Na, K and Fe in the various types of precipitates. Thus, the experimental data presented here are entirely consistent with the hypothesis of reverse weathering reactions postulated more than five decades ago by Mackenzie and Garrels (1966).

The complete conversion of diatom frustules into clay minerals, as observed by Michalopoulos et al. (2000) in sediments of the Amazon River delta, likely represents the end product of biogenic silica early diagenesis, as a result of the high availability of relatively reactive terrigenous minerals in deltaic depositional settings (Michalopoulos and Aller, 2004; Presti and Michalopoulos, 2008). The pristine appearance of the diatom frustule surfaces, the low amounts of $bSiO_2$ dissolved, and the dispersed occurrence of new precipitates in the incubations with sediment carried out in this study illustrate a less advanced stage of the interactions between $bSiO_2$ and terrigenous minerals.

The results of the laboratory and field incubations, both with and without terrigenous sediment, point to an important role of seawater Mg in the diagenesis of $bSiO_2$. The higher Mg/Si ratios of the diatoms incubated at sea may reflect the longer contact time, compared to the laboratory experiments (Fig. 6.4). The EDX analyses confirm that, for the incubations deployed at sea, Mg is present at higher concentrations within the walls of frustules (Fig. 6.12), but is also more abundantly represented in new precipitates (Fig. 6.9, 6.10, and 6.11). Particularly characteristic for the incubations with terrigenous sediment deployed in the Mozambique Channel are the Mg-rich silicate pore infillings of the frustules (Fig. 6.9).

The precipitation of Mg-rich silicate minerals is in line with the experiments of Wollast et al. (1968), who demonstrated that, under alkaline conditions (pH > 8) sepiolite-type minerals readily precipitate out of seawater upon addition of dissolved silicate. Kastner et al. (1977) further proposed that Mg plays a significant role in the later diagenetic transformation of $bSiO_2$ to opal-CT. However, to our knowledge, early diagenetic interactions between $bSiO_2$ and seawater Mg have not been studied before. The results of the incubations suggest that these interactions decrease $bSiO_2$ solubility and, hence, may enhance the sedimentary removal of Si and Mg from the oceans.

Iron (Fe) plays an important role in the early diagenesis of $bSiO_2$ and the associated formation of authigenic silicate minerals in anoxic coastal marine sediments (Michalopoulos and Aller, 1995; Michalopoulos and Aller, 2004; Michalopoulos et al., 2000). The results of the incubations presented here provide further direct evidence for the transfer of Fe from the terrigeneous sediment minerals to the diatom frustules. The products of the transfer of Fe, however, differ between the incubations carried out in the laboratory and those deployed at sea. The differences appear to be related to the redox conditions in the two series of incubations.

In the laboratory incubations, fully oxygenated seawater was used in the preparation of the suspensions, and the headspace above the suspensions consisted of regular air. Under these oxic conditions, the Fe and P-rich precipitates observed in the laboratory experiments where frustules and terrigeneous sediment were suspended together (Fig. 6.7) are most likely ferric iron oxyhydroxides resulting from the oxidative precipitation of ferrous iron solubilized from the sediments. Such Fe(III) precipitates are commonly found in the upper oxic layers of nearshore sediments (Hyacinthe and Van Cappellen, 2004 and references therein). Furthermore, ferric iron oxyhydroxides formed in the presence of high levels of dissolved silicate exhibit enhanced sorption capacities for phosphate (Mayer and Jarrell, 2000), which may explain the significant amounts of phosphate associated with the precipitates produced in the laboratory incubations ($P/Fe \approx 0.4$, Fig. 6.8).

In the incubations deployed at sea, the evidence does not support the formation of ferric iron oxyhydroxides, probably because of more reducing conditions. The experimental suspensions had no headspace, and were prepared using seawater with dissolved oxygen well below saturation (approximately 90 μM, personal communication, Erica Koning). Iron is mainly associated with Mg and Mn in the precipitates observed in the incubations with terrigeneous sediment. The relatively constant proportions among the three metals (Fig. 6.10c) suggest that iron is present as Fe^{2+} in the precipitates.

Early work by Lewin (1961) showed that iron under the ferrous form has a more pronounced effect on the dissolution of $bSiO_2$, compared to ferric iron. This author observed a significant decline in the silica dissolution rate when diatom frustules were incubated in ferrous phosphate solution, but not in ferric chloride solution. The inhibitory effect of Fe^{2+} could be related to its incorporation in the silica structure, as suggested by the EDX measurements presented here (Fig. 6.12).

6.5 Conclusions

The results of the long-term incubation experiments provide direct experimental evidence for a significant decrease in apparent silica solubility of diatom frustules upon exposure to seawater, on the time scale of 1-2 years. The apparent silica solubility decreases even further in the presence of fine-grained deltaic sediments. Chemical interactions involve the transfer of chemical elements from seawater (e.g., Mg, K) and from the clay-rich sediments (e.g., Al, Fe, Mn) to the frustules. The latter may result in the formation of a variety of new mineral precipitates, often deposited on the surfaces of the frustules. The precipitates include alumino-silicate and magnesian silicate phases. Under oxic conditions, phosphate-rich ferric iron oxyhydroxides may also form.

The decrease in silica solubility, and the reaction products of the interactions between the diatom frustules and terrigeneous sediment observed in this study correspond to the initial stages of the early diagenetic transformation of biogenic silica in marine sediments. In nearshore depositional environments containing relatively reactive terrigeneous clay minerals, further interactions may ultimately lead to the complete conversion of biogenic silica into authigenic clay minerals, as shown in previous studies. The extent and products of interactions between biogenic silica and lithogenic minerals in deep-sea sediments will need further assessment.

The interactions between biogenic silica, seawater and lithogenic minerals enhance the removal of reactive silicon from the ocean system through sedimentary burial. In addition, uptake by biogenic silica and the precipitation of secondary mineral products may affect the biogeochemical cycles of other key biological (e.g., Fe, P) and geochemical (e.g., Mg, Al) elements. While some of these processes have long been recognized, they are rarely considered in budgets and model studies of biogeochemical cycles.

References

Abelmann, A., Gersonde, R., and Spiess, V., 1988. Pliocene – Pleistocene paleoceanography in the Weddell Sea – Siliceous microfossil evidence. In: Bleil, U. and Thiede, J. Eds.), *Geological history of the polar oceans: Arctic versus Antarctic*. Kluwer Academic Publishers, Bremen.

Alexandre, A., Meunier, J.-D., Colin, F., and Koud, J.-M., 1997. Plant impact on the biogeochemical cycle of silicon and related weathering processes. *Geochim Cosmochim Acta* **61**, 677-682.

Alldredge, A. L. and Cohen, Y., 1987. Can Microscale Chemical Patches Persist in the Sea? Microelectrode Study of Marine Snow, Fecal Pellets. *Science* **235**, 689-691.

Alldredge, A. L. and Gotschalk, C., 1988. In Situ Settling Behavior of Marine Snow. *Limnol Oceanogr* **33**, 339-351.

Alldredge, A. L., Granata, T. C., Gotschalk, C. C., and Dickey, T. D., 1990. The Physical Strength of Marine Snow and its Implications for Particle Disaggregation in the Ocean. *Limnol Oceanogr* **35**, 1415-1428.

Alldredge, A. L. and Silver, M. W., 1988. Characteristics, dynamics and significance of marine snow. *Prog Oceanog* **20**, 41-82.

Anderson, G. F., 1986. Silica, diatoms and a freshwater productivity maximum in Atlantic coastal plain estuaries, Chesapeake Bay. *Estuar Coast Shelf Sci* **22**, 183-197.

Archer, D., Lyle, M., Rodgers, K., and Froelich, P., 1993. What controls opal preservation in tropical deep-sea sediments? *Paleoceanography* **8**, 7-21.

Baeyens, W., van Eck, B., Lambert, C., Wollast, R., and Goeyens, L., 1997. General description of the Scheldt estuary. *Hydrobiologia* **366**, 1-14.

Barker, P., 1992. Differential diatom dissolution in Late Quaternary sediments from Lake Manyara, Tanzania: an experimental approach. *J Paleolimnol* **7**, 235-251.

Barker, P., Fontes, J. C., Gasse, F., and Druart, J. C., 1994. Experimental dissolution of diatom silica in concentrated salt-solutions and implications for paleoenvironmental reconstruction. *Limnol Oceanogr* **39**, 99-110.

Beck, L., Gehlen, M., Flank, A.-M., Van Bennekom, A. J., and Van Beusekom, J. E. E., 2002. The relationship between Al and Si in biogenic silica as determined by PIXE and XAS. *Nuclear Instruments and Methods in Physics Research Section B: Beam Interactions with Materials and Atoms* **189**, 180-184.

Berger, W. H. and Herguera, J. C., 1992. Reading the sedimentary record of the ocean's productivity. In: Palkowski, P. G. and Woodhead, A. D. Eds.), *Primary production and biogeochemical cycles in the sea*. Plenum Press, New York.

Bidle, K. D. and Azam, F., 1999. Accelerated dissolution of diatom silica by marine bacterial assemblages. *Nature* **397**, 508-512.

Bidle, K. D. and Azam, F., 2001. Bacterial Control of Silicon Regeneration from Diatom Detritus: Significance of Bacterial Ectohydrolases and Species Identity *Limnol Oceanogr* **46**, 1606-1623.

Birks, H. J. B., Line, J. M., Juggins, S., Stevenson, A. C., and Ter Braak, C. J. F., 1990. Diatoms and pH reconstruction. *Philos Trans R Soc Lond B Biol Sci* **327**, 263-278.

Boudreau, B. P., 1990. Asymptotic Forms and Solutions of the Model for Silica-Opal Diagenesis in Bioturbated Sediments. *J Geophys Res* **95**, 7367-7379.
Brady, P. V. and Walther, J. V., 1990. Kinetics of quartz dissolution at low temperatures. *Chem Geol* **82**, 253.
Brzezinski, M. A., 1985. The Si:C:N ratio of marine diatoms: interspecific variability and the effect of some environmental variables. *J Phycol* **21**, 347-357.
Brzezinski, M. A., Alldredge, A. L., and O'Bryan, L. M., 1997. Silica Cycling Within Marine Snow. *Limnol Oceanogr* **42**, 1706-1713.
Brzezinski, M. A., Jones, J. L., Bidle, K. D., and Azam, F., 2003. The balance between silica production and silica dissolution in the sea: Insights from Monterey Bay, California, applied to the global data set. *Limnol Oceanogr* **48**, 1846-1854.
Brzezinski, M. A., Olson, R. A., and Chisholm, S. W., 1990. Silicon availability and cell-cycle progression in marine diatoms. *Mar Ecol Prog Ser* **67**, 83-96.
Chen, C.-T. A. and Marshall, W. L., 1982. Amorphous silica solubilities IV. Behavior in pure water and aqueous sodium chloride, sodium sulfate, magnesium chloride, and magnesium sulfate solutions up to 350°C. *Geochim Cosmochim Acta* **46**, 279-287.
Claquin, P., Martin-Jezequel, V., Kromkamp, J. C., Veldhuis, M. J. W., and Kraay, G. W., 2002. Uncoupling of silicon compared with carbon and nitrogen metabolisms and the role of the cell cycle in continuous cultures of thalassiosira pseudonana (Bacillariophyceae) under light, nitrogen, and phosphorous control. *J Phycol* **38**, 922-930.
Conley, D. J., 1997. Riverine contribution of biogenic silica to the oceanic silica budget. *Limnol Oceanogr* **42**, 774-777.
Conley, D. J. (2002) Terrestrial ecosystems and the global biogeochemical silica cycle. *Global Biogeochem Cycles* **16**, 10.1029/2002GB001894.
Conley, D. J. and Kilham, S. S., 1989. Differences in silica content between marine and freshwater diatoms. *Limnol Oceanogr* **34**, 205-213.
Corzo, A., Morillo, J. A., and Rodríguez, S., 2000. Production of transparent exopolymer particles (TEP) in cultures of Chaetoceros calcitrans under nitrogen limitation. *Aquat Microb Ecol* **23**, 63-72.
Datnoff, L. E., Snyder, G. H., and Korndörfer, G. H., 2001. Silicon in Agriculture. Elsevier Science, Amsterdam.
Davis, C. O., 1976. Continuous culture of marine diatoms under silicate limitation. II. Effect of light intensity on growth and nutrient uptake of *Skeletonema constantum*. *J Phycol* **12**, 291-300.
de Keizer, A., van der Ent, E. M., and Koopal, L. K., 1998. Surface and volume charge densities of monodisperse porous silicas. *Colloid Surface A* **142**, 303-313.
DeMaster, D. J., 1981. The supply and accumulation of silica in the marine environment. *Geochim Cosmochim Acta* **45**, 1715-1732.
DeMaster, D. J., 2002. The accumulation and cycling of biogenic silica in the Southern Ocean: revisiting the marine silica budget. *Deep Sea Res II* **49**, 3155-3167.
Derry, L. A., Kurtz, A. C., Ziegler, K., and Chadwick, O. A., 2005. Biological control of terrestrial silica cycling and export fluxes to watersheds. *Nature* **433**, 728-731.
Dixit, S. and Van Cappellen, P., 2002. Surface chemistry and reactivity of biogenic silica. *Geochim Cosmochim Acta* **66**, 2559-2568.
Dixit, S. and Van Cappellen, P. (2003) Predicting benthic fluxes of silicic acid from deep-sea sediments. *J Geophys Res* **108**, 10.1029/2002JC001309.

Dixit, S., Van Cappellen, P., and van Bennekom, A. J., 2001. Processes controlling solubility of biogenic silica and pore water build-up of silicic acid in marine sediments. *Mar Chem* **73**, 333-352.

Dove, P. M., 1994. The dissolution kinetics of quartz in sodium chloride solutions at 25 degrees to 300 degrees C. *Am J Sci* **294**, 665-712.

Dove, P. M., 1999. The dissolution kinetics of quartz in aqueous mixed cation solutions. *Geochim Cosmochim Acta* **63**, 3715-3727.

Dove, P. M. and Crerar, D. A., 1990. Kinetics of quartz dissolution in electrolyte solutions using a hydrothermal mixed flow reactor. *Geochim Cosmochim Acta* **54**, 955-969.

Dove, P. M. and Elston, S. F., 1992. Dissolution kinetics of quartz in sodium-chloride solutions – analysis of existing data and a rate model for 25-Degrees-C. *Geochim Cosmochim Acta* **56**, 4147-4156.

Dove, P. M. and Nix, C. J., 1997. The influence of the alkaline earth cations, magnesium, calcium, and barium on the dissolution kinetics of quartz. *Geochim Cosmochim Acta* **61**, 3329-3340.

Drapeau, D. T., Dam, H. G., and Grenier, G., 1994. An Improved Flocculator Design for Use in Particle Aggregation Experiments. *Limnol Oceanogr* **39**, 723-729.

Dugdale, R. C. and Wilkerson, F. P., 1998. Silicate regulation of new production in the equatorial Pacific upwelling. *Nature* **391**, 270-273.

Dugdale, R. C., Wilkerson, F. P., and Minas, H. J., 1995. The role of a silicate pump in driving new production. *Deep Sea Res I* **42**, 697-719.

Durbin, E. G., 1977. Studies in the autoecology of the marine diatom *Thalassiosira nordenskioeldii.* II. The influence of cell size on growth rate and carbon. nitrogen, chlorophyll *a* and silica content. *J Phycol* **13**, 150-155.

Einarsson, Á., 2004. Lake Myvatn and the River Laxá: An introduction. *Aquat Ecol* **38**, 111-114.

Epstein, E., 1999. Silicon. *Annu Rev Plant Physiol Plant Mol Biol* **50**, 641-664.

Falkner, K. K., Church, M., Measures, C. I., LeBaron, G., Thouron, D., Jeandel, C., Stordal, M. C., Gill, G. A., Mortlock, R., Froelich, P., and Chan, L. H., 1997. Minor and trace element chemistry of Lake Baikal, its tributaries, and surrounding hot springs. *Limnol Oceanogr* **42**, 329-345.

Fleming, B. A., 1986. Kinetics of reaction between silicic acid and amorphous silica surfaces in NaCl solutions. *J Colloid Interface Sci* **110**, 40.

Fowler, S. W. and Fisher, N. S., 1983. Viability of marine phytoplankton in zooplankton fecal pellets. *Deep Sea Res* **30**, 963-969.

Fraysse, F., Cantais, F., Pokrovsky, O. S., Schott, J., and Meunier, J. D., 2006a. Aqueous reactivity of phytoliths and plant litter: Physico-chemical constraints on terrestrial biogeochemical cycle of silicon. *J Geochem Explor* **88**, 202-205.

Fraysse, F., Pokrovsky, O. S., Schott, J., and Meunier, J.-D., 2006b. Surface properties, solubility and dissolution kinetics of bamboo phytoliths. *Geochim Cosmochim Acta* **70**, 1939-1951.

Fritz, S. C., Juggins, S., Battarbee, R. W., and Engstrom, D. R., 1991. Reconstruction of past changes in salinity and climate using a diatom-based transfer function. *Nature* **352**, 706-708.

Frohlich, F., 1989. Deep-sea biogenic silica: new structural and analytical data from infrared analysis – geological implications. *Terra Nova* **1**, 267-273.

Gallinari, M., Ragueneau, O., Corrin, L., DeMaster, D. J., and Treguer, P., 2002. The importance of water column processes on the dissolution properties of biogenic silica in deep-sea sediments I. Solubility. *Geochim Cosmochim Acta* **66**, 2701-2717.

Gehlen, M., Beck, L., Calas, G., Flank, A.-M., Van Bennekom, A. J., and Van Beusekom, J. E. E., 2002. Unraveling the atomic structure of biogenic silica: evidence of the structural association of Al and Si in diatom frustules. *Geochim Cosmochim Acta* **66**, 1601-1609.

Gehlen, M. and Van Raaphorst, W., 2002. The role of adsorption-desorption surface reactions in controlling interstitial $Si(OH)_4$ concentrations and enhancing Si(OH)₄ turnover in shallow shelf seas. *Cont Shelf Res* **22**, 1529-1547.

Gendron-Badou, A., Coradin, T., Maquet, J., Frohlich, F., and Livage, J., 2003. Spectroscopic characterization of biogenic silica. *J Non-Cryst Solids* **316**, 331-337.

Gensemer, R. W., 1990. Role of aluminum and growth rate on changes in cell size and silica content of silica-limited populations of *Asterionella ralfsii* var. *Americana* (Basillariophyceae).. *J Phycol* **26**, 250-258.

Grauer, R. and Stumm, W., 1982. Die Koordinationschemie oxidischer Grenzflächen und ihre Auswirkung auf die Auflösungskinetik oxidischer Festphasen in wäßrigen Lösungen. *Colloid Polym Sci* **260**, 959.

Greenwood, J. E., Truesdale, V. W., and Rendell, A. R., 2001. Biogenic silica dissolution in seawater – in vitro chemical kinetics. *Prog Oceanog* **48**, 1-23.

Gun'ko, V. M., Mironyuk, I. F., Zarko, V. I., Voronin, E. F., Turov, V. V., Pakhlov, E. M., Goncharuk, E. V., Nychiporuk, Y. M., Vlasova, N. N., and Gorbik, P. P., 2005. Morphology and surface properties of fumed silicas. *J Colloid Interface Sci* **289**, 427-445.

Hamm, C. E., Merkel, R., Springer, O., Jurkojc, P., Maier, C., Prechtel, K., and Smetacek, V., 2003. Architecture and material properties of diatom shells provide effective mechanical protection. *Nature* **421**, 841-843.

Harrison, P. J., Conway, H. L., and Dugdale, R. C., 1976. Marine diatoms grown in chemostats under silicate or ammonium limitation. I. Cellular chemical composition and steady-state growth kinetics of Skeletonema costatum. *Mar Biol* **35**, 177-186.

Harrison, P. J., Conway, H. L., Holmes, R. W., and Davis, C. O., 1977. Marine diatoms grown in chemostats under silicate or ammonium limitation. III. Cellular chemical composition and morphology of Chaetoceros debilis, Skeletonema costatum, and Thalassiosira gravida. *Mar Biol* **43**, 19-31.

Hasle, G. R., 1983. Thalassiosira punctigera (Castr.) comb, nov., a widely distributed marine planktonic diatom. *Nord J Bot* **3**, 593-608.

Heaney, P. J., 1994. Structure and chemistry of the low pressure silica polymorphs. In: Heaney, P. J., Prewitt, C. T., and Gibbs, G. V. Eds.), *Silica: Physical behavior, geochemistry, and materials applications*. Mineralogical Society of America, Washington, DC.

Hecky, R. E., Mopper, K., Kilham, P., and Degens, E. T., 1973. The amino acid and sugar composition of diatom cell-walls. *Mar Biol* **19**, 323-331.

House, W. A., 1994. The role of surface complexation in the dissolution kinetics of silica: Effects of monovalent and divalent ions at 25°C. *J Colloid Interface Sci* **163**, 379-390.

Humborg, C., Conley, D., Rahm, L., Wulff, F., Cociasu, A., and Ittekkot, V., 2000. Silicon retention in river basins: Far-reaching effects on biogeochemistry and aquatic food webs in coastal marine environments. *Ambio* **29**, 45-50.

Hurd, D. C., 1972. Factors affecting solution rate of biogenic opal in seawater. *Earth Planet. Sci. Lett.* **15**, 411.

Hurd, D. C., 1973. Interactions of biogenic opal, sediment and seawater in the Central Equatorial Pacific. *Geochim Cosmochim Acta* **37**, 2257.

Hurd, D. C. and Birdwhistell, S., 1983. On producing a more general model for biogenic silica dissolution. *Am J Sci* **283**, 1-28.

Hurd, D. C. and Theyer, F., 1974. Changes in physical and chemical properties of biogenic silica from the Central Equatorial Pacific. I. Solubility, specific surface area, and solution rate constants of acid-cleaned samples. In: Gibb, T. R. P. J. (Ed.), *Analytical Methods in Oceanography*. American Chemical Society, Washington D. C.

Hyacinthe, C. and Van Cappellen, P., 2004. An authigenic iron phosphate phase in estuarine sediments: composition, formation and chemical reactivity. *Mar Chem* **91**, 227-251.

Iler, R. K., 1979. *The Chemistry of Silica*. Wiley- Interscience, New York.

Ittekkot, V., Unger, D., Humborg, C., and Tac An, N., 2006. The Silicon Cycle*SCOPE*. Island Press, Washington.

Jahnke, R. A. and Jahnke, D. B., 2000. Rates of C, N, P and Si recycling and denitrification at the US Mid-Atlantic continental slope depocenter. *Deep Sea Res I* **47**, 1405-1428.

Jourabchi, P., Van Cappellen, P., and Regnier, P., 2005. Quantitative interpretation of pH distributions in aquatic sediments: A reaction-transport modeling approach. *Am J Sci* **305**, 919-956.

Juillet-Leclerc, A., 1984. Cleaning process for diatomaceous samples*Eighth International Diatom-Symposium*, Paris, France.

Kamatani, A., 1982. Dissolution rates of silica from diatoms decomposing at various temperatures. *Mar Biol* **68**, 91-96.

Kamatani, A. and Riley, J. P., 1979. Rate of dissolution of diatom silica walls in seawater. *Mar Biol* **55**, 29-35.

Kamatani, A., Riley, J. P., and Skirrow, G., 1980. The dissolution of opaline silica of diatom tests in sea water. *J Oceanogr Soc Jpn* **36**, 201-8.

Kamiya, H. and Shimokata, K., 1976. The role of salts in the dissolution of powdered quartz. In: J, C. and T, P. Eds.)*International symposium on Water-Rock Interactions*. Czechoslovakian Geological Survey, Prague, Czechoslovakia.

Karlsson, M., Craven, C., Dove, P., and Casey, W., 2001. Surface charge concentrations on silica in different 1.0 M metal-chloride background electrolytes and implications for dissolution rates. *Aquat Geochem* **7**, 13-32.

Kastner, M., Keene, J. B., and Gieskes, J. M., 1977. Diagenesis of siliceous oozes – I. Chemical controls on the rate of opal-A to opal-CT transformation – an experimental study. *Geochim Cosmochim Acta* **41**, 1041-1051, 1053-1059.

Kemp, A. E. S., Pearce R B, Grigorov I, Rance J, Lange C B, Quilty P, and I., S., 2006. Production of giant marine diatoms and their export at oceanic frontal zones: Implications for Si and C flux from stratified oceans. *Global Biogeochem Cycles* **20**.

Kemp, A. E. S., Pike, J., Pearce, R. B., and Lange, C. B., 2000. The "Fall dump" – a new perspective on the role of a "shade flora" in the annual cycle of diatom production and export flux. *Deep Sea Res II* **47**, 2129-2154.

Khalil, K., Rabouille, C., Gallinari, M., Soetaert, K., DeMaster, D. J., and Ragueneau, O., 2007. Constraining biogenic silica dissolution in marine sediments: A comparison between diagenetic models and experimental dissolution rates. *Mar Chem* **106**, 223-238.

King, S. L., Froelich, P. N., and Jahnke, R. A., 2000. Early diagenesis of germanium in sediments of the Antarctic South Atlantic: in search of the missing Ge sink. *Geochim Cosmochim Acta* **64**, 1375-1390.

Koning, E., Brummer, G.-J., Van Raaphorst, W., Van Bennekom, J., Helder, W., and Van Iperen, J., 1997. Settling, dissolution and burial of biogenic silica in the sediments off Somalia (northwestern Indian Ocean). *Deep Sea Res II* **44**, 1341-1360.

Koning, E., Gehlen, M., Flank, A. M., Calas, G., and Epping, E., 2007. Rapid post-mortem incorporation of aluminum in diatom frustules: Evidence from chemical and structural analyses. *Mar Chem* **106**, 97-111.

Koning, E., van Iperen, J. M., van Raaphorst, W., Helder, W., Brummer, G.-J. A., and van Weering, T. C. E., 2001. Selective preservation of upwelling-indicating diatoms in sediments off Somalia, NW Indian Ocean. *Deep Sea Res I* **48**, 2473-2495.

Laruelle, G. G., Roubeix, V., Sferratore, A., Brodherr, B., Ciuffa, D., Conley, D. J., Durr, H. H., Garnier, J., Lancelot, C., Le Thi Phuong, Q., Meunier, J. D., Meybeck, M., Michalopoulos, P., Moriceau, B., Ni Longphuirt, S., Loucaides, S., Papush, L., Presti, M., Ragueneau, O., Regnier, P. A. G., Saccone, L., Slomp, C. P., Spiteri, C., and Van Cappellen, P., 2008. The global biogeochemical cycle of silicon: Role of the land-ocean transition and sensitivity to anthropogenic perturbations. *Global Biogeochem Cycles* **Submitted**.

Lasaga, A. C. and Gibbs, G. V., 1990. Ab-initio quantum mechanical calculations of water-rock interactions: Adsorption and hydrolysis reactions. *Am J Sci* **290**, 263-295.

Lawson, D. S., Hurd, D. C., and Pankratz, H. S., 1978. Silica dissolution rates of phytoplankton assemblages at various temperatures. *Am J Sci* **278**, 1373-1393.

Legrand, A. P., 1998. The surface properties of silicas. Wiley, New York.

Lemaire, E., Abril, G., De Wit, R., and Etcheber, H., 2002. Distribution of phytoplankton pigments in nine European estuaries and implications for an estuarine typology. *Biogeochemistry* **59**, 5-23.

Lewin, J. C., 1961. The dissolution of silica from diatom walls. *Geochim Cosmochim Acta* **21**, 182-198.

Lisitzin, A. P., 1985. The silica cycle during the last ice age. *Palaeogeogr Palaeoclimatol Palaeoecol* **50**, 241-270.

Lotter, A. F., Birks, H. J. B., Hofmann, W., and Marchetto, A., 1997. Modern diatom, cladocera, chironomid, and chrysophyte cyst assemblages as quantitative indicators for the reconstruction of past environmental conditions in the Alps.1. Climate. *J Paleolimnol* **18**, 395-420.

Loucaides, S., Behernds, T., and Van Cappellen, P., 2009. Surface reactivity of biogenic silica: surface versus bulk charge density. *Geochim Cosmochim Acta* **Submitted**.

Loucaides, S., Van Cappellen, P., and Behrends, T., 2008. Dissolution of biogenic silica from land to ocean: The role of salinity and pH. *Limnol Oceanogr* **53**, 1614-1621.

Lucas, C. C. and Dolan, M. E., 1939. Studies of the solubility of quartz and silicates. *Canadian Medical Association Journal* **40**, 126-134.

Lyklema, J., 1968. The structure of the electrical double layer on porous surfaces. *J Electroanal Chem* **18**, 341-348.

Mackenzie, F. T. and Garrels, R. M., 1965. Silicates: Reactivity with Sea Water. *Science* **150**, 57-58.

Mackenzie, F. T. and Garrels, R. M., 1966. Chemical mass balance between rivers and oceans. *Am J Sci* **264**, 507-525.

Mackenzie, F. T., Stoffyn, M., and Wollast, R., 1978. Aluminum in Seawater: Control by Biological Activity. *Science* **199**, 680-682.

Malej, A. and Harris, R. P., 1993. Inhibition of copepod grazing by diatom exudates: a factorin the development of mucus aggregates. *Mar Ecol Prog Ser* **96**, 33-42.

Martin-Jezequel, V., M., H., and Brzezinski, M. A., 2000. Silicon metabolism in diatoms: implications for growth. *J Phycol* **36**, 821-840.
Mayer, T. D. and Jarrell, W. M., 2000. Phosphorus sorption during iron(II) oxidation in the presence of dissolved silica. *Water Res.* **34**, 3949-3956.
McManus, J., Hammond, D. E., Berelson, W. M., Kilgore, T. E., Demaster, D. J., Ragueneau, O. G., and Collier, R. W., 1995. Early diagenesis of biogenic opal: Dissolution rates, kinetics, and paleoceanographic implications. *Deep Sea Res II* **42**, 871-903.
Menzel, D. W., Hulburt, E. M., and Tyther, J. H., 1963. The effects of enriching Sargasso sea water on the production and species composition of the phytoplankton. *Deep Sea Research and Oceanographic Abstracts* **10**, 209-219.
Michalopoulos, P. and Aller, R. C., 1995. Rapid Clay Mineral Formation in Amazon Delta Sediments. *Science* **270**, 614-617.
Michalopoulos, P. and Aller, R. C., 2004. Early diagenesis of biogenic silica in the Amazon delta: alteration, authigenic clay formation, and storage. *Geochim Cosmochim Acta* **68**, 1061-1085.
Michalopoulos, P., Aller, R. C., and Reeder, R. J., 2000. Conversion of diatoms to clays during early diagenesis in tropical, continental shelf muds. *Geology* **28**, 1095-1098.
Millero, F. J., 1995. Thermodynamics of the carbon dioxide system in the oceans. *Geochim Cosmochim Acta* **59**, 661-677.
Moriceau, B., Garvey, M., Ragueneau, O., and Passow, U., 2007. Evidence for reduced biogenic silica dissolution rates in diatom aggregates. *Mar Ecol Prog Ser* **333**, 129-142.
Moyle, P. R. and Dolley, T. P., 2002. With or without salt: A comparison of marine and continental-lacustrine diatomite deposits. *B. USGS* **2209-D**.
Muller, B., Maerki, M., Schmid, M., Vologina, E. G., Wehrli, B., Wuest, A., and Sturm, M., 2005. Internal carbon and nutrient cycling in Lake Baikal: sedimentation, upwelling, and early diagenesis. *Global Planet Change* **46**, 101-124.
Nelson, D. M. and Brzezinski, M. A., 1997. Diatom growth and productivity in an oligotrophic midocean gyre: A 3-yr record from the Sargasso Sea near Bermuda. *Limnol Oceanogr* **42**, 473-486.
Nelson, D. M. and Dortch, Q., 1996. Silicic acid depletion and silicon limitation in the plume of the Mississippi River: evidence from kinetic studies in spring and summer. *Mar Ecol Prog Ser* **136**, 163-178.
Nelson, D. M., Treguer, P., Brzezinski, M. A., Leynaert, A., and Queguiner, B., 1995. Production and Dissolution of Biogenic Silica in the Ocean – Revised Global Estimates, Comparison with Regional Data and Relationship to Biogenic Sedimentation. *Global Biogeochem Cycles* **9**, 359-372.
Osthols, E., 1995. Thorium sorption on amorphous silica. *Geochim Cosmochim Acta* **59**, 1235-1249.
Paasche, E., 1973. Silicon and the ecology of marine plankton diatoms. I. Thalassiosira pseudonana (Cyclotella nana) grown in a chemostat with silicate as limiting nutrient. *Mar Biol* **19**, 117-126.
Paasche, E., 1980. Silicon Content of Five Marine Plankton Diatom Species Measured with a Rapid Filter Method. *Limnol Oceanogr* **25**, 474-480.
Passow, U., 2000. Formation of transparent exopolymer particles, TEP, from dissolved precursor material. *Mar Ecol Prog Ser* **192**, 1-11.
Passow, U., 2002. Transparent exopolymer particles (TEP) in aquatic environments. *Prog Oceanog* **55**, 287-333.

Passow, U., Engel, A., and Ploug, H., 2003. The role of aggregation for the dissolution of diatom frustules. *FEMS Microbiol Ecol* **46**, 247-255.

Passow, U., Shipe, R. F., Murray, A., Pak, D. K., Brzezinski, M. A., and Alldredge, A. L., 2001. The origin of transparent exopolymer particles (TEP) and their role in the sedimentation of particulate matter. *Cont Shelf Res* **21**, 327-346.

Patrick, S. and Holding, A. J., 1985. The effect of bacteria on the solubilization of silica in diatom frustules. *Journal of applied bacteriology* **59**, 7-16.

Perram, J. W., 1973. Structure of the double layer at the oxide/water interface. *J Chem Soc Farad T 2* **69**, 993-1003.

Perram, J. W., Hunter, R. J., and Wright, H. J. L., 1973. Charge and potential at the oxide/solution interface. *Chem Phys Lett* **23**, 265-269.

Pitzer, K. S., 1973. Thermodynamics of Electrolytes. I. Theoretical Basis and General Equations. *J Phys Chem.* **77**, 268-277.

Platt, T., Subba Rao, D. V., Smith, J. C., Li, W. K., Irwin, B., Horne, E. P. W., and Sameoto, D. D., 1983. Photosynthetically-Competent Phytoplankton from the Aphotic Zone of the Deep Ocean. *Mar Ecol Prog Ser* **10**, 105-110.

Pondaven, P., Gallinari, M., Chollet, S., Bucciarelli, E., Sarthou, G., Schultes, S., and Jean, F., 2007. Grazing-induced Changes in Cell Wall Silicification in a Marine Diatom. *Protist* **158**, 21-28.

Pondaven, P., Ragueneau, O., Treguer, P., Hauvespre, A., Dezileau, L., and Reyss, J. L., 2000. Resolving the 'opal paradox' in the Southern Ocean. *Nature* **405**, 168-172.

Prelot, B., Janusz, W., Thomas, F., Villieras, F., Charmas, R., Piasecki, W., and Rudzinski, W., 2002. Adsorption of cadmium ions at the electrolyte/silica interface: I. Experimental study of surface properties. *Appl Surf Sci* **196**, 322-330.

Presti, M. and Michalopoulos, P., 2008. Estimating the contribution of the authigenic mineral component to the long-term reactive silica accumulation on the western shelf of the Mississippi River Delta. *Cont Shelf Res* **28**, 823-838.

Rabouille, C., Gaillard, J.-F., Treguer, P., and Vincendeau, M.-A., 1997. Biogenic silica recycling in surficial sediments across the Polar Front of the Southern Ocean (Indian Sector). *Deep Sea Res II* **44**, 1151-1176.

Ragueneau, O., Gallinari, M., Corrin, L., Grandel, S., Hall, P., Hauvespre, A., Lampitt, R. S., Rickert, D., Stahl, H., Tengberg, A., and Witbaard, R., 2001. The benthic silica cycle in the Northeast Atlantic: annual mass balance, seasonality, and importance of non-steady-state processes for the early diagenesis of biogenic opal in deep-sea sediments. *Prog Oceanog* **50**, 171-200.

Ragueneau, O., Lancelot, C., Egorov, V., Vervlimmeren, J., Cociasu, A., Deliat, G., Krastev, A., Daoud, N., Rousseau, V., Popovitchev, V., Brion, N., Popa, L., and Cauwet, G., 2002. Biogeochemical Transformations of Inorganic Nutrients in the Mixing Zone between the Danube River and the North-western Black Sea. *Estuar Coast Shelf Sci* **54**, 321-336.

Ragueneau, O., Schultes, S., Bidle, K. D., Claquin, P., and Moriceau, B. (2006) Si and C interactions in the world ocean: Importance of ecological processes and implications for the role of diatoms in the biological pump. *Global Biogeochem Cycles* **20**, 10.1029/2006GB002688.

Ragueneau, O., Treguer, P., Leynaert, A., Anderson, R. F., Brzezinski, M. A., DeMaster, D. J., Dugdale, R. C., Dymond, J., Fischer, G., Francois, R., Heinze, C., Maier-Reimer, E., Martin-Jezequel, V., Nelson, D. M., and Queguiner, B., 2000. A review of the Si cycle in

the modern ocean: recent progress and missing gaps in the application of biogenic opal as a paleoproductivity proxy. *Global Planet Change* **26**, 317-365.
Reitz, A., Pfeifer, K., de Lange, G. J., and Klump, J., 2004. Biogenic barium and the detrital Ba/Al ratio: a comparison of their direct and indirect determination. *Mar Geol* **204**, 289-300.
Renders, P. J. N., Gammons, C. H., and Barnes, H. L., 1995. Precipitation and dissolution rate constants for cristobalite from 150 to 300[degree sign]C. *Geochim Cosmochim Acta* **59**, 77-85.
Rickert, D., Schluter, M., and Wallmann, K., 2002. Dissolution kinetics of biogenic silica from the water column to the sediments. *Geochim Cosmochim Acta* **66**, 439-455.
Ridderinkhof, H. and Quartly, G., 2006. RRS Discovery Cruise Report: Cruise D301B and D302. NIOZ/NOCS.
Riese, A. C., 1982. Adsorption of radium and thorium onto quartz and kaolinite: A comparison of solution/surface equilibrium models. PhD, Colorado School of Mines.
Rimstidt, J. D. and Barnes, H. L., 1980. The kinetics of silica-water reactions. *Geochim Cosmochim Acta* **44**, 1683-1699.
Rocha, C. L. D. L., 2006. Opal-based isotopic proxies of paleoenvironmental conditions. *Global Biogeochem Cycles* **20**.
Roubeix, V., Becquevort, S., and Lancelot, C., 2008. Influence of bacteria and salinity on diatom biogenic silica dissolution in estuarine systems. *Biogeochemistry* **88**, 47-62.
Roubeix, V., Rousseau, V., and Lancelot, C., Diatom succession and silicon removal from freshwater in estuarine mixing zones: From experiment to modelling. *Estuar Coast Shelf Sci* **In Press, Corrected Proof**.
Ryves, D. B., Juggins, S., Fritz, S. C., and Battarbee, R. W., 2001. Experimental diatom dissolution and the quantification of microfossil preservation in sediments. *Paleogeography, Paleoclimatology, Peleoecology* **172**, 99-113.
Sahai, N. and Sverjensky, D. A., 1997. Evaluation of internally consistent parameters for the triple-layer model by the systematic analysis of oxide surface titration data. *Geochim Cosmochim Acta* **61**, 2801-2826.
Schink, D. R., Fanning, K. A., and Pilson, M. E. Q., 1974. Dissolved silica in the upper pore waters of the Atlantic Ocean Floor. *J Geophys Res* **79**, 2243-2250.
Schmidt, M., Botz, R., Rickert, D., Bohrmann, G., Hall, S. R., and Mann, S., 2001. Oxygen isotopes of marine diatoms and relations to opal-A maturation. *Geochim Cosmochim Acta* **65**, 201-211.
Schultes, S., 2004. The role of mesozooplankton grazing in the biogeochemical cycle of silicon in the Southern Ocean. PhD, University of Bremen.
Simon, M., Grissart, H.-P., Schweitzer, B., and Ploug, H., 2002. Microbial ecology of organic aggregates in aquatic ecosystems. *Aquat Microb Ecol* **28**, 175-211.
Sionneau, T., Bout-Roumazeilles, V., Biscaye, P. E., Van Vliet-Lanoe, B., and Bory, A., 2008. Clay mineral distributions in and around the Mississippi River watershed and Northern Gulf of Mexico: sources and transport patterns. *Quaternary Sci Rev* **27**, 1740-1751.
Smetacek, V., 2000. Oceanography: The giant diatom dump. *Nature* **406**, 574-575.
Sonnefeld, J., 1996. The influence of an acid treatment on the surface charge density of silica gel. *Colloid Polym Sci* **274**, 1137-1144.
Sonnefeld, J., Lobbus, M., and Vogelsberger, W., 2001. Determination of electric double layer parameters for spherical silica particles under application of the triple layer model using surface charge density data and results of electrokinetic sonic amplitude measurements. *Colloid Surface A* **195**, 215-225.

Spencer, C. P., 1983. Marine biogeochemistry of silicon. In: Aston, S. R. (Ed.), *Silicon geochemistry and biogeochemistry*. Academic Press, London.
Staats, N., Stal, L. J., De Winder, B., and Mur, L. R., 2000. Oxygenic photosynthesis as driving process in exopolysaccharide production of benthic diatoms. *Mar Ecol Prog Ser* **193**, 261-269.
Stoffyn, M., 1979. Biological Control of Dissolved Aluminum in Seawater: Experimental Evidence. *Science* **203**, 651-653.
Struyf, E., Dausse, A., Van Damme, S., Bal, K., Gribsholt, B., Boschker, H. T. S., Middelburg, J. J., and Meire, P., 2006. Tidal marshes and biogenic silica recycling at the land-sea interface. *Limnol Oceanogr* **51**, 838-846.
Stumm, W., 1992. *Chemistry of the solid-water interface*. Wiley Interscience, New York.
Sverjensky, D. A. and Sahai, N., 1996. Theoretical prediction of single-site surface-protonation equilibrium constants for oxides and silicates in water. *Geochim Cosmochim Acta* **60**, 3773-3797.
Tadros, T. F. and Lyklema, J., 1968. Adsorption of potential-determining ions at the silica – aqueous electrolyte interface and the role of some cations. *J Electroanal Chem* **17**, 267-275.
Tanaka, M., Takahashi, K., and Sahoo, Y. V., 2004. Speciation of dissolved silicates in natural waters cantaining alkaline and alkaline-earth ions
A case study – waters from arid lands (North West China). *Anal Bioanal Chem* **378**, 789-797.
Taylor, N. J., 1985. Silica incorporation in the diatom *Coscinodiscus granii* as affected by light intensity. *British Phycological Journal* **20**, 365-374.
Tréguer, P., Kamatani, A., Gueneley, S., and Queguiner, B., 1988. Kinetics of Dissolution of Antarctic Diatom Frustules and the Biogeochemical Cycle of Silicon in the Southern Ocean. *Polar Biol* **9**, 397-403.
Tréguer, P., Nelson, D. M., Vanbennekom, A. J., Demaster, D. J., Leynaert, A., and Queguiner, B., 1995. The silica balance in the world ocean – a reestimate. *Science* **268**, 375-379.
Truesdale, V., Greenwood, J., and Rendell, A., 2005. The Rate-equation for Biogenic Silica Dissolution in Seawater – New Hypotheses. *Aquat Geochem* **11**, 319-343.
Turner, J. T., Ianora, A., Esposito, F., Carotenuto, Y., and Miralto, A., 2002. Zooplankton feeding ecology: does a diet of Phaeocystis support good copepod grazing, survival, egg production and egg hatching success? *J Plankton Res* **24**, 1185-1195.
Van Bennekom, A. J., Fred Jansen, J. H., Van der Gaast, S. J., Van Iperen, J. M., and Pieters, J., 1989. Aluminium-rich opal: an intermediate in the preservation of biogenic silica in the Zaire (Congo) deep-sea fan. *Deep Sea Res* **36**, 173-190.
Van Bennekom, A. J., L, B. A. G., and F, N. R., 1991. Dissolved aluminium in the Weddell-Scotia Confluence and effect of Al on the dissolution kinetics of biogenic silica. *Mar Chem* **35**, 423-434.
Van Beueskom, J. E. E., Van Bennekom, A. J., Treguer, P., and Morvan, J., 1997. Aluminium and silicic acid in water and sediments of the Enderby and Crozet Basins. *Deep Sea Research Part II: Topical Studies in Oceanography* **44**, 987.
Van Beusekom, J. E. E., 1989. Wechselwirkungen zwischen gelösten Aluminium und Phytoplankton in marinen Gewässern. Ph.D. thesis, Hamburg University.
Van Cappellen, P., 1996. Reactive surface area control of the dissolution kinetics of biogenic silica in deep-sea sediments. *Chem Geol* **132**, 125-130.
Van Cappellen, P., Dixit, S., and Gallinari, M., 2002a. Biogenic silica dissolution and the marine Si cycle: kinetics, surface chemistry and preservation. *Oceanis* **28**, 417-454.

Van Cappellen, P., Dixit, S., and Van Beusekom, J. E. E. (2002b) Biogenic silica dissolution in the oceans: Reconciling experimental and field-based dissolution rates. *Global Biogeochem Cycles* **16**, 10.1029/2001GB001431.
Van Cappellen, P. and Qiu, L., 1997a. Biogenic silica dissolution in sediments of the Southern Ocean. I. Solubility. *Deep Sea Res II* **44**, 1109-1128.
Van Cappellen, P. and Qiu, L., 1997b. Biogenic silica dissolution in sediments of the Southern Ocean. II. Kinetics. *Deep Sea Res II* **44**, 1129-1149.
van der Weijden, A. J. and van der Weijden, C. H., 2002. Silica fluxes and opal dissolution rates in the northern Arabian Sea. *Deep Sea Res I* **49**, 157-173.
Van Lier, J. A., DeBruyn, P. L., and Overbeek, J. T. G., 1960. The solubility of quartz. *J Phys Chem.* **64**, 1675-1682.
Viollier, E., Michard, G., Jezequel, D., Pepe, M., and Sarazin, G., 1997. Geochemical study of a crater lake: Lake Pavin, Puy de Dome, France. Constraints afforded by the particulate matter distribution in the element cycling within the lake. *Chem Geol* **142**, 225-241.
Vrieling, E. G., Beelen, T. P. M., van Santen, R. A., and Gieskes, W. W. C., 2000. Nanoscale uniformity of pore architecture in diatomaceous silica: A combined small and wide angle X-ray scattering study. *J Phycol* **36**, 146-159.
Vrieling, E. G., Gieskes, W. W. C., and Beelen, T. P. M., 1999a. Silicon deposition in diatoms: Control by the pH inside the silicon deposition vesicle. *J Phycol* **35**, 548-559.
Vrieling, E. G., Poort, L., Beelen, T. P. M., and Gieskes, W. W. C., 1999b. Growth and silica content of the diatoms *Thalassiosira weissflogii* and *Navicula salinarum* at different salinities and enrichments with aluminum. *Eur J Phycol* **34**, 307-316.
Wang, Y., Bryan, C., Xu, H., and Gao, H., 2003. Nanogeochemistry: Geochemical reactions and mass transfers in nanopores. *Geology* **31**, 387-390.
Wells, J. D., Koopal, L. K., and de Keizer, A., 2000. Monodisperse, nonporous, spherical silica particles. *Colloid Surface A* **166**, 171-176.
Weres, O., Yee, A., and Tsao, L., 1981. Kinetics of silica polymerization. *J Colloid Interface Sci* **84**, 379-402.
Willey, J. D., 1974. The effect of pressure on the solubility of amorphous silica in seawater at 0[deg]C. *Mar Chem* **2**, 239.
Willey, J. D., 1980. Effects of aging on silica solubility: A laboratory study. *Geochim Cosmochim Acta* **44**, 573-578.
Wirth, G. S. and Gieskes, J. M., 1979. The initial kinetics of the dissolution of vitreous silica in aqueous media. *J Colloid Interface Sci* **68**, 492-500.
Wollast, R., 1974. The silica problem. In: Goldberg, E. D. (Ed.), *The Sea*. Wiley Interscience, New York.
Zhuravlev, L. T., 1993. Surface characterization of amorphous silica – a review of work from the former USSR. *Colloid Surface A* **74**, 71-90.

Summary

Silicon (Si) is the second most abundant element in the Earth's crust after oxygen. Weathering of silicate rocks at the earth's surface is the ultimate source of dissolved silicate (dSi) which is an essential nutrient for numerous organisms, both in the oceans and on land. The biological fixation of dSi under the form of structural elements composed of amorphous biogenic silica ($bSiO_2$) initiates the biological cycle of Si and links the silicon and carbon cycles.

The oceanic biogeochemical cycle of Si gained significant attention during the last few decades mainly because of the role of diatoms in the biological CO_2 pump. Diatoms are efficient exporters of organic matter from the surface ocean and by far the single most important group of oceanic primary producers. Unlike other algal species, however, diatoms are limited by the availability of dSi, which they require to synthesize their amorphous silica frustules.

Since $bSiO_2$-rich sediments are distributed in a variety of depths and latitudes and across all climatic zones of the ocean, biosiliceous fossils have a great potential as proxies for paleoproductivity. However, the great spatial and temporal inconsistencies between production, export and burial of $bSiO_2$ significantly hinder the interpretation of the sedimentary record. The large variability in preservation efficiency reflects the great variety of (interacting) biotic and abiotic processes involved in the recycling of $bSiO_2$. A sound knowledge of these processes is essential to better understand the functioning of the Si cycle in the past, present, and future oceans

Chapter 2 provides a review of the processes involved in determining the fate of $bSiO_2$ in the ocean. It starts with processes that take place during, and shortly following, the life cycle of diatoms, including parameters known to affect the silicification of diatom frustules during biomineralization. The important role of bacteria in initiating the chemical dissolution of $bSiO_2$ in the water column is highlighted, as well as the roles of aggregation and grazing. The chapter further deals with the geochemical aspects of $bSiO_2$ dissolution. It provides the theoretical background for the dissolution process and discusses different factors known to affect the dissolution kinetics and solubility of $bSiO_2$. Finally, the geochemical processes taking place in the water column during sinking, and in the sediments after deposition are reviewed.

The dissolution rate of diatom frustules is a function of the degree of undersaturation in respect to $bSiO_2$. Therefore, the solubility of $bSiO_2$ is an important parameter controlling the recycling efficiency of diatom frustules in the water column and sediments. As for any other mineral phase, the solubility of $bSiO_2$ is a function of ambient temperature and pressure. While an extensive body of data exists describing the dependence of $bSiO_2$ solubility on temperature, the effect of pressure on solubility has not yet been determined experimentally. Chapter 3 presents results from laboratory and field experiments describing the effect of pressure on the solubility of $bSiO_2$ between 1-700 bar and temperatures between 2 and 21°C. Our results suggest that the solubility of diatom frustules gradually decreases from 1 to ~200 bar by about 10%. Around 200 bar, however, our data imply a reversal in the pressure dependence. At 700 bar the solubility is about 15% higher than at atmospheric pressure.

In Chapter 4, we investigate the acid-base properties of a range of marine and continental biosiliceous materials. We present an improved titration procedure capable of producing accurate determinations of the build-up of electrical charge, in part by eliminating artifacts due to dissolution. The results of the acid-base titrations are interpreted using an equilibrium surface

complexation model. The large variability in charging observed among the various biosiliceous materials is explained by the existence of two pools of ionizable sites, one at the surface and one inside the $bSiO_2$ particle. Dissolution rate constants correlate positively with the external charge, rather than the total charge build-up, as expected if dissolution only involves the removal of silicate units from the outer surfaces of the particles. Older biosiliceous materials exhibit lower proportions of internal groups, while a decrease in the relative amount of internal silanols is also observed for diatom frustules artificially aged in seawater. The progressive reduction with time of the internal *versus* external silanol concentration ratio represents one of the aging mechanisms altering the material properties that affect the recycling and preservation of $bSiO_2$ in earth surface environments.

Fixation of $bSiO_2$ by land plants, but also by riverine and lacustrine diatoms, has been proposed to be of similar magnitude as that by marine diatoms. Therefore, a major fraction of the dSi load of the world's rivers may in fact originate from the dissolution of plant litter, soil phytoliths, and freshwater diatom frustules, rather than directly from the chemical weathering of silicate rocks. Although the global significance of the biogeochemical cycle of Si on land is now recognized, the vast majority of studies on $bSiO_2$ dissolution have focused on the marine environment. Chapter 5 presents the results of a study on the dissolution kinetics of $bSiO_2$ along a salinity and pH gradient representative of the estuarine freshwater to seawater transition. Based on a series of flow-through reactor experiments, we demonstrate that the dissolution rates of a range of biosiliceous material are on average 5 times higher in seawater than in freshwater, as a result of the higher salinity and pH. This large enhancement of the dissolution rate of $bSiO_2$ in seawater helps explain differences in the recycling efficiency of silica in marine and freshwater ecosystems. Furthermore, it implies that the large amounts of continental $bSiO_2$ supplied by rivers could be an important, and so far overlooked, source of nutrient Si in coastal marine environments.

It has long been suspected that early diagenetic interactions in continental margin sediments exert a major control on the biogeochemical cycle of Si and, ultimately, on the siliceous productivity of the oceans. Early diagenetic reactions involving $bSiO_2$ have also been invoked to explain variations in asymptotic pore water dSi concentrations and benthic dSi fluxes in the deep and coastal ocean. Even though direct evidence for such processes in abyssal sediments is not yet available, the evidence suggests that interactions between $bSiO_2$ and lithogenic silicate minerals may be an ocean-wide phenomenon, whose role in the marine biogeochemical cycling of Si remains to be fully assessed.

In Chapter 6, results are presented of long-term (10-22 months) batch reactor experiments, carried out in the laboratory or deployed along moorings, where cultured diatom frustules were incubated in the presence or absence of clay-rich delta sediments from the Mississippi and Congo Rivers. The results provide direct experimental evidence for a significant decrease in apparent silica solubility of diatom frustules upon exposure to seawater, on the time scale of 1-2 years. The apparent silica solubility decreases even further in the presence of fine-grained deltaic sediments. Chemical analyses provide evidence for chemical interactions involving the transfer of chemical elements from seawater (e.g., Mg, K) and from the clay-rich sediments (e.g., Al, Fe, Mn) to the frustules. Furthermore, microscopic observations reveal the formation of a variety of new mineral precipitates, often deposited on the surfaces of the frustules. The precipitates include alumino-silicate and magnesian silicate phases. Under oxic conditions, however, phosphate-rich ferric iron oxyhydroxides also form. Overall, the interactions between $bSiO_2$, seawater and lithogenic minerals enhance the removal of reactive silicon from the ocean system through sedimentary burial. In addition, uptake by $bSiO_2$ and the precipitation of secondary mineral products may

affect the biogeochemical cycles of other key biological (e.g., Fe, P) and geochemical (e.g., Mg, Al) elements.

Samenvatting

Silicium (Si) is na zuurstof het meest voorkomende element in de aardkorst. Verwering van silicaatgesteenten aan het aardoppervlak is de ultieme bron van opgelost silica (dSi). Dit opgeloste silica is een essentiële voedingsstof voor vele organismen in zowel de oceanen als op het land. Het vastleggen van dSi door organismen in amorfe biogene silica ($bSiO_2$) is de eerste stap in de biologische silicium cyclus en koppelt deze cyclus met die van koolstof.

De laatste decennia heeft de biogeochemische cyclus van Si in de oceanen veel aan aandacht gewonnen, voornamelijk door de rol die diatomeeën spelen in de biologische CO_2 pomp. Diatomeeën zijn efficiënte exporteurs van organisch materiaal vanuit de ondiepe naar de diepere oceaan en ze zijn verreweg de belangrijkste primaire producenten in de oceaan. Een groot verschil met andere algen is dat diatomeeën gelimiteerd zijn door de beschikbaarheid van dSi voor het bouwen van hun amorfe silica schaaltjes.

Sedimenten rijk aan bSiO2 worden afgezet op verschillende diepten in de oceanen, op diverse breedtegraden en in alle klimaatzones. Daarom zijn fossielen van biogene silica potentieel belangrijke en breed toepasbare indicatoren voor paleoproductiviteit. De interpretatie van het sedimentaire record wordt ernstig beperkt door de laterale en temporele verschillen in productie, export en afzetting van $bSiO_2$. De grote variabiliteit in de efficiëntie van $bSiO_2$ behoud in het sediment weerspiegelt de diversiteit aan biotische en abiotische processen die het hergebruik door oplossing van $bSiO_2$ beïnvloeden. Een gedegen kennis van deze processen is van belang voor een beter begrip van het functioneren van de silicium cyclus in de oceanen van het heden, verleden en de toekomst.

Hoofdstuk 2 geeft een overzicht van de processen die bepalend zijn voor het lot van $bSiO_2$ in de oceanen. Allereerst worden de processen tijdens en vlak na de levenscyclus van diatomeeën behandeld, waaronder parameters die bekend staan als invloedrijk op de bouw van diatomeeënschaaltjes. De belangrijke rol van bacteriën bij chemische oplossing van $bSiO_2$ in de waterkolom, en de rol van aggregatie en begrazing worden aangestipt. Verder komen de geochemische aspecten van de oplossing van $bSiO_2$ aan bod. Een theoretische achtergrond voor het oplossingsproces wordt gegeven en factoren die de kinetiek van oplossing en de oplosbaarheid van $bSiO_2$ beïnvloeden worden behandeld. Tot slot volgt een overzicht van de geochemische processen die plaatsvinden in de waterkolom tijdens het bezinken, en in het sediment na afzetting.

De oplossingssnelheid van de biogene silica schaaltjes is afhankelijk van de onderverzadiging met betrekking tot $bSiO_2$. De oplosbaarheid van $bSiO_2$ is daarom een belangrijke parameter in het hergebruik van Si uit diatomeeënschaaltjes in de waterkolom en het sediment. Net als voor elk ander mineraal is de oplosbaarheid van bSiO2 een functie van temperatuur en druk. De temperatuursafhankelijkheid van de oplosbaarheid van $bSiO_2$ is al uitgebreid bestudeerd, terwijl de afhankelijkheid van druk nog niet experimenteel bepaald is.

Hoofdstuk 3 presenteert de resultaten van laboratorium- en veldexperimenten waarin het effect van drukverschillen van 1 tot 700 bar bij 2 en 21°C op de oplosbaarheid van $bSiO_2$ bestudeerd wordt. De oplosbaarheid van diatomeeënschaaltjes neemt geleidelijk af tot 90% van de atmosferische waarde wanneer de druk oploopt van 1 tot ongeveer 200 bar. Rond 200 bar zien we een omkeerpunt in de drukafhankelijkheid van de oplosbaarheid. Bij 700 bar is de oplosbaarheid 15% hoger dan bij atmosferische druk.

In hoofdstuk 4 onderzochten we de zuur-base eigenschappen van verschillende biogene silica monsters van marine en continentale oorsprong. We ontwikkelden een verbeterde titratie methode die nauwkeurige bepalingen van de opbouw van lading aan het oppervlak mogelijk maakt. Deze verbetering was voornamelijk mogelijk door het uitsluiten van artefacten ontstaan door oplossing van het materiaal. De resultaten van de zuur-base titraties zijn geïnterpreteerd met behulp van een thermodynamisc oppervlaktecomplexatiemodel. De grote variatie in de opbouw van lading aan het oppervlak van de verschillende biogene silica monsters kan verklaard worden door middel van twee populaties van ioniseerbare groepen: een aan het oppervlak en een binnenin het $bSiO_2$ deeltje. De oplossingssnelheid correleert met de externe ladingsopbouw, niet de totale ladingsopbouw. Dit is te verwachten wanneer de oplossing van $bSiO_2$ alleen het verwijderen van silica eenheden van de buitenkant van de deeltjes omvat. Ouder biogeen silica vertoont lagere hoeveelheden van de interne ioniseerbare groepen. De relatieve hoeveelheid van deze interne silanolgroepen neemt ook af wanneer diatomeeënschaaltjes kunstmatig verouderd worden in zeewater. De progressieve afname met de tijd van de verhouding interne *versus* externe silanolgroepen is een mechanisme dat de materiaaleigenschappen van $bSiO_2$ verandert en daarmee het behoud en het hergebruik van $bSiO_2$ aan het aardoppervlak beïnvloedt.

Men denkt dat de vastlegging van silica door landplanten en zoetwaterdiatomeeën van dezelfde orde van grootte is als de vastlegging van silica door mariene diatomeeën. Het is daarom goed mogelijk dat een belangrijk deel van het opgeloste silica in de rivieren afkomstig is van opgelost plantenmateriaal, humus en de schaaltjes van zoetwaterdiatomeeën in plaats van van verwering van silicaatgesteenten. Ondanks het erkende mondiale belang van het terrestrische deel van de biogeochemische cyclus van silicium heeft het merendeel van de $bSiO_2$ studies zich gericht op het mariene deel. Hoofdstuk 5 beschrijft de studie naar de kinetiek van $bSiO_2$ oplossing langs een saliniteits- en pH-gradient die representatief is voor de overgang van estuarien zoetwater naar zeewater. Met een serie doorstroom-reactor experimenten laten we zien dat de snelheid van oplossing van biogene silica monsters gemiddeld vijf keer sneller is in zeewater dan in zoetwater als gevolg van de hogere saliniteit en pH. Deze verhoging van de oplossingssnelheid van $bSiO_2$ in zeewater verklaart de verschillen in efficiëntie van hergebruik van silica in mariene en zoetwater ecosystemen. Bovendien betekent dit dat de grote hoeveelheid continentaal $bSiO_2$ aangevoerd door de rivieren een belangrijke, tot nog toe genegeerde, bron van silica nutriënt kan zijn in de ondiep mariene milieus.

Dat vroeg-diagenetische processen in sedimenten op het continentale plat een grote controle uitoefenen op de biogeochemische cyclus van silicium en de silica productiviteit van de oceanen wordt al lang vermoed. Vroeg-diagenetische reacties met $bSiO_2$ zijn ook genoemd ter verklaring van asymptotische poriewater dSi concentraties en benthische dSi fluxen in de diepe en ondiepe oceanen. Hoewel direct bewijsmateriaal voor dezelfde processen in sedimenten op de abyssale vlakte nog niet voorhanden is, zijn er indicaties dat de interactie tussen biogene en lithogene silica een oceaanbreed fenomeen is. Het is daarom van belang de rol hiervan in de mariene biogeochemische cyclus van silicium te doorgronden.

Hoofdstuk 6 toont de resultaten van langdurige (10-22 maanden) incubatie experimenten uitgevoerd in het laboratorium of uitgezet langs meertrossen. In deze experimenten werden gecultiveerde diatomeeënschaaltjes geïncubeerd in de aan- of afwezigheid van kleirijke sedimenten uit de delta's van de Mississippi en Kongo rivieren. Uit deze experimenten halen we direct bewijsmateriaal voor een belangrijke afname in de schijnbare oplosbaarheid van diatomeeënschaaltjes tijdens de blootstelling aan zeewater over een periode van 1 tot 2 jaar. De schijnbare silica oplosbaarheid neemt zelfs sterker af in de aanwezigheid van fijnkorrelig

deltasediment. Chemische analyses tonen aan dat interacties plaatsvinden door middel van overdracht van elementen uit het zeewater (Mg, K) en uit de kleirijke sedimenten (Al, Fe, Mn) naar de schaaltjes. Observaties op microscopisch niveau laten de neerslag van verschillende mineralen zien, vaak op het oppervlak van de schaaltjes zelf. Deze neerslag bestaat onder andere uit aluminosilicaten en magnesiumsilicaten. Onder zuurstofrijke omstandigheden slaan ook fosfaatrijke ijzeroxyhydroxiden neer. Samenvattend kan gezegd worden dat de interacties tussen biogene en lithogene silica het behoud van $bSiO_2$ in het sediment, en daarmee de verwijdering van reactief silica uit de oceanen door begraving in het sediment versterkt. Daarnaast kan de opname van $bSiO_2$ en het neerslaan van secundaire mineralen een grote rol spelen in de biogeochemische cycli van andere biologisch (Fe, P) en geochemisch (Mg, Al) belangrijke elementen.

Περιληψη

Το πυρίτιο (Si) είναι το δεύτερο σε αφθονία στοιχείο στο φλοιό της Γης μετά το οξυγόνο. Η διάβρωση πυριτιούχων πετρωμάτων (χαλαζιακά) του στερεού φλοιού της γης αποτελεί την βασική πηγή προέλευσης διαλυτοποιημένου πυριτίου, απαραίτητο στοιχείο ως πηγή ενέργειας πολλών οργανισμών, ξηράς και θάλασσας. Η βιολογική χρήση του πυριτίου ως δομικό συστατικό, κοινώς η δημιουργία άμορφου χαλαζία ή αλλιώς οπάλιου ($bSiO_2$), ξεκινά τον βιογεωχημικό κύκλο του πυριτίου και τον συνδέει με τον αντίστοιχο του άνθρακα.

Ειδικά τις τελευταίες δεκαετίες, ιδιαίτερη προσοχή έχει δοθεί στον ωκεανικό βιογεωχημικό κύκλο του πυριτίου, εξ'αιτίας του ρόλου των διατόμων στη βιολογική χρήση του διοξιδίου του άνθρακα. Τα διάτομα συμβάλλουν σημαντικά στη μεταφορά οργανικής ύλης από την επιφάνεια των ωκεανών, και αποτελούν την πιο σημαντική ομαδα φυτοπλανγκτού λόγω συμβολής τους στην πρωτογενή παραγωγή των ωκεανών. Σε αντίθεση με άλλα είδη φυτοπλανκτού, τα διάτομα εξαρτώνται σημαντικά από την διαθεσιμότητα του πυριτίου, το οποίο και χρειάζονται για τη δόμηση του σκελετού τους.

Ιζήματα πλούσια σε οπάλιο είναι ευρύτατα διανεμημένα σε ποικίλα βάθη, γεωγραφικά πλάτη και εξαπλώνονται σε όλες τις κλιματικές ζώνες των ωκεανών. Αυτός είναι και ο λόγος που οπαλιογενή απολιθώματα έχουν σημαντική χρήση ως δείκτες συνθηκών πρωτογενούς παραγωγής μέσα στο γεωλογικό χρόνο. Παρόλ'αυτά, υπάρχει ακόμα μεγάλη δυσκολία στην ακριβή καταγραφή ιζηματογένεσης λόγω τεράστιων αποκλίσεων στους συσχετισμούς μεταξύ χώρου, εποχής, μεταφοράς και ενταφής του $bSiO_2$. Στη διαδικασία ανακύκλωσης του πυριτίου μεγάλο ρόλο παίζουν οι ποικίλες και αλληλεπιδρώμενες βιολογικές -και μη- χημικές αντιδράσεις, οι οποίες όμως προκαλούν και τις μεγάλες ανακατατάξεις σε μια επιτυχή διατήρηση και αποθήκευση πυριτίου. Είναι απαραίτητη η περαιτέρω γνώση των βιογεωχημικών διεργασιών για καλύτερη κατανόηση της λειτουργίας του κύκλου του πυριτίου στους ωκεανούς του παρελθόντος, παρόντος και μέλλοντος.

Το δεύτερο κεφάλαιο αποτελεί σύνοψη των γνωστών εως σήμερα διεργασιών που επηρεάζουν την πορεία του πυριτίου μέσα στους ωκεανούς. Οι διεργασίες αυτές διαδραματίζονται γύρω από τον κύκλο ζωής των διατόμων, συμπεριλαμβάνοντας τις παραμέτρους που συμβάλλουν στην πυριτίωση των διατομικών κυττάρων κατά τη διάρκεια βιο-ορυκτογένεσης. Έμφαση δίνεται στη σημαντική δράση βακτηριδίων, εναρκτήρια της χημικής διαλυτοποίησης του πυριτίου στο νερό, στην οποία περιλαμβάνονται διαδικασίες όπως της συνάθροισης και διατροφής (grazing). Αυτό το κεφάλαιο επιπλέον ασχολείται με τις γεωχημικές παραμέτρους του $bSiO_2$ εν διαλύσει. Εδώ παρουσιάζεται το θεωριτικό υπόβαθρο που σχετίζεται με τη διαδικασία διαλυτοποίησης και παραθέτει γνωστούς και ποικίλους παράγοντες που επηρεάζουν κινητικές διάλυσης και τη διαλυτότητα του βιογενούς πυριτίου. Τέλος, γίνεται και αναφορά στις γεωχημικές διεργασίες που διαδραματίζονται στο νερό κατά τη διάρκεια βύθισης αλλά και μέσα στα ιζήματα μετά την απόθεση.

Ο ρυθμός διάλυσης των διατόμων εξαρτάται από το βαθμό υποκορεσμού σε βιογενές πυρίτιο. Για το λόγο αυτό η διαλυτότητα του πυριτίου παίζει κατευθυντήριο ρόλο στην επαρκή ανακύκλωση του οπαλιωμένου υλικού των διατόμων, τόσο στο νερό όσο και μέσα στο ίζημα. Σχετικώς με άλλες ορυκτές φάσεις, η διαλυτότητα του $bSiO_2$ είναι άμεσα εξαρτώμενη από τη γύρω θερμοκρασία και πίεση. Παρ'όλο που έχουν γίνει ήδη εκτεταμένες αναφορές πάνω στον

συσχετισμό διαλυτότητας του $bSiO_2$ και θερμοκρασίας, η επίδραση της πίεσης δεν έχει ερευνηθεί επαρκώς. Το τρίτο κεφάλαιο παρουσιάζει αποτελέσματα από εργασίες εργαστηρίου αλλά και υπαίθρου, περιγράφοντας την επίδραση της πίεσης στη διαλυτότητα του $bSiO_2$ μεταξύ 1 έως 700 bar και σε θερμοκρασία από 2 έως 21ºC. Τα παραγόμενα αποτελέσματα της παρούσης έρευνας δείχνουν πως η διαλυτότητα του οπαλιογενή «σκελετού» των διατόμων ελαττώνεται κατά ~10% μεταξύ πιέσεων από 1 έως και 200 bar. Παρολ'αυτά, κατά τα 200 bar τα αποτελέσματά μας ενισχύουν τη θεωρία της ανάστροφης συσχέτισης μεταξύ διαλυτότητας και πίεσης. Στα 700 bar περίπου, η διαλυτότητα αυξάνεται κατά 15% περισσότερο από ότι σε συνθήκες ατμόσφαιρας.

Στο τέταρτο κεφάλαιο ερευνούμε τις ιδιότητες οξέως/βάσεως για ένα εύρος θαλάσσιων και ηπειρωτικών βιο-πυριτιωμένων (οπαλιωμένων) υλικών. Παρουσιάζουμε εδώ μια βελτιωμένη τεχνική τιτλοδότησης που έχει τις ικανότητες να παράγει ακριβείς προσδιορισμούς παραγωγής ηλεκτρικού φορτίου, χάρις στην ικανότητα εξάληψης ανθρωπίνου λάθους κατά τη διάρκεια διαλυτοποίησης. Τα αποτελέσματα από τιτλοδοτήσεις οξέως/βάσεως ερμηνεύονται χρησιμοποιώντας ένα μοντέλο (πρότυπο) σύμπλοκου επιφανείας που βρίσκεται σε ισορροπία με το περιβαλλόμενο σύστημα. Η μεγάλη μεταβλητότητα φορτίου που παρατηρήθηκε στα διάφορα πυριτιωμένα υλικά μπορεί να εξηγηθεί από την ύπαρξη δύο ομάδων ιονιζόμενων περιοχών, μια που βρίσκεται στην επιφάνεια και μια στο εσωτερικό του βιο-πυριτιωμένου σωματιδίου.

Οι σταθερές ποσοστού διάλυσης συσχετίζονται θετικά με το εξωτερικό φορτίο, παρά με το συνολικό ποσό φορτίου, το οποίο είναι αναμενόμενο μόνο και εφ'όσον η διαλυτοποίηση περιλαμβάνει την απομάκρυνση μονάδων πυριτίου από τις εξωτερικές επιφάνειες των σωματιδίων. Οπαλιωμένα υλικά μεγαλύτερης ηλικίας παρουσιάζουν χαμηλότερα ποσοστά εσωτερικών ιονιζόμενων περιοχών, καθώς η μείωση στο σχετικό αριθμό εσωτερικών «silanols» παρατηρείται επιπλέον και σε «σκελετούς» διατόμων που μεγάλωσαν τεχνιτά σε νερό θαλάσσης. Η προοδευτική μείωση συγκεντρώσεων του εσωτερικού έναντι του εξωτερικού silanol αναλογικά με το χρόνο, αντιπροσωπεύει μια από τους μηχανισμούς «γήρανσης», οι οποίοι με τη σειρά τους μεταβάλλουν τις ιδιότητες του υλικού και συνεπώς επηρεάζουν την ανακύκλωση και διατήρηση του $bSiO_2$ στα επιφανειακά στρώματα της γης.

Η παραγωγή $bSiO_2$ από φυτά ξηράς, αλλά και από διάτομα ποταμών και λιμνών, έχει προταθεί ίσης σημαντικότητας με αυτήν των διατόμων θαλάσσιας προέλευσης. Γι'αυτό το λόγο, ένα μεγάλο ποσοστό του dSi που παράγεται παγκοσμίως προέρχεται και απο τα ποτάμια που μεταφέρουν υλικό από την αποσάθρωση φυτών, φυτικής ύλης ιζήματος και διατόμων γλυκού νερού, και όχι τόσο από την χημική αποσάθρωση πυριτικών πετρωμάτων (χαλαζιακά). Παρ'ολο που η παγκόσμια σημαντικότητα του χερσαίου βιογεωχημικού κύκλου του πυριτίου είναι πια αναγνωρισμένο ως ιδέα, οι περισσότερες έρευνες έχουν εστιάσει στη διαλυτότητα που σχετίζεται με το θαλάσσιο περιβάλλον. Το πέμπτο κεφάλαιο παρουσιάζει τα αποτελέσματα έρευνας σχετικής με κινηματικές διάλυσης του $bSiO_2$ και το πως επηρεάζονται αυτές από το βαθμό αλατότητας και pH, έτσι ώστε να εκπροσωπούν τη μετάβαση από συνθήκες γλυκού νερού έως θαλασσινού. Βασισμένοι σε σειρά πειραμάτων του τύπου «ροής-μέσω- αντιδραστήρα» ή αλλιώς «flow-through reactor experiments», μπορούμε να επιδείξουμε πως τα ποσοστά διάλυσης μιας μεγάλης γκάμας βιο-πυριτιωμένων υλικών είναι πέντε φορές πιο πάνω στο θαλάσσιο παρά στο γλυκό νερό, σαν αποτέλεσμα υψηλής αλατότητας και pH. Αυτή η μεγάλη αύξηση του ποσοστού διάλυσης του $bSiO_2$ στο θαλάσσιο νερό συμβάλλει στη διελεύκανση των υπάρχουσων διαφορών που παρατηρούνται στην αποδοτικότητα ανακύκλωσης πυριτίου σε θαλάσσια αλλά και σε γλυκών νερών οικοσυστήματα.

Από καιρό υπήρχε η υποψία πως οι πρώιμες διαγενετικές διεργασίες στα ιζήματα ηπειρωτικών περιθωρίων ασκούν ένα σημαντικό έλεγχο στον βιογεωχημικό κύκλο του πυριτίου και συνεπώς στην ευρύτερη παραγωγή Si στους ωκεανούς. Πρώιμες διαγενετικές διεργασίες σχετικές με $bSiO_2$

έχουν επικαλεσθεί στην επεξήγηση παραλλαγών στις ασυμπτωτικές συγκεντρώσεις dSi του νερού στους πόρους του ιζήματος και στις βενθικές ροές dSi στο βάθος των ωκεανών αλλά και σε παράκτιες περιοχές. Παρ'όλο που δεν υπάρχει άμεση απόδειξη τέτοιων διεργασιών σε ιζήματα της αβύθου (ιζήματα πυθμένα), κάποιες ενδείχεις συνιστούν αλληλοεπίδραση μεταξύ $bSiO_2$ και λιθογενών ορυκτών πλούσια σε πυρίτιο, το οποίο μπορεί και να αποτελεί ένα γενικότερο φαινόμενο στους ωκεανούς. Ο ρόλος αυτού του φαινομένου στο θαλάσσιο βιογεωχημικό κύκλο του Si είναι ακόμα υπό έρευνα.

Στο έκτο κεφάλαιο παρουσιάζονται αποτελέσματα πειραμάτων μακράς διάρκειας (10-22 μήνες) του τύπου «batch reactor», τα οποία πραγματοποιήθηκαν αρχικά στο εργαστήριο και έπειτα τοποθετήθικαν κατα μήκος προσδέσεων εντός θαλασσινού νερού. Τα διάτομα που χρησιμοποιήθηκαν καλλιεργήθηκαν και διατηρήθηκαν πότε εντός και πότε εκτός ιζήματος εμπλουτισμένου σε αργιλικά, παρμένο από τις περιοχές του Δέλτα του Μισισιπί και του Κονγκό. Τα αποτελέσματα παρέχουν άμεση εργαστηριακή ένδειξη σημαντικής πτώσης της φαινόμενης διαλυτότητας του πυριτίου των σκελετικών τμημάτων των διατόμων με την έκθεσή τους στο θαλασσινό νερό για 1 με 2 χρόνια. Η φαινόμενη διαλυτότητα πυριτίου μειώνεται ακόμα περισσότερο στην παρουσία λεπτόκοκκου δελταικού ιζήματος. Χημική ανάλυση παρέχει απόδειξη των χημικών αλληλεπιδράσεων που σχετίζουν τη μεταφορά των χημικών στοιχείων από τη θάλασσα (π.χ. Mg, K) και από τα ιζήματα πλούσια σε άργιλο (π.χ. Al, Fe, Mn) στο «σκελετικό» τμήμα των διατόμων. Επιπλέον, παρατήρηση μέσω μικροσκοπίου αποκάλυψε το σχηματισμό μιας καινούριας σειράς ορυκτών ιζημάτων, συχνά εναποθετημένα στην εξωτερική επιφάνεια των διατόμων. Τα πρωτοσχηματιζόμενα ορυκτά συνήθως περιλαμβάνουν αργιλο-πυριτικές και μαγνησιο-πυριτικές φάσεις ορυκτών. Με τη δε επίδραση οξυγόνου, είναι δυνατόν να σχηματιστούν και υδροξείδια σιδήρου πλούσια σε φώσφορο. Γενικώς, οι αλληλεπιδρασεις μεταξύ $bSiO_2$, θαλασσινού νερού και λιθογενών ορυκτών, ενισχύουν την απομάκρυνση του ενεργού πυριτίου από τα συστήματα των ωκεανών μέσω του ενταφιασμού των ιζημάτων. Επιπλέον, ο βιογεωχημικός κύκλος άλλων σημαντικών βιολογικών (π.χ. Fe, P) και γεωχημικών (π.χ. Mg, Al) στοιχείων επηρεάζεται άμεσα τόσο από την προσρόφησή τους στην επιφάνεια του $bSiO_2$, όσο και από τον σχηματισμό δευτερογενών ορυκτών.

Aknowledgements

This work would not have been possible without the help and support of colleagues, friends, and family. My immense gratitude goes to every one of them.

I would like to thank my supervisor Philippe Van Cappellen for giving me the opportunity to reach this goal and for his support and guidance over the years. Working with you has been an honor and a great experience. Many thanks also go to my co-supervisor, Thilo Behrends, for sharing his knowledge and expertise with me during my PhD studies. Thanks for all your help in the lab and for the countless long and stimulating discussions in your office. You have been a great supervisor but also a good friend.

My thanks go to all the members of the geochemistry group who helped me over the years in one way or another. Pieter Kleingeld, your exceptional technical skills and creativity have been invaluable to my research; Dineke and Helen thank you for your help in the lab; Pien thanks for always making sure that all non-scientific matters were in order. Many thanks to my former office mates Sandra and Vincent for the good times, David for his help with every little thing and most of all for being a good friend. Special thanks also go to Mariette Wolthers and Vasso Alexandratos for helping with the translations of the summary.

This thesis would not have been possible without the collaboration and input from a number of colleagues including Erica Koning, Panagiotis Michalopoullos, Massimo Presti, Vincent Roubeix, Brivaella Moriceau, and Olivier Raqueneau. It has been a pleasure working with you all.

I would like to thank my parents making it possible for me to reach this stage and my sister and grandparents for their inspiration, support and encouragement throughout all these years. Most of all, however, I would like to thank my son Dylan and my beautiful wife-to-be Katie for their endless patience during this long and often painful process. I'm sorry to have sacrificed invaluable quality time with you during the making of this thesis. Katie, thank you for believing in me. I love you!

Curriculum vitae

Socratis Loucaides was born the 22nd of March 1977 in Limassol, Cyprus. He grew up in Limassol and attended Laniteio Gymnasium and Lyceum B between the ages of 12 and 18. After his 2-year mandatory military service he began his Bachelor's studies in Environmental Science at the University of North Carolina at Asheville. He graduated with a distinction as a university research scholar in 2001. The same year he was accepted at the graduate school of the University of North Carolina – Wilmington, where he graduated 2 years later with a Master's degree in Marine Science. In 2003 he accepted a position at the Marine Environmental Laboratory of the International Atomic Energy Agency in Monaco as a research technician. In July of 2004, he joined the geochemistry group at Utrecht University where four years later he was awarded his PhD degree in Earth Science. Since February 2009, he holds a postdoc position at the National Oceanography Center Southampton.